11-7-2005

Practical Behavioral Modeling Technique of Power Amplifiers Based on Loadpull Measurements

Jiang Liu
University of South Florida

Scholar Commons Citation

Liu, Jiang, "Practical Behavioral Modeling Technique of Power Amplifiers Based on Loadpull Measurements" (2005). *USF Tampa Graduate Theses and Dissertations.*
https://digitalcommons.usf.edu/etd/743

Practical Behavioral Modeling Technique of Power Amplifiers Based on Loadpull Measurements

by

Jiang Liu

A dissertation submitted in partial fulfillment
of the requirements for the degree of
Doctor of Philosophy
Department of Electrical Engineering
College of Engineering
University of South Florida

Co-Major Professor: Lawrence P. Dunleavy, Ph.D.
Co-Major Professor: Huseyin Arslan, Ph.D.
Thomas Weller, Ph.D.
Dennis Killinger, Ph.D.
Miguel Labrador, Ph.D.

Date of Approval:
November 07, 2005

Keywords: nonlinear system, nonlinear modeling, frequency-domain modeling, large-signal network analysis,memory effect

DEDICATION

To my wife and my parents for their support and encouragement

ACKNOWLEDGEMENTS

During my journey pursuing this Ph.D degree, lots of people have given me selfless help and encouragements. This dissertation would have been impossible without them. Special thanks to my dissertation advisors, Lawrence P. Dunleavy and Huseyin Arslan, for their invaluable support, inspiration and guidance. I would also like to express my appreciation to my committee members, Dr. Thomas Weller, Dr. Dennis Killinger and Dr. Miguel Labrador. They have been very helpful and supportive during this journey.

I would like to thank Dr. Jan Verspecht. I have benefited a lot from his insight and experience in the modeling area. I am also very grateful to Modelithics for its resources and support. Especially I would like to thank Bill Clausen and John Capwell for testing models and giving me feedbacks.

My present and former colleagues have given me lots of support. I am very grateful to Balaji Lakshminarayanan for being such a wonderful officemate and for those active discussions. I would like to thank Alberto Rodriguez for his assistance in solving measurement problems. I also want to thank Anthony Webster and Ravi Varanasi for the productive collaboration and stimulating discussions. I wish to thank Tevfik Yucek. He is a wonderful friend and has helped me academically and personally.

I would like to express my appreciation to my parents, for their overwhelming love and kindness during these first thirty years of my life. Special thanks to my two big brothers and sister-in-laws for supporting me working towards my Ph.D degree.

Last but not least, I would like to thank my lovely wife. Every time when I thought I couldn't finish the degree, my wife has been there, encouraging me and providing me the strength to continue. Without her support and love, I don't know how I can achieve it.

TABLE OF CONTENTS

LIST OF TABLES

LIST OF FIGURES

PRACTICAL BEHAVIORAL MODELING TECHNIQUE OF POWER AMPLIFIERS BASED ON LOADPULL MEASUREMENTS

Jiang Liu

ABSTRACT

Accurate linear and nonlinear models for devices and components are essential for successful RF/microwave computer aided engineering (CAE). The modeling techniques can be categorized in different levels based on the abstraction of the model as well as the application of the models at various design phases. This dissertation deals with behavioral modeling techniques for nonlinear RF components, especially amplifiers.

There is an increasing demand for accurate behavioral models of RF and microwave components, or integrated circuit (IC) blocks used in wireless system designs. Accurate behavioral models help designers evaluate and select the appropriate components at simulation phase, thereby cutting development cost.

However, there isn't a practical (or flexible) solution for accurate and effective behavioral model generation. This dissertation tries to tackle this problem. Power amplifiers and devices are the main components studied in this dissertation.

The primary focus is on the characterization of the loadpull performance of power amplifiers and devices. Major contributions of this dissertation include development of advanced loadpull measurement procedures, large-signal load-aware behavioral model, and a load-aware behavioral model with memory-effect capabilities.

There are two advanced loadpull measurements documented in this dissertation: the AM-PM loadpull measurement and the digital demodulation loadpull measurement. These two measurements may have been used internally by some research groups, however, according to the best knowledge of the author, they haven't received much attention in the literature. This is the first published work on these two topics.

It is shown in this work that the AM-PM performance can be strongly dependent on the load conditions. This property provides important information about the nonlinearities of power amplifiers and is used herein to create better behavioral models.

This newly developed digital demodulation loadpull measurement procedure enables system designers to evaluate power amplifiers directly against digital communication system parameters such as error vector magnitude (EVM). Two example measurements are given to demonstrate the measurement system setup and the correlations between traditional nonlinear figure-of-merits and system metrics.

A new behavioral modeling technique / procedure is developed based on loadpull AM-AM and AM-PM measurements. The large-signal scattering function theory is applied in the technique to formulate the model. The created model is able to automatically detect the load impedance and generate corresponding nonlinear properties. Three example models are presented to demonstrate the capability of this technique to predict accurately the output power contours, 50 ohm large-signal S21, and 3rd order intermodulation products (through additional file-based model).

Finally, a modeling technique is demonstrated to enable predicting the linear memory effect within a varying load condition. The nonlinear block used in the traditional two-box model structure is replaced with the large-signal loadpull model mentioned above. By adding this new feature, the resulting model is able to predict the load-related AM-AM and AM-PM properties, which will improve the accuracy of ACPR prediction.

CHAPTER 1

INTRODUCTION

1.1 Background and motivation

Computer aided engineering (CAE) software packages play an important role in research and development of wireless communication systems. They help predict the component or sub-system performance prior the hardware prototype implementation, cut the development cost and reduce the time to market. Accurate models for devices/sub-systems are the key for the successful application of CAE software. If the models are not accurate, no matter how fast or precise the simulators are, the final simulation results won't match prototype measurements. A significant amount of research has been devoted towards the development of various types of devices/components models.

In general, there are three types of modeling techniques widely used in CAE tools. They are physical device modeling, equivalent circuit modeling and behavioral modeling. Physical device models provide the most complex and complete information about the device studied; however they require substantial computer resources, detailed device information typically unavailable to designers. Physical models are therefore not suitable for circuit designs.

Equivalent circuit models can be considered as an abstraction of the physical models; circuits of elemental electrical components are arranged in physically-motivated topologies to represent the electrical characteristics of the devices. The main challenge of this technique is to find a proper circuit structure and optimize the elements' values to match the performance of the devices.

Behavioral models are another level of abstraction of the device. They are a set of mathematical expressions, and corresponding fitting coefficients, that can represent the input-output relationship. Behavioral models provide the minimal set of input information about the device construction as compared to other two types of models. They also require the least amount of simulation time and are suitable for system level designs [1].

Behavioral models can be derived from two different approaches. The first approach is to measure samples of the component of interest and to create the model based on the measurement results. The second approach is to use simulation data from low-level models (physical models or equivalent models) and create the behavioral models for higher level simulation to reduce the simulation times. Figure 1.1 illustrates the two approaches.

Behavioral modeling is receiving more and more interest recently. This is because of the increasing integration level in wireless products, e.g. cellular phones and personal digital assistants (PDA). Designers prefer to using off-the-shelf functional components, like low noise amplifiers (LNA) and power amplifiers (PAs), directly in their products to minimize the discrete components in the system and cut the final cost. Accurate behavioral models for these components are very important for this practice to be successful.

This has motivated the research work documented in this dissertation. Specifically, this dissertation tries to address the behavioral modeling problems for power amplifiers, which are an important component in current wireless systems.

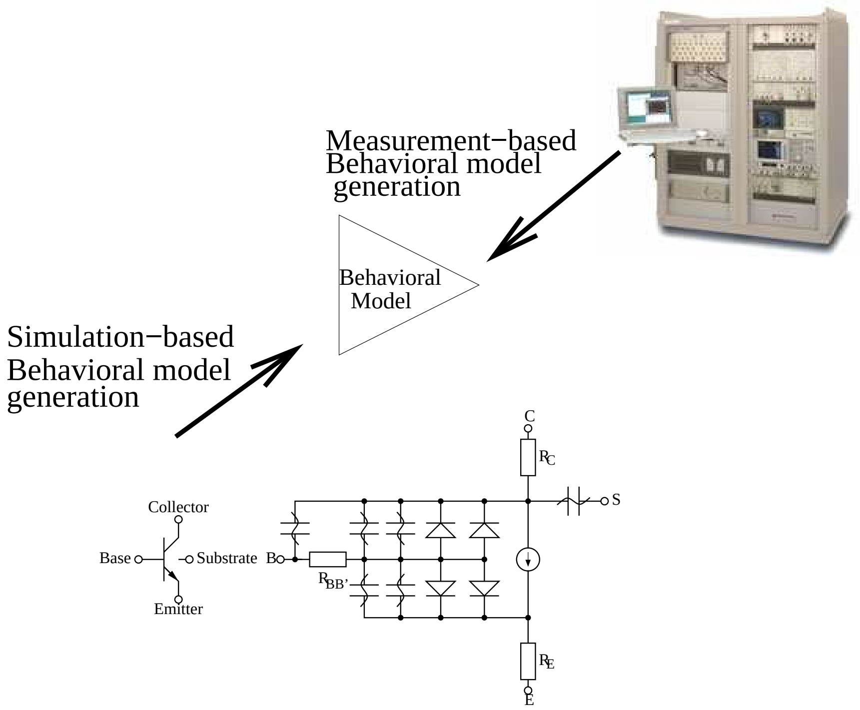

Figure 1.1 Generation of behavioral model from different data sources: measurement-based or simulation-based.

1.2 Contribution of the dissertation

An ideal behavioral model for an power amplifier should be able to predict the nonlinear performance, such as gain compression and intermodulation distortion at different input power levels under various source/load conditions. Moreover, it should be able to predict the dynamic effects of amplifiers under modulated signal stimuli. Lots of research using different approaches has been done to achieve this goal. However, according to the literature review that is given in Chapter 2, this goal hasn't been met yet.

The dissertation documents a behavioral model that can meet the requirement of an accurate nonlinear power amplifier model through easily obtained measurements. The contribution of this dissertation can be summarized as the following:

- Two advanced loadpull measurement procedures have been developed for behavioral modeling;
- A behavioral modeling technique is demonstrated to create large-signal scattering function model based on loadpull gain and phase compression; example models have been illustrated showing the effectiveness of this technique;
- A new behavioral model is proposed to combine the loadpull model with the linear filtering model to enable the prediction of memory effect at different load conditions; this feature makes the model ready for accurate system level modeling.

1.3 Organization

The organization of this dissertation is listed below. In chapter 2, a detail literature review about the current behavioral modeling efforts is provided. Different techniques are introduced briefly and their limitations are discussed.

In chapter 3, two advanced loadpull measurement procedures are presented, namely loadpull AM-PM measurement and loadpull EVM measurement. It is shown in the chapter that the load impedances will affect the phase compression property of amplifiers. This information is used later to develop the large-signal behavioral models. Also the EVM of an amplifier under various load conditions is measured and compared with the intermodulation distortion. Similarities are observed for these two figure-of-merits.

Chapter 4 is devoted entirely to introduce the proposed modeling technique based on loadpull gain and phase compression measurements. General review of the large-signal scattering function theory is given. The proposed model exploits the same concept by extending the small-signal S-parameter model to address the nonlinear effects. An optimization process is developed to fit the model parameters to match the measurement datasets. Three example models are presented that show the capability of this modeling technique for predicting nonlinear performance under varied load situations.

A new behavioral model is proposed in Chapter 5 to predict the memory effect under varied loadpull conditions. This is achieved by combining the model designed in Chapter 4 and a linear filtering function. Experimental results are given out proving the effectiveness of this method. In Chapter 6, conclusions are drawn and future studies are recommended.

CHAPTER 2

LITERATURE REVIEW ON CURRENT BEHAVIORAL MODELING TECHNIQUES FOR POWER AMPLIFIERS

2.1 Introduction

Generally speaking, the models used in CAE tools can be grouped into three categories: physical device models, equivalent circuit transistor models and behavioral models. Physical device models are based on the description of carrier transport physics. These kind of models provide invaluable insight into how the devices operate as well as their electrical properties, such as DC, AC and transient performances. However, The completeness of these models require detailed (often proprietary) information about device geometries and fabrication properties. The models generate huge demand for computing power, as well. Therefore, they are not suitable for circuit designs.

Equivalent circuit models are composed of electrical elements such as resistors, capacitors, inductors, and nonlinear current or voltage sources, which can characterize the electrical properties of transistors. There are all kinds of equivalent circuits for different types of transistors, such as BJT, CMOS or MESFET. This kind of modeling technique doesn't depend on the device physics to derive the electrical properties from the carrier transport equations. Compared with physical device models, the equivalent models require much less computation power. However, the limitation associated with this modeling technique is that it is difficult to come up with a suitable circuit structure and fit the parameters to match the measured properties.

Behavioral models provide another level of abstraction to represent the device performance. They are a set of mathematical expressions that describe the essential electrical properties. Most of the time, only the input-output relationship is of interest. So the behavioral modeling reduces to find a suitable equation to match the output to the input. Typically, a simulation using behavioral models will require the least amount of time. The cost of this technique is that the model is only as accurate as the data given and the appropriateness of the equations to represent the measured behavior.

In this research, the focus is on the behavioral modeling of nonlinear power amplifiers. Power amplifiers (PAs) are critical components in wireless communication systems. Often they are the final stage for the signal amplification. They provide high gain to the input signal, enabling the signal to transmit through the radio channel and be detected by the receiver. On the other hand, they can create large in-band and out-of-band distortion and interference that needs to be taken care of, otherwise the output signal won't be detected correctly. Hence, their performance, to a large extent, decides whether the whole system can work properly or not. Accurate models of PAs are required for system evaluation and verification.

Numerous modeling techniques have been reported in the past several years. The research efforts range from simulating the compression properties of a PA under one-tone stimulus to capturing transient input-output relationship in the time-domain. In Section 2.3, the basic theories of these modeling techniques are reviewed and summarized. Despite these reported techniques, there are still some questions that need to be answered. In Section 2.4, several of the problems are pointed out for the current research methods. These problems will be addressed in the dissertation. To begin, let's briefly review in the following section the basic nonlinear phenomena that are incurred by the PAs.

2.2 Introduction of nonlinear phenomena

The power amplifiers (PA) nonlinear effects are usually presented in frequency generation and distortion. Typical nonlinear phenomena include the following:

- harmonic distortion
- AM-AM and AM-PM conversion
- intermodulation and intercept point
- adjacent channel power ratio
- dynamic range.

The following example is provided to illustrate these concepts.

One simple way a nonlinear PA can be represented is by the polynomial function shown in Equation 2.1:

$$y(t) = k_1 x(t) + k_2 x(t)^2 + k_3 x(t)^3 \tag{2.1}$$

where $x(t)$ and $y(t)$ are the input and output signal of the component respectively. We will use this representation of PA nonlinearity to illustrate and define the above listed nonlinear phenomena. Assume the input signal $x(t)$ is a single stimulus frequency, i.e.

$$x(t) = A\cos(\omega t) \tag{2.2}$$

by substituting $x(t)$ into Equation 2.1, following expression is obtained through expansion:

$$y(t) = \frac{1}{2}k_2 A^2 + (k_1 A + \frac{3}{4}k_3 A^3)\cos(\omega t) + \frac{1}{2}k_2 A^2\cos(2\omega t) + \frac{1}{4}k_3 A^3\cos(3\omega t) \tag{2.3}$$

Although there is only one frequency excitation ω at the input, several new frequencies, 2ω and 3ω, are generated due to the nonlinear operation of the PAs. These frequencies are defined as the harmonics of the excitation frequency, i.e. $m\omega$, where m is an integer. Often the excitation frequency is also called fundamental frequency. The harmonic distortion (HD) is defined as the ratio of the harmonic to the fundamental response. For the single-tone example shown above (Equation 2.3, the second harmonic distortion denoted as HD_2 can be written as

$$HD_2 = \frac{k_2 A^2}{2k_1 A} \tag{2.4}$$

Notice that the fundamental tone consists of two items, one from the original input and the other from the third order mixing product of $2\omega - \omega$, $k_3 x(t)^2$. This part is considered as interference from higher order harmonics that contaminates the first order linear response. When computing the HD, only the response of the fundamental frequency should be considered.

AM-AM and AM-PM are defined as the shift in amplitude or phase of the fundamental tone at the output port due to the changes in the input signal amplitude. For this example, the fundamental tone at the output is $k_1 A + \frac{3}{4} k_3 A^3$, including a linear term and the contribution of the 3rd order mixing product. Because the output power is finite, k_3 has to be a negative value to make a stable system. This causes compression in the fundamental frequency power level. This is denoted as AM-AM effect or gain compression. One figure of merit for AM-AM is the 1dB compression point (P1dB), where the gain decreases by 1 dB compared to the original value.

Furthermore, if the 3rd order product is not in-phase with the input, that would cause the phase shift in the fundamental tone, which can be easily observed in the frequency domain according to:

$$Y(\omega) = k_1 A + \frac{3}{4} k_3 A^3 e^{j\theta} \tag{2.5}$$

where θ is the phase difference of the linear and 3rd term. This effect is referred to AM-PM conversion. Obviously, AM-PM occurs when the PA is driven into a high compression region. Figure 2.1 shows the AM-AM and AM-PM effect of an ISL3990 power amplifier. The compression and phase shift of the fundamental tone are obvious with the increment of the input tone. The 1dB compression point occurs at the input level of -6 dBm.

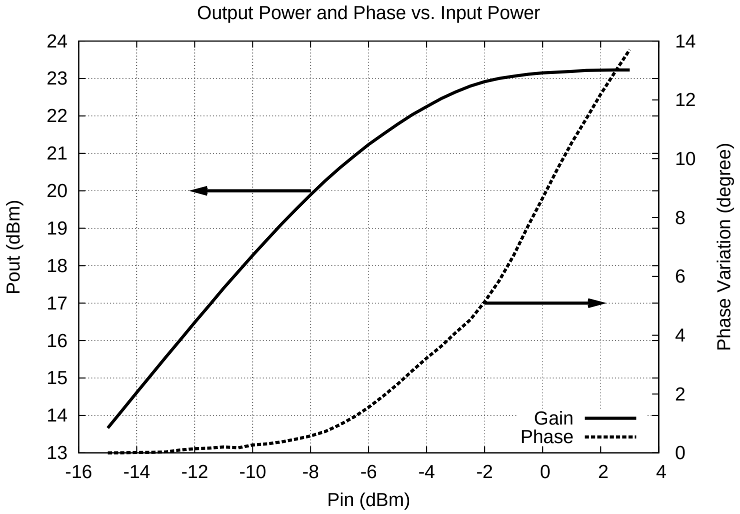

Figure 2.1 AM-AM and AM-PM performance of ISL3990 PA at 5.24 GHz.

Now let's assume the input $x(t)$ is a two-tone excitation, i.e.

$$x(t) = A(cos(\omega_1 t) + cos(\omega_2 t)) \tag{2.6}$$

the expansion of Equation 2.1 leads to the result shown following:

$$
\begin{aligned}
y(t) \;=\; & k_2A^2 + (k_1A + \frac{9}{4}k_3A^3)(cos(\omega_1 t) + cos(\omega_2 t)) \\
& + \frac{1}{2}k_2A^2(cos(2\omega_1 t) + cos(2\omega_2 t)) \\
& + k_2A^2(cos(\omega_1 t - \omega_2 t) + cos(\omega_1 t + \omega_2 t)) \\
& + \frac{1}{4}k_3A^3 cos(3\omega_1 t) + cos(3\omega_2 t)) \\
& + \frac{3}{4}k_3A^3(cos(-\omega_2 t + 2\omega_1 t) + cos(\omega_2 t + 2\omega_1 t) \\
& + cos(\omega_1 t - 2\omega_2 t) + cos(\omega_1 t + 2\omega_2 t))
\end{aligned} \tag{2.7}
$$

For this case, besides the harmonics of the fundamental input tones, more frequency components are observed that obey the relationship $m\omega_1 \pm n\omega_2$, the mixing of the two input excitation tones. These components are defined as the intermodulation (IM) products. Figure 2.2 shows a typical output spectrum of a nonlinear component.

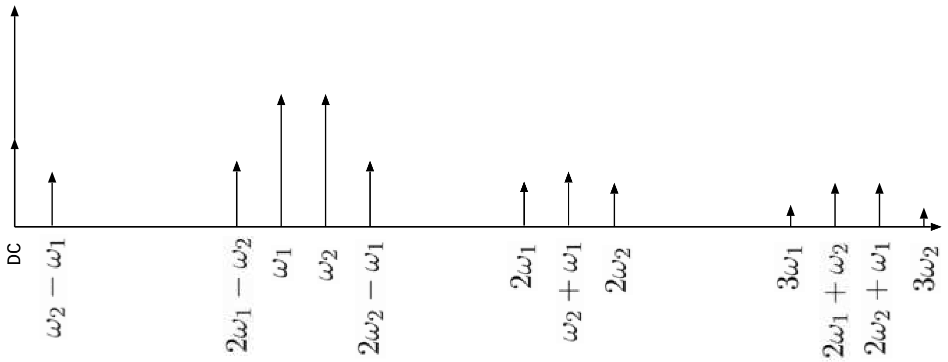

Figure 2.2 Output spectrum of a nonlinear component under two-tone excitation.

Of the multiple IM products, $2\omega_1 - \omega_2$ and $2\omega_2 - \omega_1$ are of most interest because they are close to the fundamental frequency and difficult to filter out. The power level of these two IMs, $\frac{3}{4}k_3A^3$, is proportional to the cube of the input signal amplitude A, while the fundamental tone at the output is approximately linear to that, assuming the input power level is low and neglecting contribution from other IM products. There is a 3:1 ratio between the amplitudes of the IM3 and the fundamental tone, which can be observed from Figure 2.3.

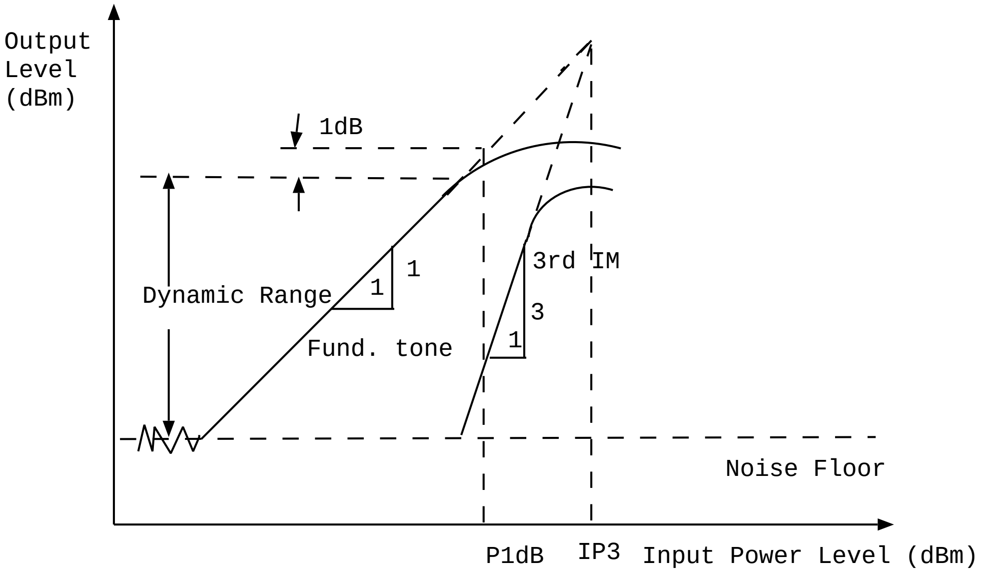

Figure 2.3 Illustration of the third order intercept point concept.

As can be seen, the extrapolation of the power of the fundamental and the third order IM (IM3) products will intersect. The intersection point is defined as the third order intercept point (IP3). Although this point is totally a theoretical value, it is a useful quantity to estimate the IM3 distortion.

For digital communication applications where complex modulation techniques are utilized, the sinusoidal representation of the stimulus signal is no longer valid to simulate the distortion effect. For this situation, ACPR is often used to represent the distortion effect. As the name implies, ACPR represents the spectral leakage to the nearby channels due to the distortion effect and is quantified as the power ratio between the adjacent channel and the main channels, as defined in Equation 2.8:

$$ACPR = \frac{P_{adjacent}}{P_{main}} \tag{2.8}$$

Obviously, the ACPR measurement depends on the definition of the main channel and the adjacent channel (which is often given out in the specifications of wireless communication systems, like W-CDMA or IS-95). Figure 2.4 illustrates the spectral regrowth effect. Significant power leakage out of the main channel can be seen in the figure.

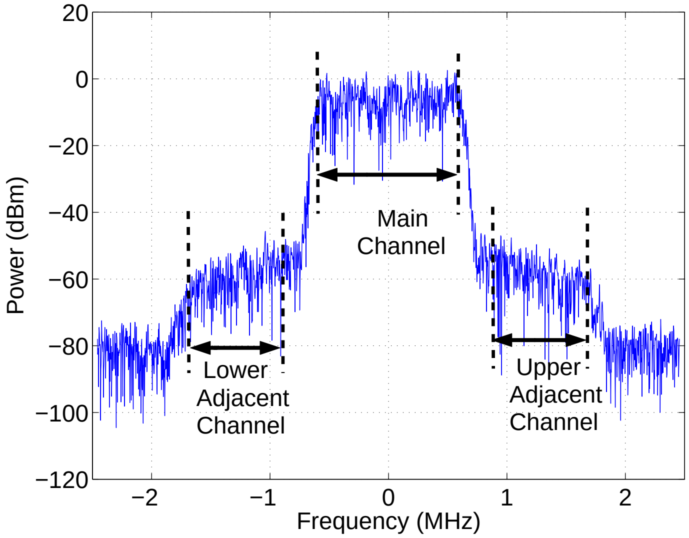

Figure 2.4 Illustration of the spectral regrowth effect and the ACPR concepts. The main channel and adjacent channel are give out, which will be used for ACPR calculation.

Another important concept is the dynamic range (DR), shown in Figure 2.3, that defines the region where the nonlinear component preserves linear performance due to low power input. It is limited at the lower side by the noise floor while the upper level is usually equal to 1dB compression point.

The measurement result of a real PA is given out in Figure 2.5 to demonstrate the IM effect. Measured IM3, IM5 and IM7 (third, fifth and 7th order IM products) and the fundamental frequency are illustrated. Notice there is a drop in IM3 power level around an input power of -13 dBm. This phenomenon is often called as "sweet spot" where the IM distortion will be much better than at other power levels. This is caused by the destructive summation of different contributors to the IM3. This effect can be exploited in PA designs to get higher output power level and efficiency and at the same time maintain low IM3 distortion.

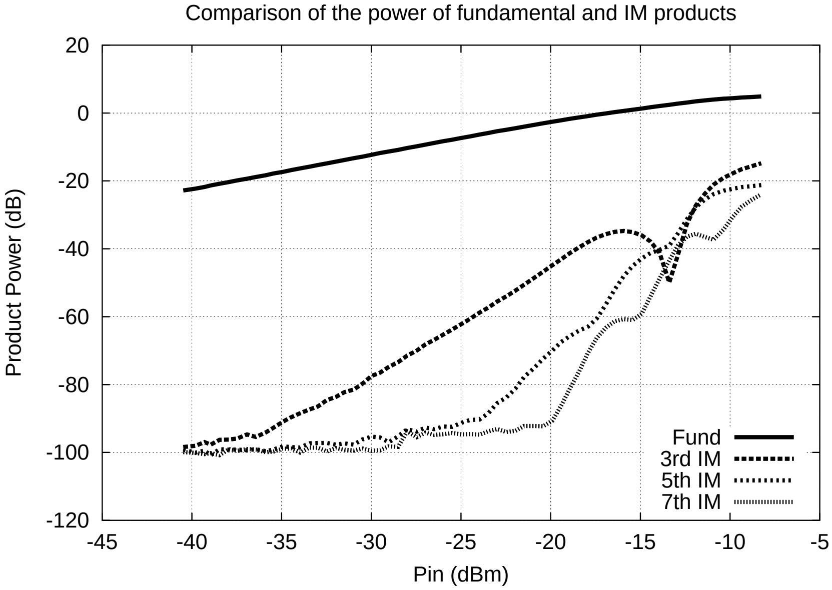

Figure 2.5 Measurement example of IMs of a MAX2371 amplifier.

Obviously, the example model shown in Equation 2.1 cannot predict the higher order IM products, simply because of the low order of the polynomial. This also demonstrates the importance of modeling for accurate simulation and prediction of circuit/system performance. In the following section, current state of art modeling techniques for PAs are introduced in detail.

2.3 Review of behavioral modeling techniques of PAs

There are two practical approaches to model PAs: circuit-level modeling and behavioral modeling. In circuit-level modeling, one has to have a good knowledge of the PA's structure; the model performance relies greatly on the accurate model for the nonlinear devices used in the circuit. Figure 2.6 gives an example 1.9GHz PCS power amplifier design using a packaged FET device, lumped components and distributed matching circuits. The accuracy of the simulation of the PA depends on the models for the elements in the circuits, especially the nonlinear FET device. Usually the nonlinear devices such as BJTs or MOSFET are represented by an equivalent circuit, in which one or several nonlinear elements are included. These nonlinear elements are often referred as the basic nonlinearities [2]. Typical nonlinear elements include:

- nonlinear conductance
- nonlinear transconductance
- nonlinear resistance
- nonlinear transresistance

Behavioral modeling, on the other hand, is simply a mathematical and/or data-file-based characterization of the essential nonlinear properties of the given circuit [1]. It treats the PA system as a black box; the only thing that matters is the relationship between the input and output signals. Once the input/output signals are obtained, either from measurements or simulation, mathematical equations, data-file-based look-up-table (LUT) or neural network structures can then be created to replicate and predict the performance of the PAs. This method is especially useful for system engineers who are only interested in the interaction of the PAs with other blocks in a system. That's because by using behavioral models, the simulation time

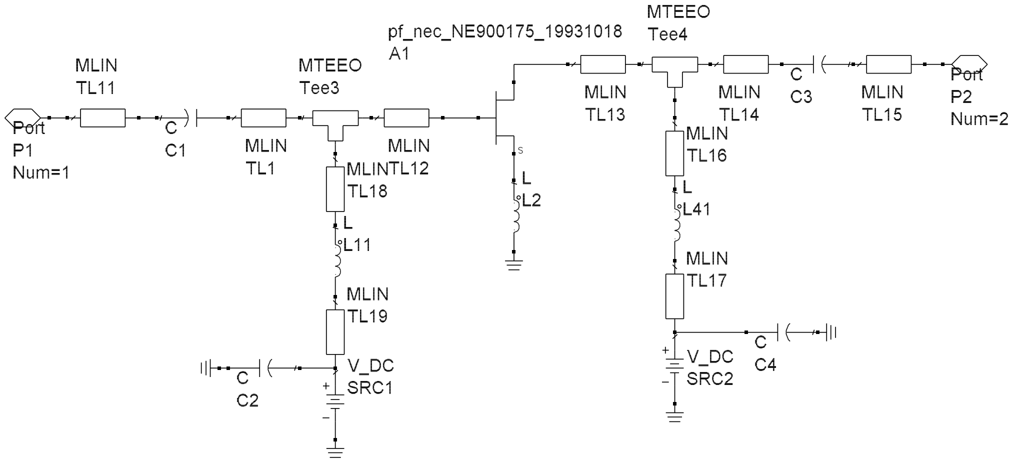

Figure 2.6 An example 1.9 GHz PCS power amplifier.

will be decreased significantly, therefore increasing the engineers' productivity. In fact, behavioral modeling is indispensable because it is practically impossible to simulate the entire system at the transistor level with the complex digitally modulated signal as the input [1].

The input-output relationship of a PA is described by the nonlinear parameters introduced in the Section 2.2. AM-AM and AM-PM are two most widely used parameters in PA behavioral modeling, because these parameters capture significant part of the PA nonlinearities and they can be easily modeled. A model that predicts only the AM-AM and AM-PM effects is often referred to a memoryless model, or mild memory model. Here "memoryless" PA means that the current output signal from the PA under study is only determined by the current input signal and is not affected by previous input or output signal samples. A "memory" model indicates that the current output signal is affected by both the present input as well as previous input/output signals. The "memory" effect can be observed, in the frequency-domain, as the asymmetric IMD performance of IM products, e.g. power level differences for the upper and lower IM3 and IM5. Or it is shown as the dynamic AM-AM and AM-PM curves by looking at the time-domain signal samples. The memory effect is caused by several issues, including input and output tuned network, low frequency dispersion, electrothermal interactions and bias circuitry [3], [4]. Memory effects of a PA influence the performance of the system significantly, and therefore, need to be treated carefully [5].

2.3.1 Memoryless models

Among the varieties of the mathematical expressions for AM-AM and AM-PM modeling, Saleh's model and the polynomial functions are utilized and reported extensively in the literature. Equation 2.1 given in Section 2.2 is a typical polynomial model for a PA. The model can be easily created using curve-fitting algorithm if the measured data is available. One can use separate expressions to model the AM-AM and AM-PM respectively, or using complex power series to integrate the two effects together [6]. By increasing the order of the polynomial, accurate replication of the AM-AM and AM-PM data can be obtained. The polynomial models are widely utilized for PA characterization [6, 7, 8, 9, 10, 11]. Zhou pointed out that polynomial is not suitable for strong nonlinearities such as hard limiters but are appropriate for weakly nonlinear devices [12]. A significant limitation of this method is that the model may behave badly for extrapolation.

Saleh proposed in [13] two rational functions to model the AM-AM and AM-PM effects of a travelling-wave tube amplifier (TWTA). This model is utilized in [14, 15, 16, 17]. The models are given out in Equation 2.9 and Equation 2.10:

$$A(r) = \frac{\alpha_a r}{1 + \beta_a r^2} \tag{2.9}$$

$$\Phi(r) = \frac{\alpha_\phi r^2}{1 + \beta_\phi r^2} \tag{2.10}$$

The application of this model needs to be careful because this model was developed primarily for TWTAs and it may not suitable for solid-state power amplifier (SSPA) modeling. As mentioned in [18], SSPAs have a more linear performance in the small-signal region (low power) than TWTAs in the saturation region (high power); the output power of the SSPAs tends to approach asymptotically a saturation value while TWTAs may present a "roll-over" effect.

Ghorbani [19] proposed a similar model and added two more fitting elements to remedy the limitation of the Saleh's model, as shown in Equation 2.11 and 2.12. Intuitively, the last item in the function should help compensating the "roll-over" effect.

$$A(r) = \frac{x_1 r^{x_2}}{1 + x_3 r^{x_2}} + x_4 r \tag{2.11}$$

$$\phi(r) = \frac{y_1 r^{y_2}}{1 + y_3 r^{y_2}} + y_4 r \tag{2.12}$$

Rapp [20] presented an AM-AM model that aims at SSPAs . In Equation 2.13, α is the saturation level at the output and β is the smoothing factor [18].

$$A(r) = \frac{r}{(1 + (\frac{|r|}{\alpha})^{2\beta})^{\frac{1}{2\beta}}} \tag{2.13}$$

White [18] compared the previous 3 mathematical models and proposed a new 4 parameter expression that aims at Ka-band SSPAs, as given out in Equation 2.14. Compared to the limitations in Rapp's model in reproducing the gradual transition between linear region and saturation region, the White's model uses an exponential term to describe this gradual transition and a Rayleigh term to linearize the typical operating of the Ka-band SSPAs.

$$A(r) = a(1 - e^{-br}) + cre^{-dr^2} \tag{2.14}$$

White also proposed an AM/PM model, given in Equation 2.15. However, this model is not good for this purpose, since it cannot represent the nonlinear progression of the phase changes with respect to the input amplitude.

$$\phi(r) = \begin{cases} f(1 - e^{-g(r-h)}), & r \geq h \\ 0, & r < h \end{cases} \tag{2.15}$$

The hyperbolic tangent function is also a very powerful nonlinear transformation for modeling the targeted curves. Since hyperbolic tangent function is bounded between -1 and 1, it can characterize the property that the output power from a amplifier is limited. A simple application of this function in amplifier modeling is shown in Equation 2.16 and Equation 2.17. The equation is the extension of the functions utilized in [21].

$$A(r) = a\tanh(b|r|) + c|r| \tag{2.16}$$

$$\Phi(r) = d + e|r|\tanh(|r|) \tag{2.17}$$

These modeling methods are used to model the AM-AM and AM-PM measurement results of a power amplifier sample shown in Figure 2.1 for performance comparison. This power amplifier is designed for 802.11a wireless local area network (WLAN) applications. Figure 2.7 illustrates the performance of different models on AM-AM prediction. The Ghorbani model's performance is not acceptable, as can be seen from the figure. All the other models can match the measured dataset (black) closely, except the early "roll-over" effect the Saleh model presents. However, when the input signal exceeds the measurement range, the performance of the extrapolation from different models is quite different. Polynomial model and White model increase significantly. Rapp model is kept flat, simulating the saturation level. And the Tanh model presents the decrement. Since the output power of a general power amplifier tends to drop to some extent when the input power hits the saturation region, the Tanh model and the Saleh model are more realistic. Among these two models, Tanh model has a better match for measurement dataset. Therefore, the Tanh model has the best performance among the six mathematical models for this example amplifier.

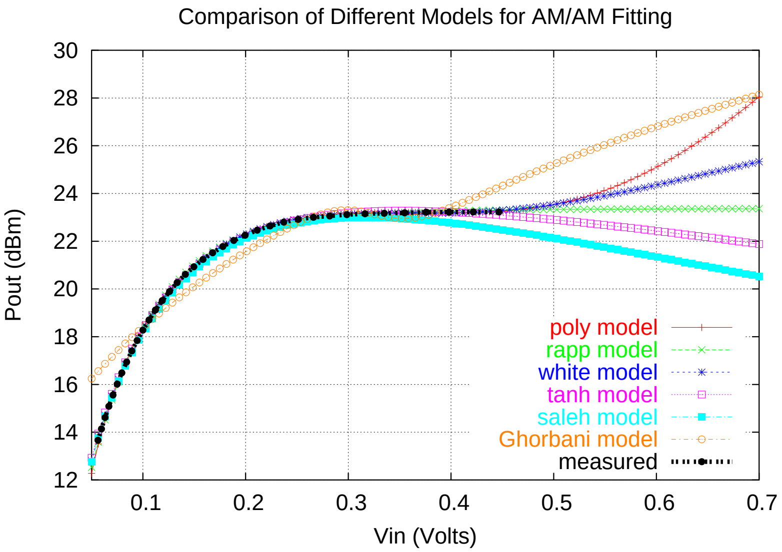

Figure 2.7 Comparison of different models for a power amplifier sample. This power amplifier is designed for 802.11a WLAN applications at 5.2 GHz.

Besides the mathematical models described above, several other models are also reported. Hischke et al. [22] applied third order spline function in amplifier modeling. Spline function is composed of multiple polynomials connected at specified break points. Compared to polynomial functions, it has more flexibility and is good at modeling sharp transitions. However, since most PAs have smooth transition characteristics, it is not a good option considering the added complexity.

O'Toole et al. [23] used neural network-Bessel transform to model the behavioral of a memoryless PA. The reported ACPR simulation result using wideband code division multiple access (WCDMA) signal shows 1 dB improvement over traditional behavioral models. Fourier-exponential series is also applied to model PAs' transfer characteristics to help design efficient predistorter [24].

Honkanen et al. [25] and [26] proposed a bipolar amplifier model that has a substantiated semi-physical basis. The transfer characteristic of the bipolar amplifier at low input power region is represented by an exponential function that takes into account the bias condition. The saturated region is modeled by Rapp's model to capture the smooth transition between the two regions. A cross-over factor is added to model the weak conduction of the transistors at very low input power levels. Usually this effect is concealed by noise floor and cannot be observed from gain compression measurement. Two-tone measurements are required to reveal it. The detailed model is listed in Equation 2.18

$$V_{out}(V_{in}) = \frac{\text{sign}(V_{in})V_{out}^{'}(|V_{in}|)}{(1+(\frac{V_{out}^{'}(|V_{in}|}{A_0})^{2p})^{\frac{1}{2p}}}(\tanh(|V_{in}|))^{\frac{1}{c}} \tag{2.18}$$

where $V_{out}^{'}(|V_{in}|)$ is:

$$V_{out}^{'}(|V_{in}|) = \begin{cases} e^{kV_b}(e^{kV_{in}}-1), & V_{in}+V_b \le V_{in,tr} \\ v(V_{in}+V_b)+b-e^{kV_b}+1, & V_{in}+V_b > V_{in,tr} \end{cases}$$

Good IM3 and IM5 simulation results are reported. The limitation of the model is that this method is based on the BJT physics and cannot be used for FET amplifiers due to the physical differences of the input/output transfer processes.

2.3.2 Memory effect modeling

The memory effect of a PA describes the input-output relationship in time-domain and can be observed in dynamic AM-AM and AM-PM curves. When inspected in frequency domain using two-tone measurements, it is shown in the IM asymmetry and IMD variation [27]. The memory effect is more significant in systems that have large signal bandwidth, e.g. WCDMA multi-carrier system and 802.11a WLAN system. Reasons for the memory effect include ([27], [28] and [29]):

- frequency response of the match networks,
- Non-constant impedance in DC bias circuits,
- nonlinear capacitances of the transistors,
- and self-heating effects

As an example of the memory effect, a Murata GaAs XM5060 power amplifier sample was measured at different carrier frequencies. Figure 2.8 and Figure 2.9 illustrate the variation of the gain and phase of the power amplifier at different frequencies [30] [31]. According to the figures, this amplifier has less distortion at the higher frequencies (higher P1dB and less AM-PM distortion) and a smaller gain compared to lower frequencies. Notice that the variation of the gain/phase may be different for different PAs, depending on the circuit design.

Based on the fact that the AM-AM and AM-PM curves are similar to each other, Poza [32] was able to simulate the frequency effect by scaling and shifting the gain

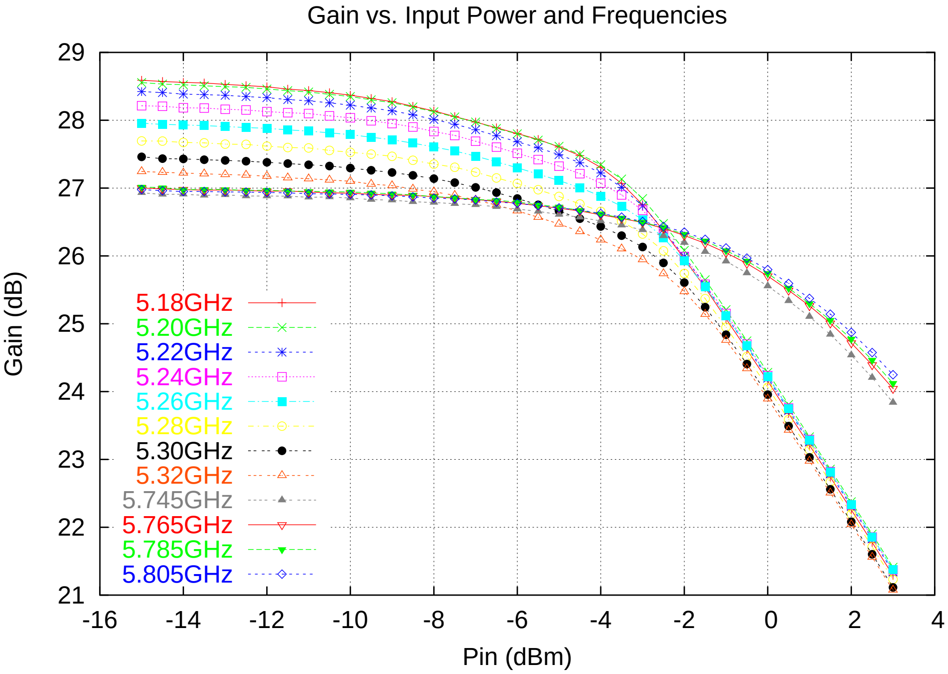

Figure 2.8 Measured AM-AM of a Murata XM5060 PA for 5GHz 802.11a WLAN applications.

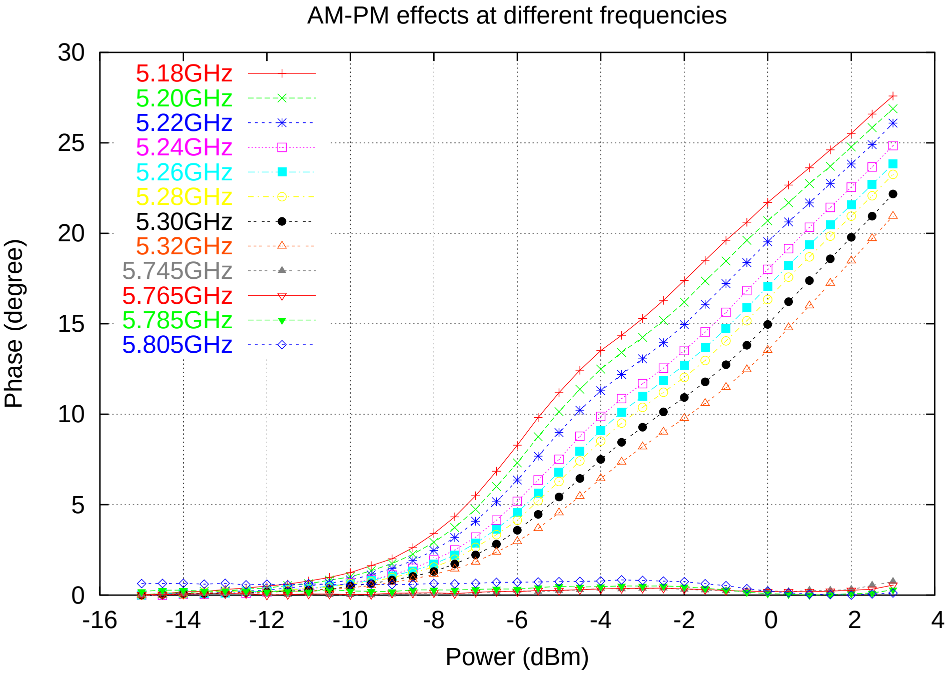

Figure 2.9 Measured AM-PM of a Murata XM5060 PA for 5GHz 802.11a WLAN applications.

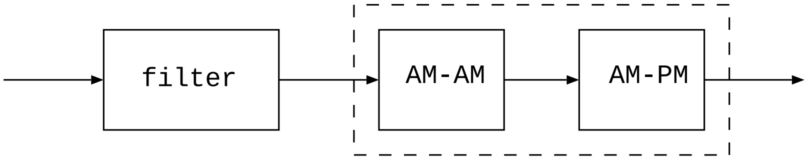

Figure 2.10 Two box model: nonlinear effect and memory effect are separated into two blocks [13].

curves. This is a straightforward approach and can be easily implemented. The downside is that the curves measured at different frequencies may not maintain their shape, which determines that this method is at best an approximation. Saleh extended his memoryless model [13] by finding the model parameters at any frequency and grouping them together to provide frequency dependency. The limitation of this method, similarly to Poza's model, lies in that the shape of the curves is determined by the rational functions and is not flexible for PAs with varying shapes of AM-AM and AM-PM curves. Elaborate fitting algorithms are needed for best fit.

The disadvantage of the previous methods is that they use one-tone measurement results, assuming the memory effect captured in this way is accurately enough. However, as pointed out in [33], when a wideband signal is passed through the system, the model cannot predict the interaction between the instantaneous tones. Another limitation is that the model cannot predict the variation in the AM-AM and AM-PM with varying tone spacings, which usually appears in two-tone measurement results.

To capture the dynamic properties of the gain and phase compression, several models have been proposed, e.g. [32, 13, 34, 35]. Generally, these models have a two-box or three-box structure, as shown in Figure 2.10 and Figure 2.11. The underlying assumption is that the nonlinear effect and the memory effect can be separated without losing accuracy.

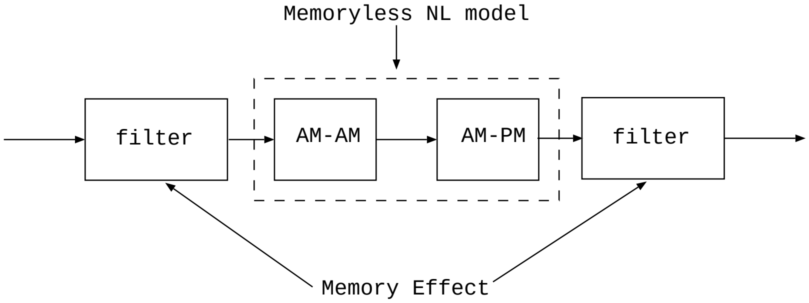

Figure 2.11 Three box model:two filter functions are used to model the memory effect [35].

Launay [34] applied moving average (MA) filter to address the problem, which is shown in Equation 2.19 and 2.20. One frequency is chosen as the reference and the coefficients of the nonlinear model is derived by fitting the model to the AM-AM and AM-PM measured results. At this frequency, the filter attenuation is unitary. Then the coefficients of the filter are estimated by solving Equation 2.21

$$G(\tilde{z}) = \sum a_n \tilde{z}^n \text{ (nonlinear model)} \tag{2.19}$$

$$H(f) = \sum_{k=0}^{P-1} a_k(V_e) e^{j2\pi kf/P} \text{ (filter model)} \tag{2.20}$$

$$\sum_{k=0}^{P-1} a_k(V_e) e^{j2\pi f_j T_e k} = \frac{V_e(f_{ref})}{V_e(f_j)} \tag{2.21}$$

f_j is the j^{th} frequency, T_e is the sampling period, and P is the size of the MA filter.

Similarly, a multi-tap polynomial model is proposed in [5] and [36]. This method characterizes the in-phase and quadrature components separately. A two-tap model shows the estimated ACPR error is within 0.7 dB [36]. In [37] the authors used a Wiener filter to model the small-signal memory effect and the Saleh model for nonlinearity. The Wiener filter used in this case basically is a convolution operation on the input signal. Optimal memory length (taps of the Wiener filter) can be found to obtain the minimum mean-square error (MSE).

To observe the PAs' performance in a realistic situation, digitally modulated signals and multi-sine signals are used in PA measurements and characterization, such as the work reported in [38], [39], and [40]. Auto-regression moving average (ARMA) models are derived from these measurements, which can be generalized in Equation 2.22:

$$A(q)y(t) = q^{n_k}\frac{B(q)}{C(q)}u(t) + \frac{D(q)}{F(q)}e(t) \tag{2.22}$$

where u and y are input/output signals; A, B, C, D, F are polynomial functions; q is the delay operator. The model fit reported in [38] is within the order of 96%. [39] also points out that different modulated stimulus may result in different order of memory length. For example, 11th order nonlinear ARMA model is sufficient for binary phase shift keying (BPSK) modulation, while 23rd order is required for minimum shift keying (MSK) to obtain similar accuracy.

In [35, 33] the authors gave a detail description and analysis of the two-tone measurement procedure utilized for PA modeling. A three-box model was developed based on the obtained dataset. Generally speaking, this model can be treated as an improved version of Poza and Saleh model.

Carvalho and Pedro [41] studied the origin for the asymmetric IMD performance observed in power amplifiers. A describing function combined with small-signal model was used to model the large-signal IMD performance. Ku et al [42] emphasized on the effect of the frequency spacing of the input tones on the IMD performance. A two-dimensional transfer function (frequency tone spacing and input signal power level) was developed to characterize the long time constant memory effects. A par-

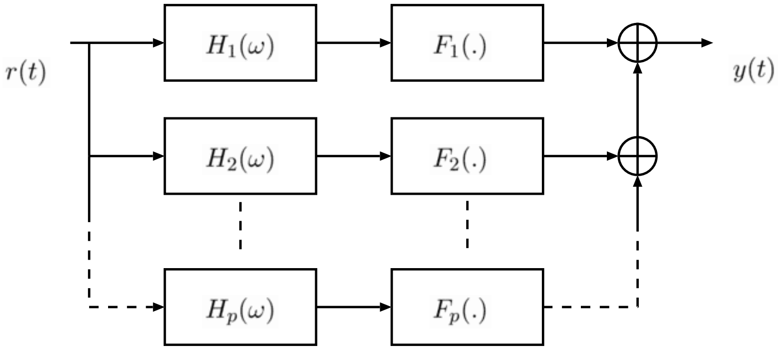

Figure 2.12 Illustration of the parallel wiener model [42].

allel Wiener model was created based on the frequency dependent transfer function. Figure 2.12 illustrates the model structure.

Maziere [43] constructed a new memory model by characterizing the relationship between the input and output envelope information. The model was based on the nonlinear differential equation shown in Equation 2.23. Only first order approximation was used in the paper.

$$\tilde{y}(t) = f_{NL}(\tilde{x}(t), \frac{d\tilde{x}(t)}{dt}, \frac{d^2\tilde{x}(t)}{d^2t}, \cdots, \frac{d^n\tilde{x}(t)}{d^nt}) \tag{2.23}$$

It turns out that the first time derivative of the input signal x(t) is the "key parameter for the characterization of the nonlinear slow dynamics, including group delay, thermal dependence and spurious modulation of bias point" [43]. Through the time derivative, the previous samples are taken into account in the model, thus capturing the "memory" effects. This approach is quite similar to the time domain state-space modeling technique reported in [44] and [45], in which nonlinear ordinary differential equations are formalized to describe the relationship between the terminal currents and voltages.

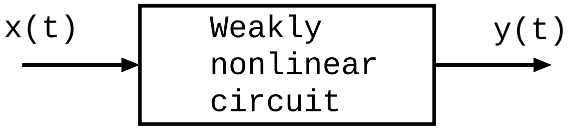

Figure 2.13 Illustration of the Volterra-series based nonlinear model.

The memory models introduced above characterize the frequency-dependent properties of PAs using linear filter(s) and separate it from the memoryless nonlinear part. Volterra-series based models, on the other hand, take a different route and treat the memory and memoryless properties together [46], as shown in Figure 2.13.

The basic form of the Volterra series is :

$$y(t) = \sum_{n=0}^{\infty} H_n[x(t)] \tag{2.24}$$

where

$$H_n[x(t)] = \int_{-\infty}^{\infty} \cdots \int_{-\infty}^{\infty} h_n(\tau_1, \tau_2, \cdots, \tau_n) x(t-\tau_1) x(t-\tau_2) \cdots x(t-\tau_n) d\tau_1 d\tau_2 \cdots d\tau_n \tag{2.25}$$

$h_n(\tau_1, \tau_2, \cdots, \tau_n)$ is so called n^{th} order Volterra kernel. This can be considered as an n^{th}-order impulse response [2]. Its corresponding Fourier transform is given by:

$$H_n(\omega_1, \omega_2, \cdots, \omega_n) = \int_{-\infty}^{\infty} \cdots \int_{-\infty}^{\infty} h_n(\tau_1, \tau_2, \cdots, \tau_n) e^{-j(\omega_1\tau_1 + \omega_2\tau_2 + \cdots + \omega_n\tau_n)} d\tau_1 d\tau_2 \cdots d\tau_n \tag{2.26}$$

Therefore, Volterra-series PA modeling is to find the n^{th} order kernel In fact, the 1st order kernel can be considered as the linear gain of the PA, while the 3rd, 5th order kernels describe the corresponding IM products. Thus, the output signal is simply a summation of all the contributing items. Since the nth kernel has time constants, if modeled properly, it can represent the memory effects. The limitation of the Volterra series modeling technique is that it is only suitable for weakly nonlinear devices. When used to describe the hard nonlinear performances, it will require very high order model which makes the kernel determination process difficult and tedious.

Large-signal scattering function model has been proposed [47, 48, 49]. The basic idea is to extend the small-signal S-parameter concept into nonlinear region through nonlinear describing functions. Elaborate measurement systems were developed to test power amplifier or devices and extract the model. In Chapter 4, this concept will be studied in detail.

Besides all the modeling methods reviewed above, there are still several other techniques, such as dynamic neural network and nonlinear time series that approach the problem from the time domain, and describing function in frequency domain, as summarized in [1] and [3].

2.4 Proposed research topics

In last section, current state of art memoryless and memory modeling techniques have been reviewed. Although with all the advances in this area, still there are some questions that haven't been answered correctly.

Generally, a behavioral model will be used in a simulation schematic with preceding and following blocks (e.g. input or output matching networks) to predict the system performance. Therefore, it is vital for the behavioral model to be able to detect automatically the source and load impedances and adjust its response accordingly.

It has been widely acknowledged that the performance of power amplifiers is significantly affected by the source and load impedances they are embedded in. This effect is called source-pulling or load-pulling. There are special measurement setups that are dedicated to capture these effects, such as the loadpull measurement systems provided by Maury Microwave [50] and Focus Microwave [51].

However, most of the behavioral models discussed so far don't provide this capability (except the large-signal scattering function models and the models having small-signal S-parameter blocks). In most cases, the load effects on the nonlinearities are not studied or not emphasized.

Therefore, how can we create a nonlinear behavioral model that can address the limitation mentioned above? What measurements should be taken for creating such a behavioral model? These are the main questions this dissertation will try to answer in the following chapters.

2.5 Conclusion

In this chapter, an extensive literature review has been presented on the current research status of behavioral modeling for power amplifiers / devices. Modeling techniques covered include mathematical memoryless models, filter-based two-box and three-box memory models, Volterra series based memory models and large-signal scattering function models. Two research topics have been proposed that are aimed to solve two aspects of the limitations of current modeling techniques.

The first research topic is on behavioral modeling of load-related nonlinearities of power amplifiers based on loadpull measurements. The second topic is on integration of memory effect modeling with the loadpull behavioral model to predict the memory effect under various load conditions. The ultimate goal is to develop a behavioral modeling technique or procedure that can easily generate behavioral models for power amplifiers or device that are based on loadpull measurements for system simulations and are ready for practical non-50 ohm applications.

CHAPTER 3

ADVANCED LOADPULL MEASUREMENTS

3.1 Introduction

Loadpull measurement has been widely used in characterization of devices and components. It provides valuable insight about the device performance under different source / load conditions and different power levels. This is very important information for power amplifier designers. Traditional loadpull measurements include one-tone and two-tone measurements, generating measured datasets for gain compression, 3rd intercept point (IP3), power added efficiency (PAE) and adjacent channel power ratio (ACPR). A thermal imaging loadpull measurement has also been described in [52].

However, with the advanced development in the baseband algorithms as well as the more and more complex modulation techniques, the traditional metrics like P1dB and IP3 obtained through one-tone or two-tone stimuli cannot predict the system performance completely, because:

- the nonlinear phase performance is not characterized properly;
- the testing signals don't reflect the realistic complex modulated RF signals. The performance of a transistor is closely related to the stimulus signal [53].

Two loadpull measurement procedures are developed to address these two limitations. Both measurement procedures are based on the Automated Test System (ATS) from Maury Microwave. Section 3.2 presents an AM-PM loadpull measurement procedure developed using the Agilent's 8719D vector network analyzer. Although the

AM-PM loadpull measurement procedure is available through some commercial measurement systems (e.g, Maury's ATS system), it is not as a routine procedure as the gain compression measurement is. Therefore, in Section 3.2, the detail analysis and instruction are given on how to make this measurement. Example measurement results are given out for an Maxim 2373 low noise amplifier sample and a Fujitsu L-band GaAs FET power device sample.

Section 3.3 presents a digital demodulation loadpull measurement procedure based on the Agilent 89610 vector signal analyzer (VSA). This new measurement procedure provides the hardware designers the capability to study the system performance (such as error vector magnitude (EVM)) directly in loadpull measurement. Example measurement results are given for Intersil 3984 power amplifier and Fujitsu L-band GaAs LDMOS device. Part of the results has been documented in [54].

3.2 AM-PM loadpull measurement procedure

3.2.1 Introduction

High spectral efficiency and data rate can be achieved through advanced digital modulation techniques like 16 Quadrature amplitude modulation (QAM) or 64 QAM, which apply both amplitude and phase modulation. The nonlinear amplitude (AM-AM) and phase (AM-PM) compression of an amplifier, therefore, deteriorates the modulation quality. For example, Park reports the simulated AM-AM and AM-PM effects on ACPR with respect to the power back-off consideration [55]. These two nonlinear effects have been studied extensively and accurately modelled in 50 ohm condition, e.g. [13] [18] and [19].

The loadpull AM-AM measurements have been widely applied to evaluate the performance of power amplifiers and devices [56], [57]. However, the AM-PM performance under loadpull conditions hasn't been given enough attention so far. Part of the reason is that the phase compression doesn't deteriorate legacy system performance significantly as gain compression does. Also the modulation techniques used were not very complex. This phase compression cannot be ignored anymore for modern complex modulation techniques, which apply closer phase distance between symbol points.

Therefore, in this study a measurement procedure is developed to characterize the load impedance's effects on the phase compression of the nonlinear amplifier. The developed AM-PM loadpull measurement procedure is based on the Agilent 8719D VNA and the Maury Automated Test System (ATS).

3.2.2 Introduction of a typical VNA structure and processing steps

Before starting the discussion of the developed measurement system, let's review the system structure and the data processing steps of a typical VNA. This review will help understand how the measurement procedure is designed. Figure 3.1 shows the system diagram of the Agilent 8719D VNA [58]. Although only the 8719D VNA is discussed in this paper, a similar procedure can be developed for other kinds of VNAs, as well.

A typical VNA is composed of four parts: the synthesized source, test set, vector receivers and display device [58]. A phase lock loop (PLL) circuit is used to synchronize the source and the receivers to make the S-parameter ratio measurements. The test set is used to separate the signal into R, A and B channels. A/R represents the S_{11} or S_{22} reflection coefficient measurement, while B/R for the S_{21} or S_{12} transmission measurement.

Figure 3.2 illustrates the data processing algorithm used in the 8719D VNA. The sampled signal is first converted to digital signal through the ADC and filtered. If

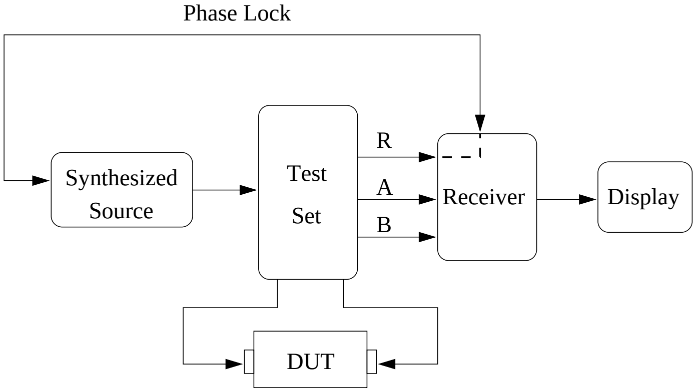

Figure 3.1 System diagram of HP8719D.

ratio measurements are desired, like S_{11}, the RATIO calculation will be performed on the sampled signals; otherwise the input signal will be kept constant and passed to the next stage. After an averaging process, the data is stored in a “RAW” array for further correction using the calibration error arrays obtained through the calibration process. Then the corrected data arrays will be formatted in the desired format and displayed on the screen.

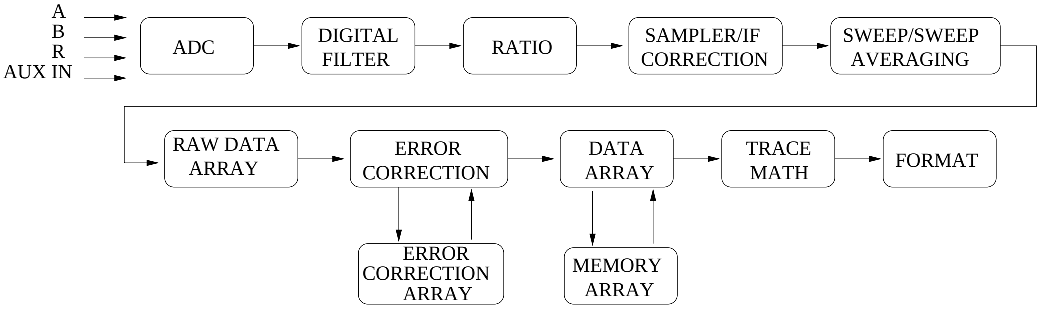

Figure 3.2 Data processing flow diagram of the HP8719D VNA.

3.2.3 AM-PM measurement through vector receiver setup

To measure AM-PM, one can either measure the swept power S_{21} or use the VNA as a vector receiver and measure the absolute vector value of the B2. For the first method, the input power level is swept and the S_{21} is collected at each power level.

The compression property can be derived by setting the S_{21} obtained at the lowest input power level as the reference and comparing the other S_{21} values to it. By comparing the amplitude of the S_{21}s, one gets the AM-AM; comparing the phase, one gets the AM-PM measurements.

The advantage of the power swept S_{21} method is that the procedure is built-in and the measurement is straightforward. The data processing is also convenient. However, this method is not flexible because it is bundled to the internal source. If it is used together with other instruments in a loadpull measurement, the integration will be troublesome since extra switches may be required.

The vector receiver method can overcome these shortcomings. By inspecting the data processing steps given out above, one notices that VNAs configured as a vector receiver perform the absolute vector measurements of the incoming signals to A/B/R ports. The sampled incoming signal is a complex value. If the input power sweeps, the measured result will be an array of complex values. The AM-PM information is contained in this RAW data array, in fact. Instead of going through all the ratio and correction processing, the RAW data array can be used directly to get the results.

As for the calibration consideration, the magnitude of the result can be corrected through receiver calibration procedure to remove the possible distortion caused by the system hardware. The phase can be calibrated in similar way as well.

There are some extra hardware setup steps required. The VNA needs to be synchronized with the external synthesizer. It needs to know which port (vector receiver) the incoming signal is sent to. The frequency of the incoming signal cannot be swept, otherwise the synchronization will be lost.

A custom 8719D VNA driver was developed to support extraction and analysis of the RAW data arrays. The measurement system diagram is shown in Figure 3.3. The incident signal is coupled to the R IN port while the reflected and transmitted signals are sampled through the input and output couplers. The sampled signal at Port 2 is stored in RAW data array. The AM-PM information can be extracted from the RAW data array by comparing the phase of the complex data array to the first value in the array (corresponding to small-signal phase).

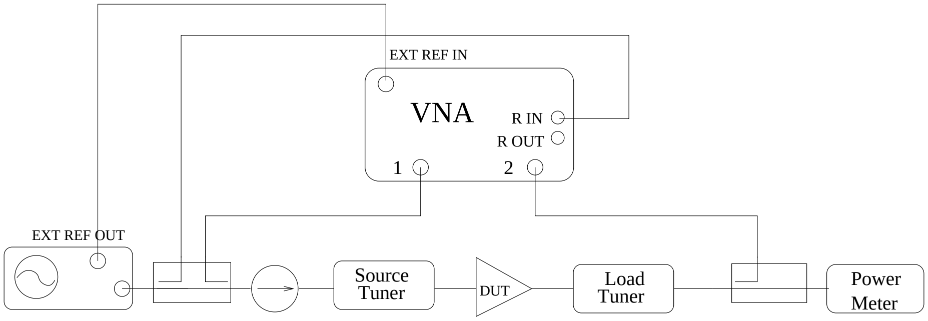

Figure 3.3 AM-PM loadpull measurement system diagram.

The extra setup steps regarding to the 8719D VNA are given below for the purpose of completeness. The sequence of the panel buttons to be pressed is given out for each step.

- System - Instrument Mode - Tuned Receiver (set the VNA in vector receiver mode);
- Menu - CW Freq - set the CW frequency of interest;
- Meas - Input Ports - B (channel B is used to sample the signal);
- Meas - Testport - 2 (test port 2 is selected as the sampling port).

3.2.4 Example AM-PM results

Two DUTs were measured using this developed AM-PM loadpull system. One device is a Maxim 2373 low noise amplifier (LNA) sample; the other is an FLL120MK high power GaAs FET sample from Fujitsu. First of all, the validity of the developed system should be checked against the VNA. Figure 3.4 shows the comparison of the measured AM-PM and AM-AM datasets for the LNA sample under 50 ohm condition from the two methods. Obviously, the result obtained using the loadpull system presents good agreement with the HP8719D result at small signal levels. The discrepancy at the high power levels is because of the significant harmonic signals generated.

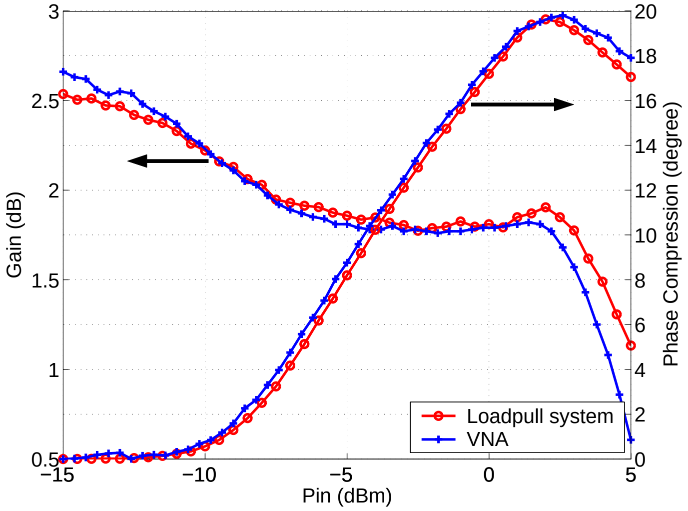

Figure 3.4 Comparison of measured AM-AM and AM-PM results from the VNA and the loadpull system for the LNA sample at 900 MHz .

Figure 3.5 presents an example AM-PM loadpull measurement result. The AM-PM compression is measured at six load impedances. For different load impedances, the characteristics of the gain compression and the phase compression change dramatically. At load points that cause high gain compression, the phase compression is also significantly different from the mild compressed cases.

Similar observation can be made from the measured results for the GaAs FET device sample at 2.14 GHz. As shown in Figure 3.6, at load points where the device shows lower gain compression, it also has smooth AM-PM curves. On the other hand, load points associated with high gain compression cause significant phase compression

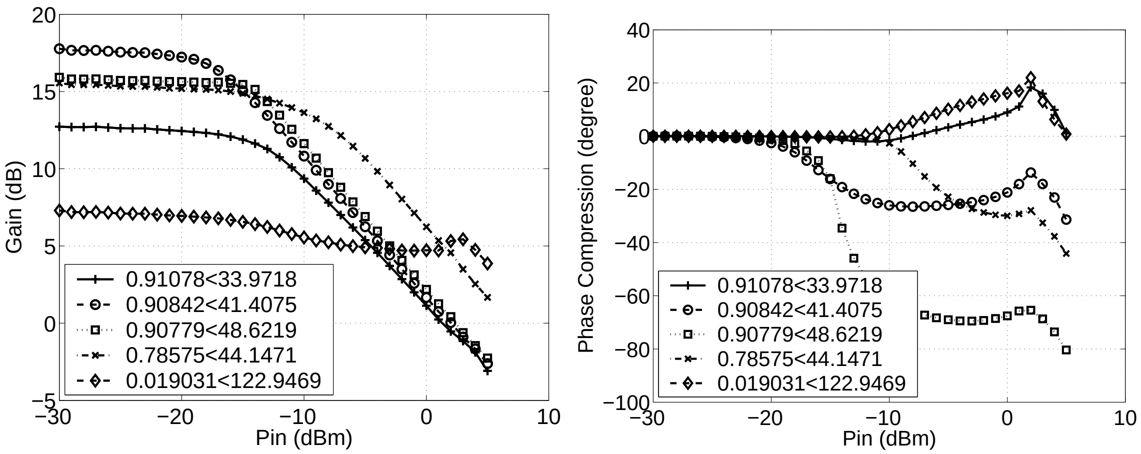

Figure 3.5 AM-AM and AM-PM loadpull measurement results at 900 MHz for the LNA sample.

even at low power levels. Since conjugate load causes higher gain, it suggests that the AM-PM compression will be high near the conjugate load area on the smith chart.

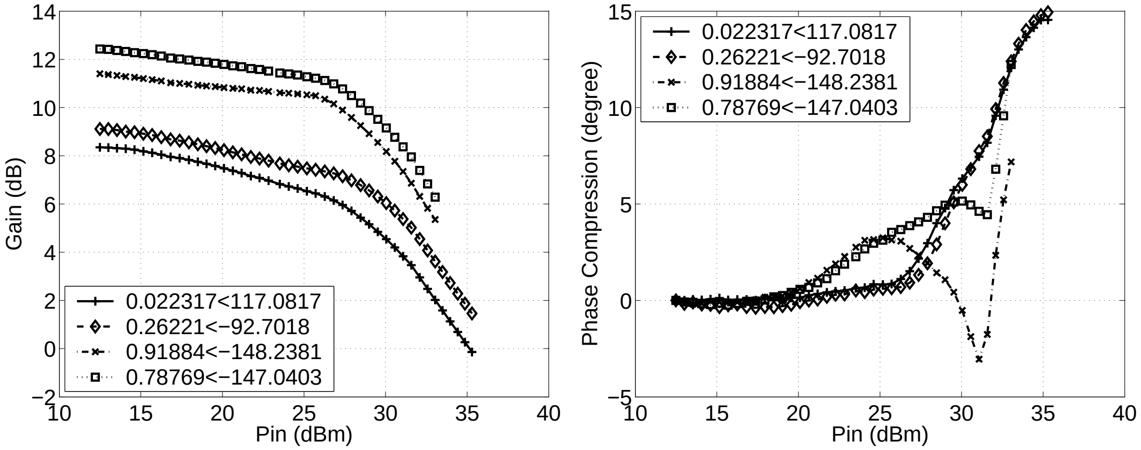

Figure 3.6 AM-AM and AM-PM loadpull measurement results at 2.14 GHz for the high power GaAs FET sample.

From the modeling viewpoint, this additional information suggests that the nonlinear model for amplifiers should be able to adjust its gain and phase compression properties with respect to different load conditions.

3.3 Digital Demodulation loadpull measurement procedure

In this section, we introduce an innovative digital demodulation loadpull measurement procedure that directly characterizes system performance of a power transistor (or amplifier) under various test conditions, together with the traditional nonlinear metrics, e.g. gain compression and intermodulation distortion (IMD). The key parameter under study in this section is the error vector magnitude (EVM).

3.3.1 Definition and measurement of EVM

EVM is a metric that quantifies the quality of digital modulated signals. It is defined as the magnitude of the phasor differences between an ideal reference signal and the measured transmitted signal after it has been compensated in timing, amplitude, frequency, phase and dc offset [59]. It can be computed (3.1):

$$EVM_{RMS} = \sqrt{\frac{\sum_{i=1}^{N} |S_{ideal}(i) - S_{meas}(i))|^2}{\sum_{i=1}^{N} |S_{ideal}(i)|^2}} \tag{3.1}$$

where $S_{ideal}(i)$ and $S_{meas}(i)$ are the i^{th} normalized ideal complex reference constellation point and the measured symbol respectively [60]. Because it changes continuously during every symbol transition, EVM is defined as the root-mean-square (RMS) value of the error vector over time.

Some studies have already been reported to successfully predict the EVM based on one-tone [61] [62] [63] or two-tone distortion [64] of power amplifiers. However, most of the work deals either with a matched 50 ohm condition or provides only the simulation results with respect to the load tuning. This new measurement procedure, as demonstrated in the following sections, provides a much more realistic and complete view of the performance of the DUT, including measurement validation of both power and source/load impacts.

Before proceeding to the discussion of the EVM loadpull measurement, let's review how a typical EVM measurement is done. Fig. 3.7 illustrates the measurement diagram [65]. The input RF signal is first down-converted to the low intermediate frequency (IF) so that the ADC can sample it adequately and down-convert it to baseband for further processing. The LO is not directly phase-locked to the incoming signal (unlike the VNA ratio measurement), therefore, it will introduce some frequency offset. The frequency offset will be translated into a phase rotation in the time domain and can be estimated and compensated through a digital processing algorithm. In fact, frequency offset is one of the measurement capabilities of a VSA.

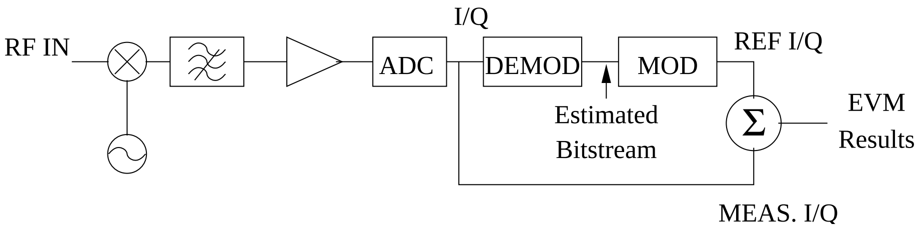

Figure 3.7 EVM measurement diagram.

Based on the sampled data stream, the ideal constellation points are recovered by first demodulating the incoming stream and then re-modulating the obtained digits. The RMS EVM is computed through averaging all the frames used in the measurement. To make the RMS EVM accurate, a large number of frames are required, e.g. 802.11a WLAN specification [66] requires at least 20 frames.

3.3.2 Measurement system and calibration consideration

The EVM loadpull measurement system is developed based on the Automatic Tuner System (ATS) from Maury Microwave and the 89610A Vector Signal Analyzer (VSA) from Agilent Technologies. Fig. 3.8 shows the integrated system setup. The ATS controls all the instruments in the measurement system and coordinates the measurement procedure. The digital demodulation measurement is performed by the VSA. An in-house program is developed to access the VSA measurement results through the common object model (COM) API interface. The program can automatically adjust the input range setup for the VSA so that the input signal can be sampled and evaluated at proper levels to obtain the optimal measurement results. The RMS EVM is averaged over several readings and then collected by the program and ported to ATS for contour analysis.

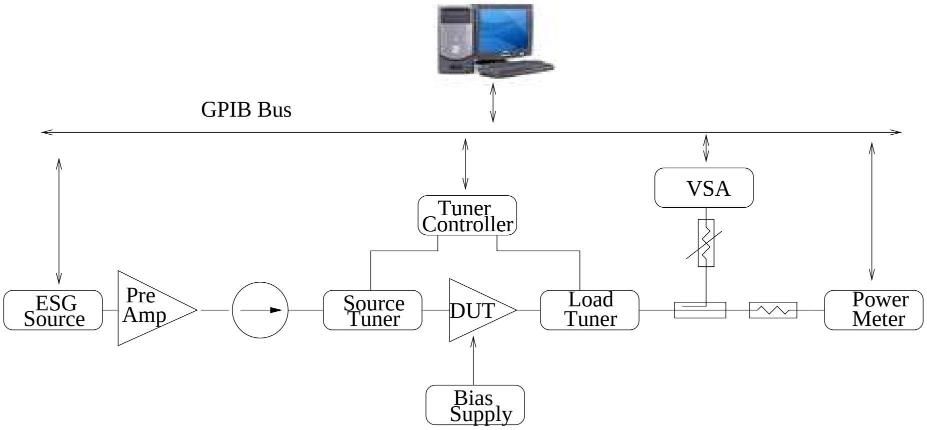

Figure 3.8 Illustration of the digital demodulation loadpull measurement system.

As the digitally modulated RF signal passes through the measurement system, some errors will be introduced, mainly due to the distortion effects of the driver amplifier preceding the DUT and the down-converter. The distortion of the down-converter can be minimized by adjusting the step attenuator. However, the distortion caused by the driver amplifier is difficult to separate. The system EVM (acting as the EVM noise floor for the measurement system) should be evaluated before performing further measurements to make sure the driver amplifier is linear enough.

This can be done by plugging a THRU between the source and load tuners and measuring the EVM associated with the THRU. A flat EVM curve across the power range of interest indicates a linear system. Otherwise, additional care should be taken regard to measured results close to the EVM noise floor indicated by the thru measurement.

Fig. 3.9 compares the system EVM and that associated with the DUT. Obviously from this figure, we can tell that the system presents significant nonlinearities due to the driver amplifier. The distortion of the driver amplifier dominates at the low and mid power range until the nonlinear power amplifier starts dominating.

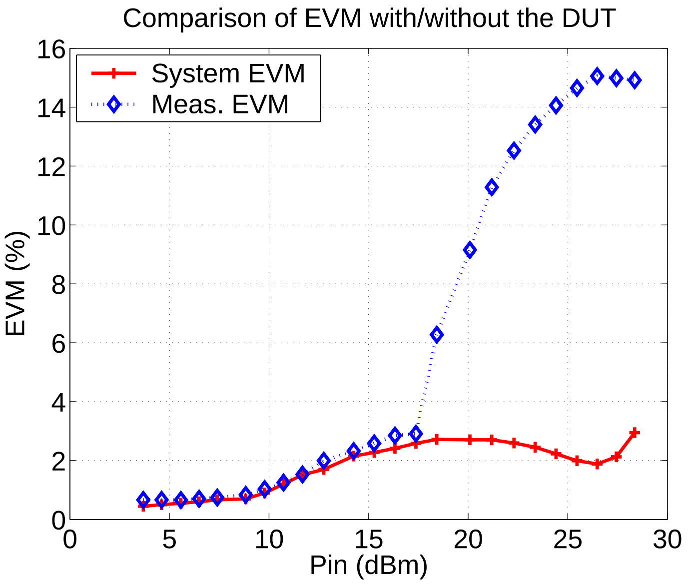

Figure 3.9 Comparison of the system EVM and measured EVM of the DUT.

Fig. 3.10 demonstrates similar phenomenon for the ACPR measurements. As can be seen, the ACPR appeared at low input power levels (up to 17dBm) is mainly the contribution of the the nonlinear driver amplifier.

Fig. 3.11 compares the measurement system EVM and the DUT EVM for a low power amplifier. In this measurement setup, there is no requirement for a driver amplifier. Therefore, the system shows little distortion; the system EVM is quite flat

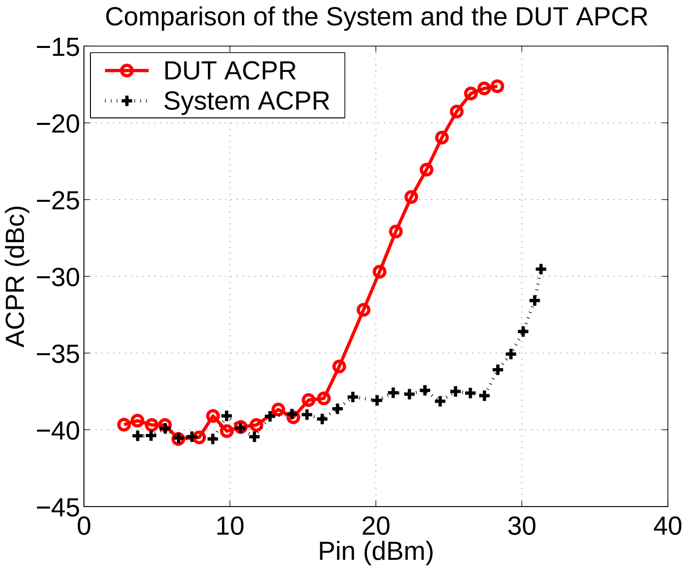

Figure 3.10 Comparison of the system ACPR and measured ACPR of the DUT.

across the whole power range. This result again emphasizes the importance of linear driver amplifier for accurate EVM measurements.

3.3.3 Example loadpull EVM measurement results

In this section, the loadpull EVM measurement datasets for two devices are demonstrated. The first device under study is a high power GaAs FET sample from Fujitsu. The typical output power at 1dB compression point is 40 dBm with a gain of 10 dB. The PAE is around 40% [67]. The load related gain and phase compression properties have been shown in Fig. 3.6.

The FET was studied at 2.14 GHz using an OFDM modulated signal to explore its capability to handle multi-carrier signals which have high peak-to-average power ratio (PAPR). High PAPR signals pose high requirements on the linearity of power amplifiers.

Fig. 3.12 compares the transducer gain (GT) and EVM performance in an example sourcepull measurement. The load is set at conjugate match and the input power is

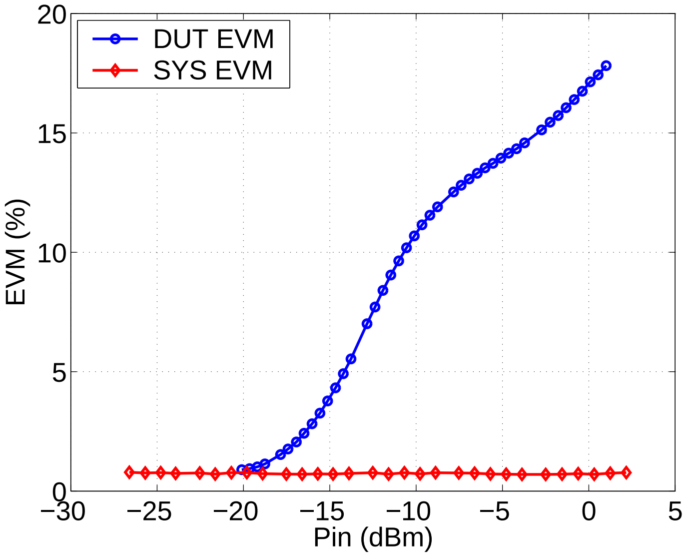

Figure 3.11 Comparison of the system and DUT EVM .

set at 22 dBm. Similar comparison is shown in Fig. 3.13 for a loadpull measurement. In both case, the test signal was a 64 carrier OFDM modulated signal.

Typically, the goal of the source tuning is to get the best gain out of the DUT, while the load tuning optimizes the total output power. If a multi-carrier signal passes through the DUT with high gain, the chance is much higher for the peaks of the signal getting distorted due to the limited power handling capability of the DUT.

On the other hand, by tuning the load to obtain the maximum output power, the signal is allowed to swing to the largest extent possible, which provides the best signal fidelity. Therefore, we might expect the EVM performance to degrade when the source impedance approaches the conjugate match, and better EVM performance for load impedance optimizing the output power. This point is demonstrated in Fig. 3.12 and Fig. 3.13.

Fig. 3.14 presents a better illustration of the source/load influence. Shown in the figure are two EVM surfaces.The lower surface is for the source pulling measurement. Comparing to Fig.3.12 and Fig. 3.13, one can see that the EVM degrades significantly

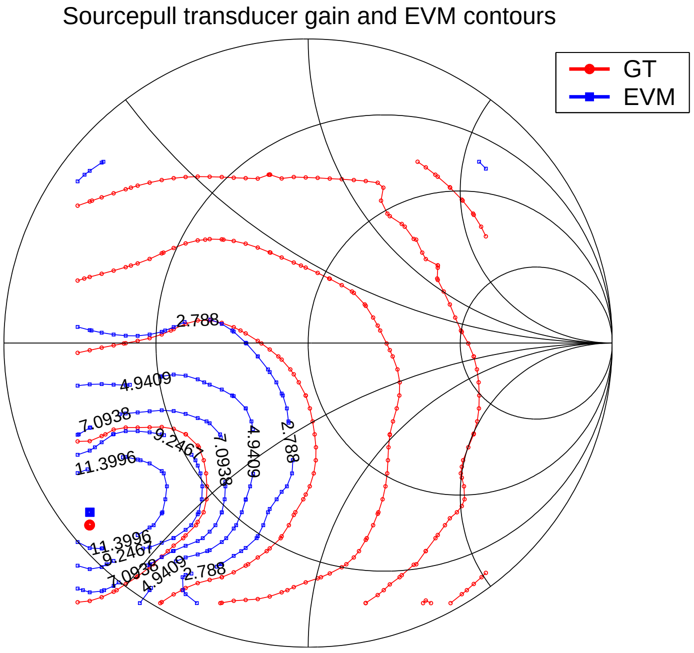

Figure 3.12 Transducer gain and EVM contours for example sourcepull measurement. The Γ_L is -0.72827-j*0.40883. The optimal Γ_S for the GT is -0.67904-j*0.60152. The maximum GT is 10.75 dB. The maximum EVM (13.75%) appears at Γ_S of -0.68003-j*0.58930.

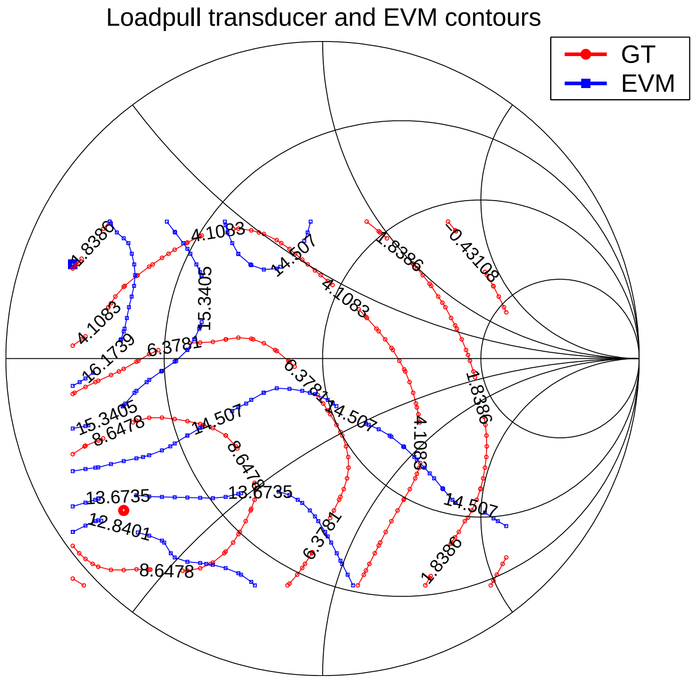

Figure 3.13 Transducer gain and EVM contours for example loadpull measurement. The Γ_S is -0.67904-j*0.60152. The optimal Γ_L for the GT is -0.72827-j*0.40883. The maximum GT is 10.87 dB. The maximum EVM (16.86%) appears at Γ_L of -0.7890+j*0.2966.

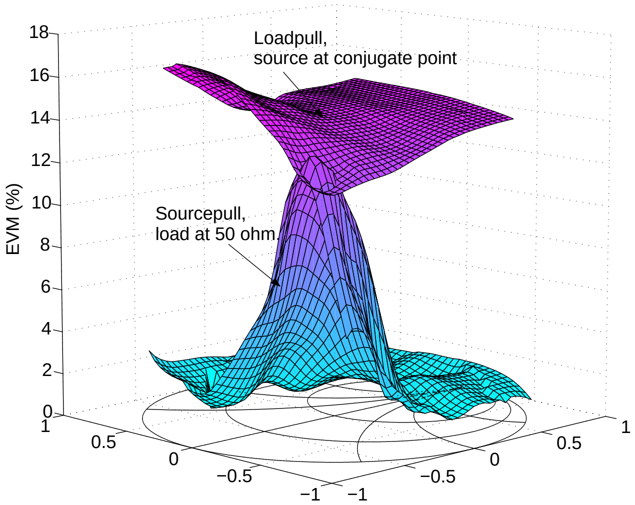

Figure 3.14 Sourcepull / loadpull EVM measurements; Pin is set at 22 dBm.

around the high gain region on the source Smith chart.The EVM load contour is relatively smoother. This might be not a perfect way to evaluate the source or load-pull effect on the EVM or other parameters. A better way is to evaluate these parameters under constant output power levels.

Fig. 3.15 shows an load tuning example to obtain the improved EVM. Two sets of swept power EVM measurements are compared. In one case, the load is tuned to obtain the optimum GT, while in the other case, the load is tuned for better EVM. The source is kept at conjugate matching point. The tuned EVM is about 2.5-3.5% better than the former case, with 0.5 dB loss of gain.

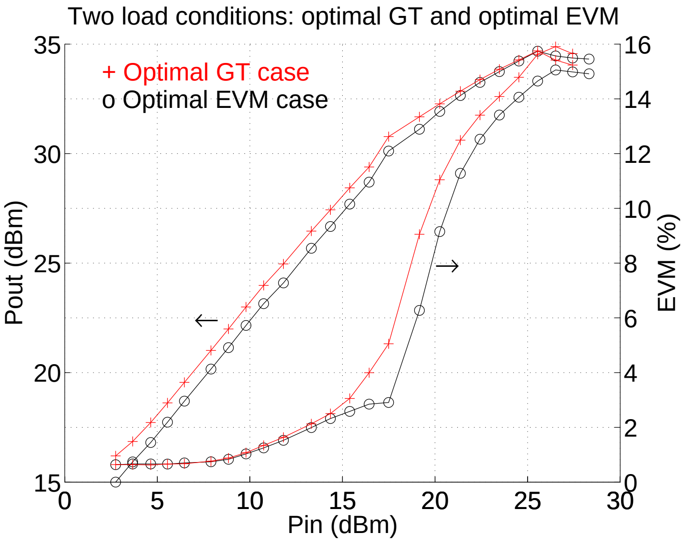

Figure 3.15 Improvement of the EVM performance by tuning the load.

The second device studied is an Intersil 3984 WLAN power amplifier sample. Traditional one-tone and two-tone loadpull measurements are performed first, followed by the EVM loadpull measurements. The power amplifier is studied at 2.45 GHz.

Figure 3.16 compares the transducer gain contours with the EVM contours at constant output power levels. The output power is 15 dBm in (a) and 18 dBm in (b). Similarity can be found for this two contours. Notice that the optimal load impedances for these two merits are different, which means tradeoffs can be made based on different application requirements.

The ACPR contours and the EVM contours are compared in Figure 3.17. Both measurements were obtained using the 54 Mbps OFDM modulated signal. The measurement results demonstrate the close relationship between the two figure-of-merits. The optimal load impedances for these two merits are very close to each other in both cases.

Similarly, the IP3 and the EVM contours are compared in Figure 3.18. At low output power level (a), the optimal load impedances for the IP3 and EVM are very close; for high output power level (b), the difference become significant. Therefore, instead of resorting to the IP3, engineers can optimize their designs against the EVM performance, which will provide better correlation between the simulation results and the system performance of the final products.

3.4 Conclusion

In this chapter, two loadpull measurements are presented. An AM-PM loadpull measurement system is introduced which is based on Agilent 8719D and Maury ATS system. It is shown that the load impedances affect the AM-PM characteristic significantly. The example measurements suggest loads that are close to conjugate load impedance will cause higher AM-PM compression and the characteristics will be much different from other cases. Modeling engineers need to be aware of this fact and take the load into account.

A newly developed digital demodulation loadpull measurement procedure is described thereafter. The evaluation of the system linearity is discussed. The importance of the driver amplifier is emphasized. Example measurement results are given, demonstrating the possible tradeoffs between the traditional figure-of-merits and the

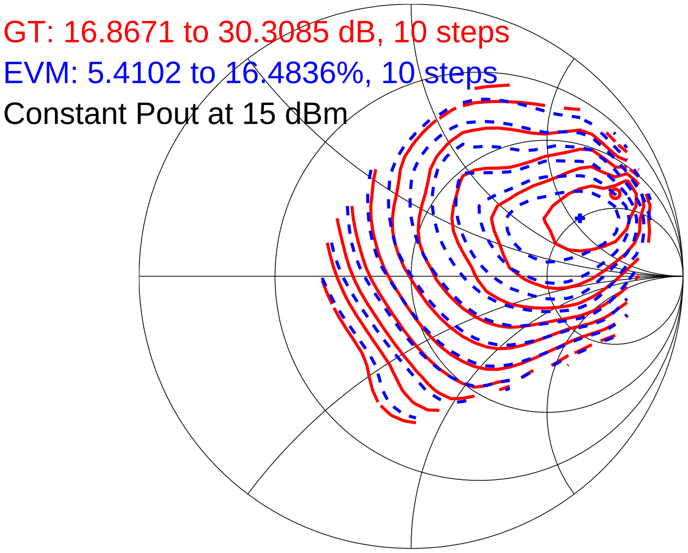

(a)

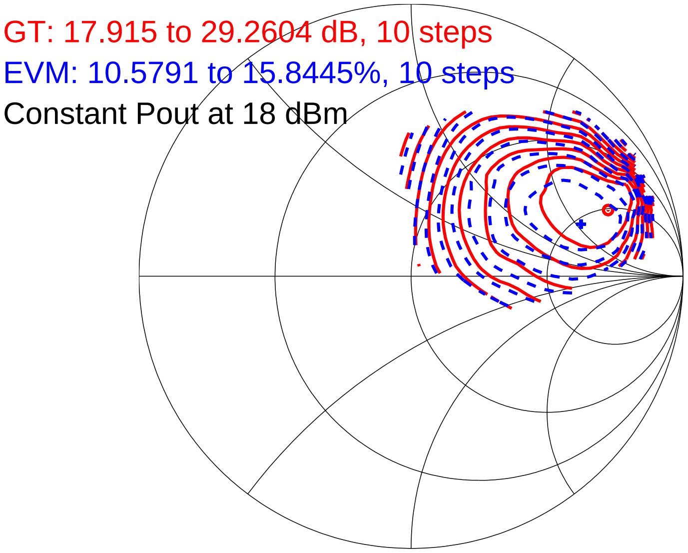

(b)

Figure 3.16 Comparison of the GT and EVM contours at constant output power level of 15 and 18 dBm.

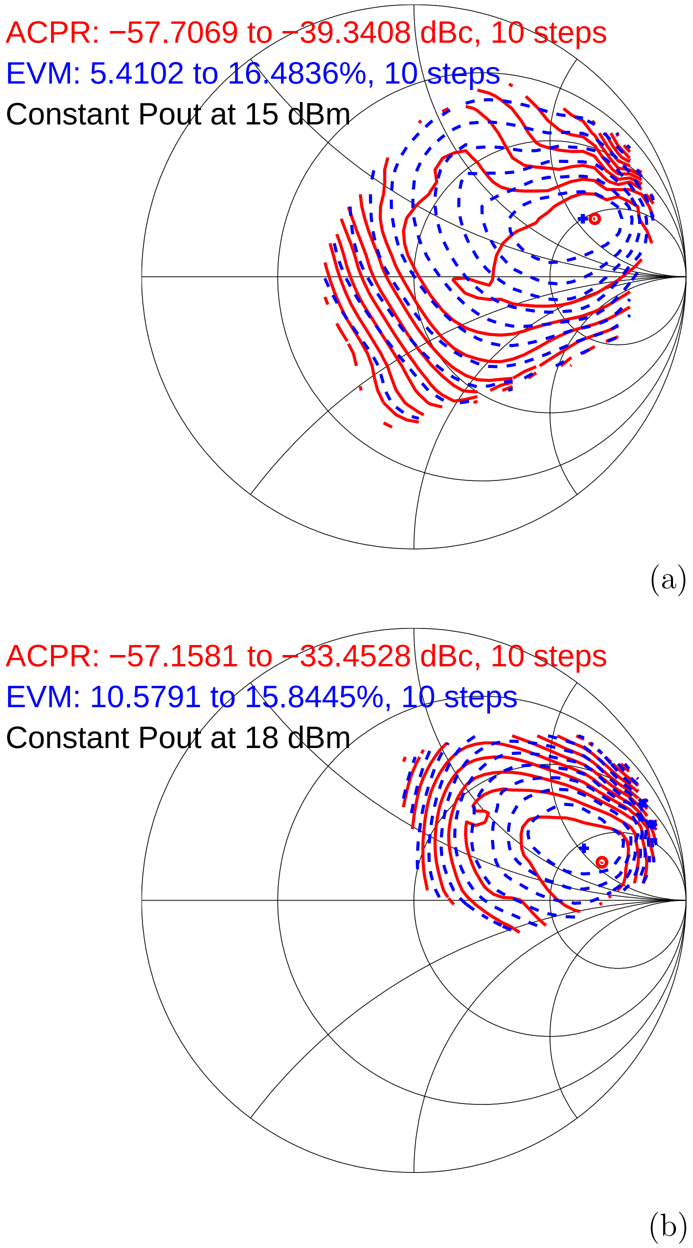

Figure 3.17 Comparison of the ACPR and EVM contours at constant output power level of 15 dBm and 18 dBm.

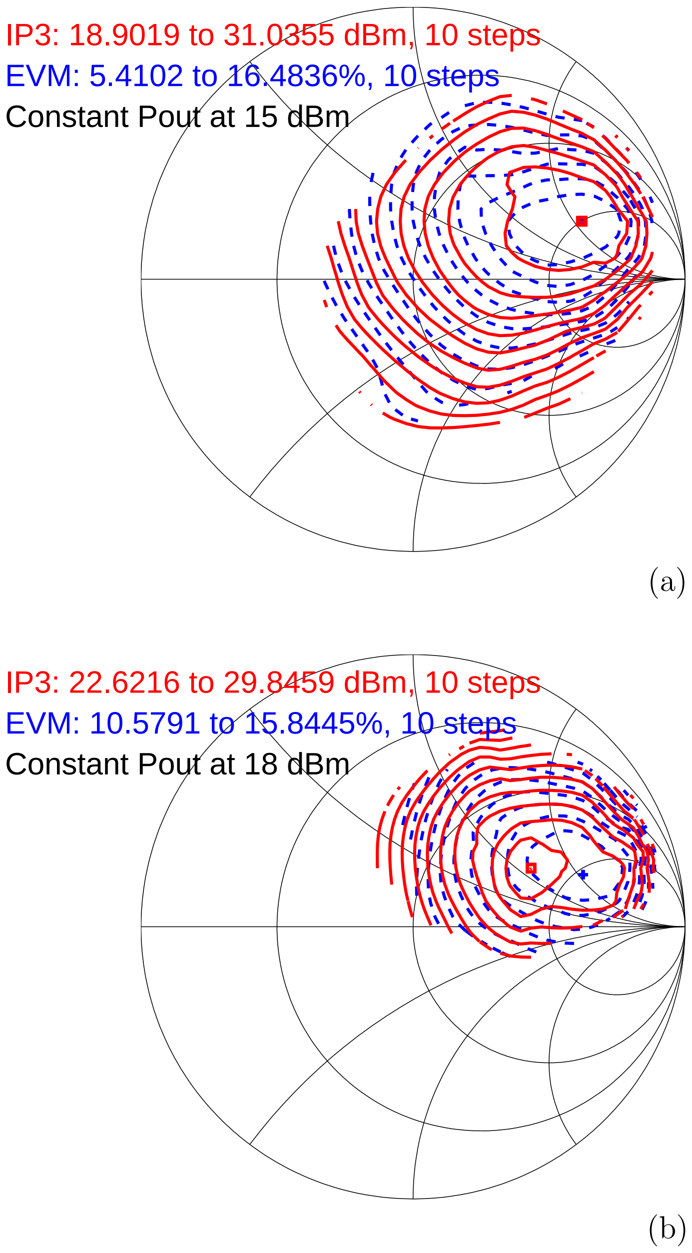

Figure 3.18 Comparison of the IP3 and EVM contours at constant output power level of 15 dBm and 18 dBm.

EVM. The designers might be able to use this information to improve their designs by tuning load impedances to find the better performance with respect to the EVM. This practice helps the designers communicate with system engineers using common metrics to come up with the system specification.

CHAPTER 4

LARGE-SIGNAL SCATTERING FUNCTION MODEL BASED ON LOADPULL MEASUREMENT DATASETS

4.1 Introduction

Small-signal Scattering parameters are widely used in RF and microwave engineering to characterize linear and mildly nonlinear devices and components. They can be thought of as a simple frequency domain behavioral model for the network studied, characterizing the relationship between the in-going and out-going waveforms at specific frequencies one at a time. Obviously, S-parameters deal with linear transferring relationships only, since the input and output frequencies are identical and no new frequencies are generated. However, with the advance of modern wireless communication systems, more and more demands are generated for nonlinear operation of devices and amplifiers to get better transmission efficiency and less power consumption. This causes distortion effects, such as harmonics and spectral regrowth, as introduced in Chapter 2. The classical S-parameter theory is no longer suitable for this situation.

Large-signal scattering function theory is proposed to address this limitation. In general, this theory extends the small-signal theory to take into account not only the fundamental, but also harmonics at different ports. The contribution of all these spectral components is formulated into nonlinear functions, therefore, making it possible to characterize the nonlinearities. A specific measurement system, called a large-signal network analyzer (LSNA), is required to measure and derive this type of large-signal behavioral model.

This theory hasn't been widely applied due to the limited access to such specialized (and costly) systems. Therefore, one question is asked: is it possible to derive practically useful large-signal behavioral models using more widely available measurement systems (for this study, the loadpull measurement system)?

This is the main research topic presented in this chapter. By closely studying the large-signal scattering function theory, the author comes to a conclusion that useful large-signal models can be derived from the loadpull measurement system, although some advanced measurement procedures are required. The procedure for deriving the behavioral model will be explained and example modeling results will be demonstrated that show good performance.

This proposed modeling technique also provides a solution to fully utilize the loadpull measurement dataset. Although the loadpull measurement has been widely applied in power devices (or amplifiers) characterization and design, derivation of an accurate behavioral model from the dataset still presents as a huge challenge. Most of the time, the loadpull measurement datasets are only used for observation of the optimal load points or as a verification for the device modeling. There are some commercially available solutions in current microwave circuit simulation software, such as the Advanced Design System (ADS) [68] and the Microwave Office [69], to generate behavioral models from the measurement datasets, however, the model has limitations, as will be pointed out in the chapter. The method proposed in the chapter shows an analytical way to exploit the datasets and presents significant advantages over the existing approaches.

The theory of the large-signal scattering function is introduced in Section 4.2. The limitations of the current modeling techniques are elaborated in Section 4.3. The detail derivation and optimization process of the proposed method is then presented in Section 4.4. Three example models are constructed. Their simulation results are compared with measurement results in Section 4.5. Good agreements observed prove the effectiveness of the proposed modeling technique.

4.2 Introduction of large-signal scattering function theory

4.2.1 Small-signal network analysis

An N-port linear network can be fully characterized by capturing the relationship between the current and voltage at each port. For example, a two port network as shown in Figure 4.1, can be fully described through Z, Y, ABCD or S-parameters.

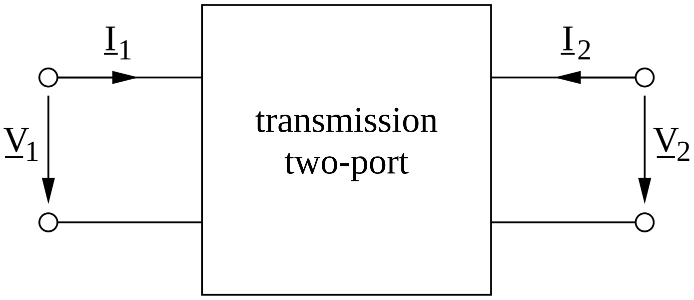

Figure 4.1 Two port network with the voltage and current definition.

For example, the Y parameter for this two-port network is given in Equation 4.1:

$$\begin{bmatrix} i_1 \\ i_2 \end{bmatrix} = \begin{bmatrix} y_{11} & y_{12} \\ y_{21} & y_{22} \end{bmatrix} \begin{bmatrix} v_1 \\ v_2 \end{bmatrix} \tag{4.1}$$

where i_n and v_n are the current and voltage at port n, y_{mn} is the admittance from port n to port m with port m shorted. The Y-parameter can be determined using short circuited outputs, i.e. the y_{mn} can be determined through Equation 4.2 by shorting the port i:

$$y_{mn} = \left.\frac{i_m}{v_n}\right|_{v_m=0} \tag{4.2}$$

Similarly, Z parameter is defined in Equation 4.3. To obtain the Z-parameter, open circuited outputs are required, as indicated in Equation 4.4.

$$\begin{bmatrix} v_1 \\ v_2 \end{bmatrix} = \begin{bmatrix} z_{11} & z_{12} \\ z_{21} & z_{22} \end{bmatrix} \begin{bmatrix} i_1 \\ i_2 \end{bmatrix} \tag{4.3}$$

$$z_{mn} = \left.\frac{v_m}{i_n}\right|_{i_m=0} \tag{4.4}$$

However, when dealing with high frequencies, these parameter definition is no longer suitable. First, the ideal short and open circuit are difficult to obtain at high frequencies. Second, the voltage and the current are difficult to measure at high frequencies. Therefore, the scattering parameter is proposed to solve these problems. The idea is to measure the incident, reflected and transmitted waveforms to capture the performance of the network studied. The ingoing wave a and outgoing wave b are defined as:

$$a = \frac{v + Z_0 \cdot i}{\sqrt{2\mathrm{Re}(Z_0)}} \qquad b = \frac{v - Z_0^* \cdot i}{\sqrt{2\mathrm{Re}(Z_0)}} \tag{4.5}$$

where Z_0 is the reference impedance.

The S-parameter is defined in Equation 4.6, as a function of frequency f:

$$\begin{bmatrix} b_1(f) \\ b_2(f) \end{bmatrix} = \begin{bmatrix} s_{11}(f) & s_{12}(f) \\ s_{21}(f) & s_{22}(f) \end{bmatrix} \begin{bmatrix} a_1(f) \\ a_2(f) \end{bmatrix} \tag{4.6}$$

The S-parameter can be determined by terminating all other ports instead of port j with matched loads to avoid reflection and interference.

$$s_{ij}(f) = \left.\frac{b_i(f)}{a_j(f)}\right|_{a_i(f)=0} \tag{4.7}$$

The Z, Y or S-parameters can be considered as behavioral models, since they deal with only the port variables and don't require information about the internal structure of the network. All the network parameter sets have one important assumption, that is the network is linear and superposition is valid. When the network shows nonlinear effects, typically through the generation of new frequencies (harmonics or mixing products), the Z, Y or S-parameters are no longer valid and more advanced methods are required to characterize the network.

4.2.2 Theory of the large-signal scattering function

The large signal scattering function has been proposed to extend the applicability of the small-signal (linear) S-parameter concept. The idea of the large-signal S-parameter was in exist since 1997. There are lots of publications on this concept, e.g. [47], [48], [70]. Recently, a new broadband version of the original theory was presented [71], which extends this modeling technique to add the frequency dimension.

As introduced in [47] and [72], the large-signal scattering function can be considered as a linearization that relates the incident and reflected wave coefficients of a weakly nonlinear time-invariant device. "Weakly nonlinear" means that the output signals are a stable, single-valued, and continuous function of the input signals around the large-signal operating point [72]. It also hints that the spectral components in the output signals are linear combinations with integer coefficients of the frequencies at the input port.

The input and output variables are defined in the frequency domain as depicted in Figure 4.2: A_{ij} denotes the complex number representing the j^{th} spectral component of the incident voltage wave at port "i" and B_{ij} denotes in a similar manner the scattered voltage waves. The relationship between the input and output wave signals can be described by Equation 4.8, with all the spectral components normalized to A_{11} in phase.

$$B_{ij} = S_{ij}(\mathrm{Re}(A_{11}), \mathrm{Re}(A_{12}), \mathrm{Im}(A_{12}), \cdots, \mathrm{Re}(A_{2N}), \mathrm{Im}(A_{2N})) \tag{4.8}$$

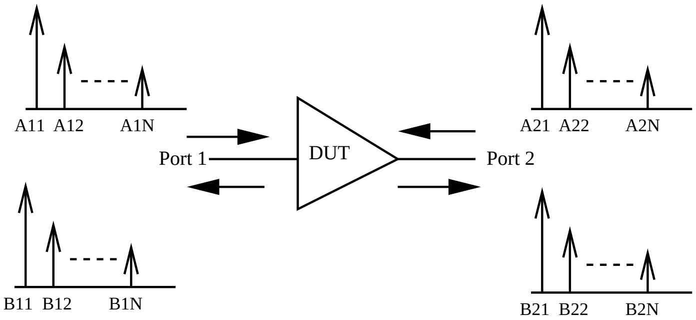

Figure 4.2 The input and output variables for a two-port network used in the large-signal scattering function are composed of the fundamental tones as well as the harmonics for both the incident and reflected waves [47].

The S_{ij} is called "large-signal scattering function". It is a complex multi-dimensional nonlinear function. If there is only one large tone present at the input and all other harmonic signals are relatively small, it is possible to simplify (or linearize) the multi-dimensional nonlinear function S_{ij}. Based on this assumption, the superposition principle holds for the harmonics, which can be expressed in Equation 4.9 [47] , [71]:

$$B_{ij}(|A_{11}|) = \sum_{q} \sum_{l=1,\cdots,M} S_{iq,jl}(|A_{11}|) P^{j-l} A_{ql} + \sum_{q} \sum_{l=1,\cdots,M} T_{iq,kl}(|A_{11}|) P^{j+l} A_{ql}^{*} \tag{4.9}$$

$$T_{p1,k1} = 0 \tag{4.10}$$

where P is the phase of A_{11}. This equation shows that the scattered wave B_{ij}, the j^{th} harmonic at port i, is the sum of incident waves and their conjugates of l^{th} harmonic at port q incident waves. The introduction of the complex conjugate terms of the incident waves is the consequence of the linearization around the time-varying operating point established by the single large-amplitude tone in the absence of perturbation [71] [72]. Equation 4.10 is required to include the fundamental tones in Equation 4.9. $S_{iq,jl}$ and $T_{iq,jl}$ are dependent on the magnitude of the A_{11} that models the nonlinear performance of the amplifiers or devices.

4.2.3 Creation of the large-signal scattering function model

The large-signal scattering function of a device can be derived from measurement results using LSNA. A LSNA (sometimes called vector nonlinear network analyzer, or VNNA) is composed of the testset, down-converter, digitizer and analysis software, as shown in Figure 4.3. The source 1 is a signal generator that can generate CW signals as well as modulated signals, if required. Source 2 provides the perturbation signal to port 1 or 2 through the switch. This signal simulates the small perturbation signal presented in the model.

The measurement system requires specific multi-tone phase calibration, in addition to the traditional VNA calibration (such as the SOLT or LRM calibration) and absolute power calibration. The phase calibration normalizes all the fundamental and harmonic spectral components to the phase of A_{11}, the dominant tone at the port 1.

To obtain the coefficients in the large-signal behavioral model for a device, several measurements are required. Let's use an example to explain this process. If we are interested in the scattered wave B_{21}, the fundamental tone at port 2. Assume this

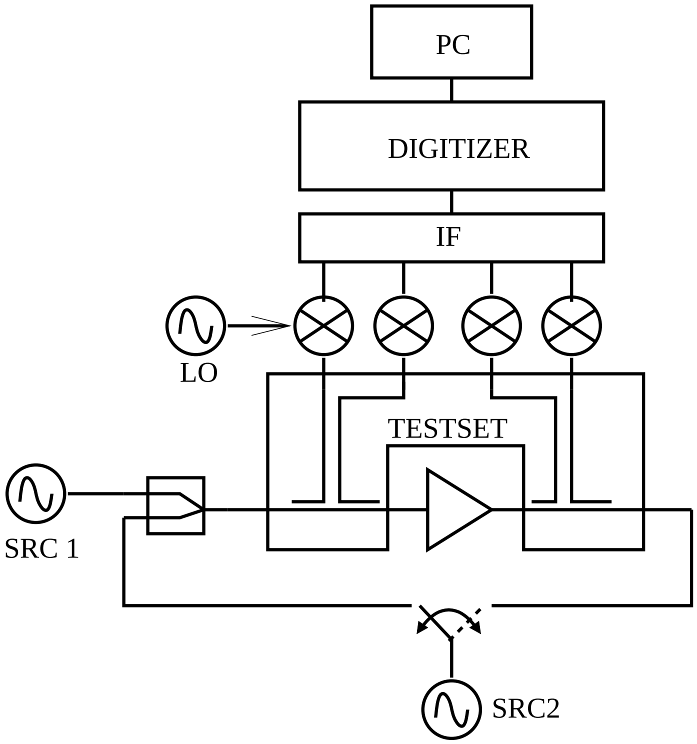

Figure 4.3 Functional block of the LSNA.

wave variable is determined by the input large signal tone A_{11} at one specific power level and the spectral components at port 2, including A_{21}, A_{22} and A_{23}. The B_{21} can be written in Equation 4.11:

$$\begin{aligned} B_{21} &= S_{21,11}A_{11} + S_{22,11}A_{21} + T_{22,11}A_{21}^{*}P^{2} \\ &\quad + S_{22,12}A_{22}P^{-1} + T_{22,12}A_{22}^{*}P^{3} + S_{22,13}A_{23}P^{-2} + T_{22,13}A_{23}^{*}P^{4} \end{aligned} \tag{4.11}$$

There are 7 unknown coefficients for this specific power level and frequency. Since superposition holds, as the theory assumes, the 7 coefficients can be obtained through three measurements:

- measurement with only the large-signal A_{11} present;

- two measurements with the small-signal perturbation A_{21} at different phase relative to the A_{11};
- two measurements with the small-signal perturbation A_{22} at different phase relative to the A_{11};
- two measurements with the small-signal perturbation A_{23} at different phase relative to the A_{11};

By combining all these measurement datasets and applying a least-square-error fit, the 7 coefficients can be determined thereafter. By sweeping the amplitude of the A_{11}, we will get a table for the 7 coefficients corresponding to each input signal amplitude. Then either a look-up-table (LUT) model or an fitting function (e.g. ANN model) can be used to implement the large-signal model in commercial microwave simulation software to simulate the device performance.

If only the fundamental frequency is considered in the large-signal model, that is the harmonic spectral components don't appear in the model, the large-signal model is reduced to so called the "Hot" S22 method [49]. Equation 4.12 illustrates this model:

$$B_2 = S_{21}(|A_1|)A_1 + S_{22}(|A_1|)A_2 + T_{22}(|A_1|)P^2 A_2^* \tag{4.12}$$

As pointed out in [48], the measurements are actually a combination of passive and active (harmonic) loadpull measurements, since the second synthesizer injects signals to the DUTs to simulate the variation in the load. This analogy suggests the possibility to approximately create the large-signal model from a general loadpull measurement dataset.

4.3 Current loadpull-based modeling technique and their limitations

There are several existing techniques to utilize the loadpull dataset for modeling purposes [73], [74] and [75]. Some commercial microwave simulation software packages provide the capabilities to read the loadpull data files into the simulator for linear or nonlinear simulation [68] and [69].

Generally these techniques can be grouped into two categories: file-based modeling and analytical modeling. As the name hints, the file-based techniques provide a solution to directly access the loadpull data file through some indexing design to find out the device performance according to a set of rules. [68], [69], [73] and [74] belong to this category.

Carlson [74] described a novel method to integrate the loadpull dataset in microwave simulation software for optimization of the load condition for different goals (e.g. output power or IP3). Instead of sweeping the amplitude and phase of the reflection coefficient of the load Γ_L, the author proposed to sweep the resistance and capacitance based on the observation of the small-signal S22 seen at the output port of the DUT. This method can capture the frequency effect through the capacitance, which makes the data processing easier. However, this method has its limitation in that it only provides a way to observe the loadpull data file and find the optimal load points for specific goals. It doesn't provide a usable behavioral model for general simulation purposes.

Olah et al [73] introduced a systematic method to create behavioral models based on the loadpull data file. The method has three steps:

- scattered data interpolation: triangulation is used to generate a set of triangular mesh; the contours are plotted by traversing these triangular patches;

- convert the triangulated scattered data to a grid (regular or uniform data) for easy usage in simulators;
- calculate the incident and scattering waves as functions of load impedances using the gridded datasets; the results are stored in a file for access during simulation.

The limitation about this method is that it requires the storage of large data files; a lot of the information might be redundant. For example, when the input signal level is low, a simple small-signal S-parameter model is enough to predict the gain at various loads. However, this method would utilize the stored B_1 and B_2 for every possible load, which will require a large data file. The extensive file access operation makes this method inefficient.

Another limitation of this method is that the file-based model requires a large number of testing load points to be able to interpolate or extrapolate smoothly on the Smith chart. Figure 4.4 illustrates this problem. As can observed, the file-based model doesn't extrapolate the output power contours properly. Analytic models are able to overcome this problem, as will be demonstrated in the examples in Section 4.5.

[75] is an example of the use of analytic methods to model the loadpull performance of a device. By expanding the linear S-parameter through a nonlinear S_{21} function, the model was able to predict the gain compression effects. This is often called "large-S21" method. This technique provides a simple solution to predict the nonlinear performance of the DUT based on the loadpull measurements. However, the large-S21 model has limited accuracy in predicting the gain/phase compression and intermodulation performance at different load conditions.

Due to the limitation of the current modeling techniques based on the loadpull measurement datasets, a new approach is proposed to address the limitations. The

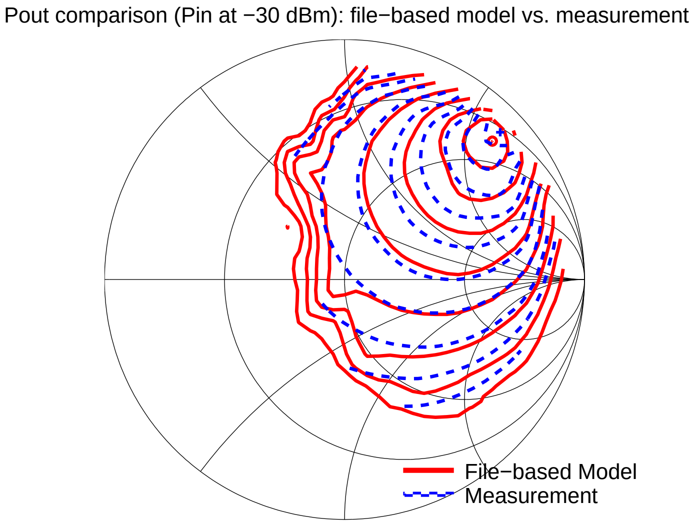

Figure 4.4 The interpolation and extrapolation problem with the file-based model. This is due to the insufficient testing points. However, as will be shown in later sections, analytic models have better performance in interpolation and extrapolation.

new modeling technique exploits the large-signal scattering function theory and derives the relationship between the incident and scattering waves through the loadpull measurement datasets. The detail analysis is given in the following section.

4.4 Behavioral model based on loadpull gain and phase compression measurements

A power amplifier can be treated as a two-port network, as shown in Figure 4.5. A typical one-tone loadpull measurement gives information about the source impedance (or reflection coefficient, Γ_S), load impedances(or reflection coefficient, Γ_L), the input power (P_{in}), the measured delivered power (P_{out}).

For simplicity, suppose the device is unilateral (i.e. $S_{12} = 0$), the input impedance of the port 1 can be expressed as Equation 4.13. This constrain can be removed if

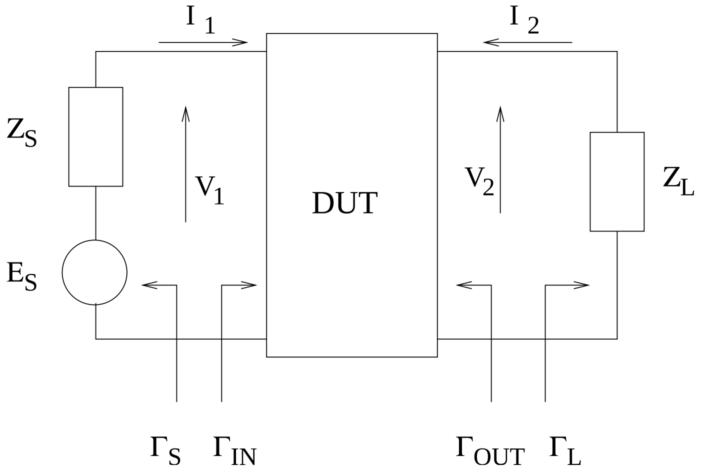

Figure 4.5 Diagram of a two-port network with a voltage source of E_s and source impedance of Z_S. The load impedance is Z_L

the input port reflected power is captured in the loadpull measurement.

$$\begin{aligned} Z_{in} &= Z_0 \frac{1+\Gamma_{IN}}{1-\Gamma_{IN}} \\ &= Z_0 \frac{1+S_{11}}{1-S_{11}} \end{aligned} \tag{4.13}$$

Based on the given information, the voltage and current at port 1 can be calculated through the following steps:

$$Z_S = Z_0 \frac{1+\Gamma_S}{1-\Gamma_S} \tag{4.14}$$

$$P_{in} = \frac{E_S^2}{8Re(Z_S)} \tag{4.15}$$

$$E_S = \sqrt{8Re(Z_S)P_{in}} \tag{4.16}$$

$$V_1 = E_S \frac{Z_{in}}{Z_{in}+Z_S} \tag{4.17}$$

$$I_1 = \frac{V_1}{Z_{in}} \tag{4.18}$$

Therefore, the incident and reflected waveforms at port 1 are calculated as:

$$A_1 = \frac{V_1 + I_1 Z_0}{\sqrt{2Re(Z_0)}} = V_1 M_1 \tag{4.19}$$

$$B_1 = \frac{V_1 - I_1 Z_0}{\sqrt{2Re(Z_0)}} = A_1 S_{11} \tag{4.20}$$

$$M_1 = \frac{Z_0 + Z_{in}}{Z_{in}\sqrt{2Re(Z_0)}} \tag{4.21}$$

The incident and reflected waveforms at port 2 are characterized based on the large-signal scattering function theory, as shown in Equation 4.22 and Equation 4.23. The phase of the A_{11}, P, is absorbed into the T_{22} coefficient.

$$B_2 = S_{21}A_1 + S_{22}A_2 + T_{22}A_2^* \tag{4.22}$$

$$A_2 = B_2\Gamma_L \tag{4.23}$$

Combining Equation 4.22 and 4.23 gives:

$$B_2 = S_{21}A_1 + S_{22}B_2\Gamma_L + T_{22}B_2^*\Gamma_L^* \tag{4.24}$$

Equation 4.24 is an implicit expression for B_2; it can be further transformed to an explicit function to simplify the model generation. Assume S_{21}, S_{22} and T_{22} are represented as:

$$S_{21} = c_1 + \mathrm{j}c_2$$

$$S_{22} = c_3 + \mathrm{j}c_4$$

$$T_{22} = c_5 + \mathrm{j}c_6$$

where $c_i, i = 1, \cdots, 6$ are unknowns to be determined.

Suppose $B_2 = B_{2r} + \mathrm{j}B_{2i}$ and $A_1 = A_{1r} + \mathrm{j}A_{1i}$. B_{2r} and B_{2i} are the real and imaginary parts of B_2 respectively. A_{1i} and A_{1i} are the real and imaginary parts of A_1 respectively. Equation 4.24 can be rewritten as:

$$(c_1 + \mathrm{j}c_2)A_1 + (k_1 + \mathrm{j}k_2)B_2 + (m_1 + \mathrm{j}m_2)B_2^* = 0 \tag{4.25}$$

where

$$k_1 + \mathrm{j}k_2 = (c_3 + \mathrm{j}c_4)\Gamma_L - 1 \tag{4.26}$$

$$m_1 + \mathrm{j}m_2 = (c_5 + \mathrm{j}c_6)P^2\Gamma_L^* \tag{4.27}$$

Arrange the real and imaginary part and we can get:

$$\begin{bmatrix} c_1A_{1r} - c_2A_{1i} \\ c_1A_{1i} + c_2A_{1r} \end{bmatrix} + \begin{bmatrix} k_1 + m_1 & -k_2 + m_2 \\ k_2 + m_2 & k_1 - m_1 \end{bmatrix} \begin{bmatrix} B_{2r} \\ B_{2i} \end{bmatrix} = 0 \tag{4.28}$$

By solving the linear function 4.28, the real and imaginary part of B_2 can be derived as:

$$\begin{bmatrix} B_{2r} \\ B_{2i} \end{bmatrix} = \frac{1}{D} \begin{bmatrix} (k_1 + k_2 - m_1 - m_2)c_1 & (-k_1 + k_2 + m_1 - m_2)c_2 \\ (k_1 - k_2 + m_1 - m_2)c_1 & (k_1 + k_2 + m_1 + m_2)c_2 \end{bmatrix} \begin{bmatrix} A_{1r} \\ A_{1i} \end{bmatrix} \tag{4.29}$$

where $D = k_1^2 - k_2^2 - m_1^2 + m_2^2$.

Obviously, in order to obtain the B_{2r} and B_{2i}, the measurements for both the magnitude and phase are required. This is why it is important to obtain the loadpull AM-PM datasets. The loadpull AM-AM measurements provide the optimization criteria for the magnitude, while the loadpull AM-PM measurements set up the rule for the phase optimization.

The magnitude can be derived from the delivered output power. The output power at port 2 is determined by the A_2 and B_2 through:

$$\begin{aligned} P_{out} &= \frac{1}{2}(|B_2|^2 - |A_2|^2) \\ &= \frac{1}{2}|B_2|^2(1 - |\Gamma_L|^2) \end{aligned} \tag{4.30}$$

Since the output power is known through the measurement, the B_2 can be expressed as:

$$|B_2| = \sqrt{\frac{2P_{out}}{1 - |\Gamma_L^2|}} \tag{4.31}$$

Optimization process can be applied to obtain the 6 unknown coefficients c_1 to c_6. The least-mean-square (LMS) errors for the magnitude and phase can be represented by Equation 4.4 and 4.4.

$$err_{mag} = \frac{\sum_n ((B_{2r}^2 + B_{2i}^2) - (\frac{1}{1 - |\Gamma_L|^2} P_{out}))^2}{n} \tag{4.32}$$

$$err_{phase} = \frac{\sum_n (\Phi(\frac{A2 + B2}{A1 + B1}) - \text{AM-PM})}{n} \tag{4.33}$$

where n is the number of load points used in the optimization process. AM-PM is the phase compression data obtained through the loadpull AM-PM measurement. It is the phase difference between the voltages at the input and output ports. The

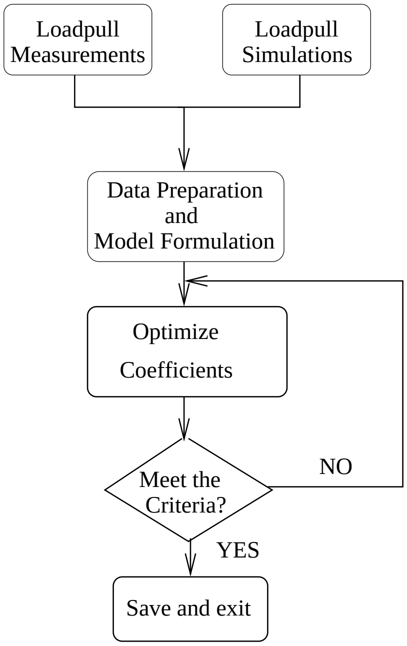

Figure 4.6 The flowchart of the Matlab program created for the behavioral model optimization based on the loadpull AM-AM and AM-PM datasets.

input and output voltages are the sum of the incident and reflected waves at the port respectively.

The analysis given above has been implemented in a Matlab program [76]. Figure 4.6 demonstrates the procedure to generate the behavioral model based on the loadpull datasets. Notice that the loadpull datasets can come from either the measurements or from simulations, depending on the applications of this modeling technique.

4.5 Experimental result 1: measurement-based behavioral model

To demonstrate the modeling technique proposed in previous section, three example models are created and compared with existing techniques. The three examples are chosen so that they show two types of applications of this behavioral modeling technique. The first two example models are created based on measurement results, showing an efficient way to integrate measurement results into design. The third ex-

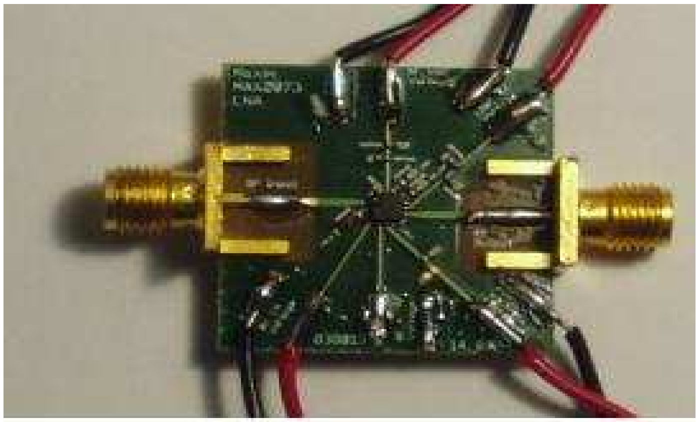

Figure 4.7 Illustration of the MAXIM 2373 LNA sample.

ample is based on the simulation results, which will lead to decrement in computing complexity and therefore the simulation time.

4.5.1 Example model of a packaged RFIC LNA

The first example component used is an MAX2373 low noise amplifier (LNA). Figure 4.7 shows this component. This component was characterized at 900 MHz. Loadpull gain and phase compression measurements were performed. Two tone loadpull measurements were performed as well. The Matlab modeling program was used to process the measurement data files and generate the model coefficients through the unconstraint nonlinear optimization procedure. In addition, a file-based model is created for characterizing the 3rd order intermodulation products.

The model was implemented in ADS 2004A using the frequency domain defined device (FDD). The advantage of using this device is that it provides the ability to define the behavior of individual frequency components separately. The model only requires two setup parameters: the fundamental frequency (RFfreq), and the frequency spacing (fspacing). For one tone simulation, the fspacing is set at 0. Therefore, the model requires minimum interaction from the users and makes it easy for usage.

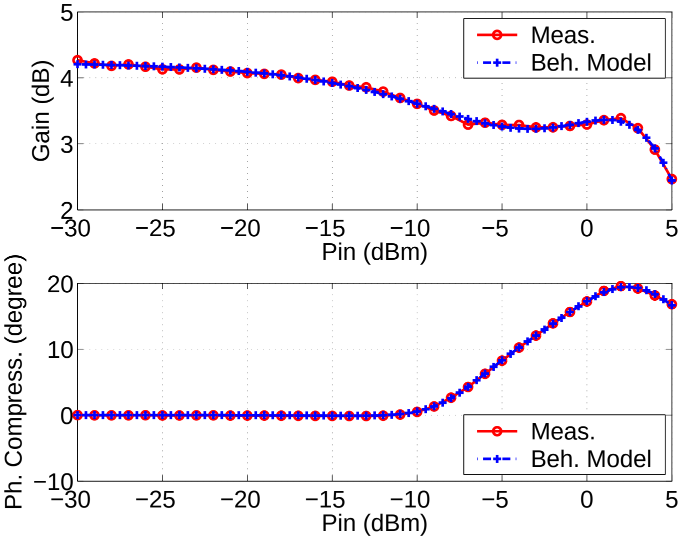

Figure 4.8 Comparison of the measured and simulated gain and phase compression at 50 ohm.

The measurement condition is summarized in the following:

- Frequency: 900 MHz;
- Input power: -30 dBm to 5 dBm;
- Two tone frequency spacing: 100 KHz;
- AGC Bias: 1.3875 V;
- Vcc bias: 2.775 V.

Figure 4.8 compares the measured and simulated gain and phase compression performance of this LNA at 50 ohm condition. The model predicts the compression property correctly.

Figure 4.9 shows the simulated output power contours compared with the measured result. The input power is low at -30dBm. Good agreement is observed. In fact, the large signal model reduces to small-signal S-parameter model when the input signal is low enough. The variation of the output power with respect to the load

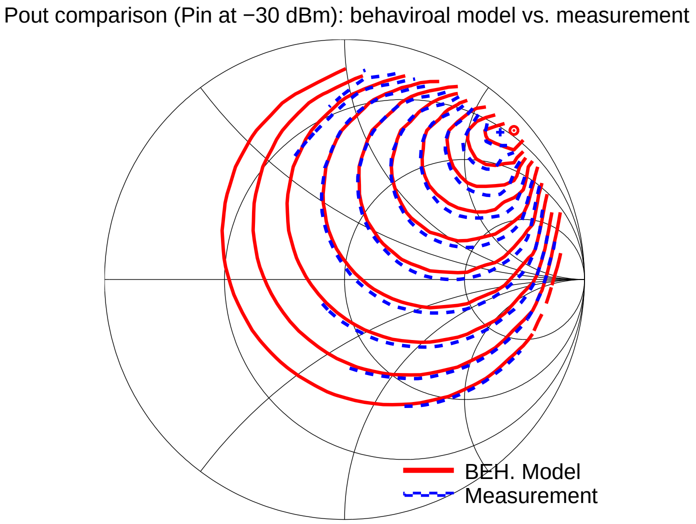

Figure 4.9 The simulated output power contours are compared with the measurements. The input power is at -30dBm.

can be characterized through the small-signal S-parameter. Detailed analysis can be found in [77]. Compared with the file-based model, obviously the analytic model provides much better interpolation and extrapolation characteristics.

However, the small-signal S-parameter cannot predict accurately nonlinear effects associated with large input signal. The simple large-S21 model provides limited prediction accuracy, compared with the proposed model, as shown in Figure 4.10. In this figure, the measured output power contour at input signal of -5dBm is compared with the large-signal model in (a) and the model based on the large-S21 technique in (b). By looking at (a), one can see that the proposed behavioral model does a decent job in predicting the change in the load impedance for optimal output power performance. However, the simple large-S21 modeling technique assumes the compression properties at all load points are the same. This explains why the large-S21 model behaves different from the proposed large-signal model.

Since only the fundamental tone is considered in the model generation, its capability to predict the intermodulation products is limited. Therefore, a file-based

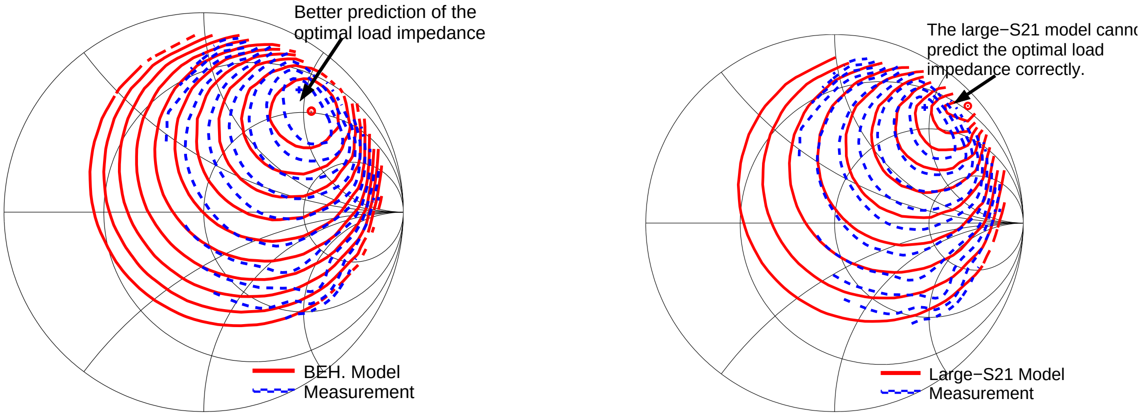

(a)

(b)

Figure 4.10 Comparison of simulated and measured output power contours. The new model and the large-S21 model are compared side by side, showing the improvement of the new model to predict the changing optimal load impedance.

Table 4.1 List of the 6 example load reflection coefficients used to test the LNA model.

(a)	0.56723+j*0.03630	(b)	0.36904+j*0.40569
(c)	0.75532+j*0.50893	(d)	0.77211+j*0.16110
(e)	0.17539+j*0.76875	(f)	0.30559-j*0.57057

model is implemented for prediction of the 3rd order intermodulation products. A contour interpolation algorithm is utilized during the generation of the data file.

Figure 4.11 illustrates the comparison of the measured and simulated IP3. The input power is -20dBm. As can be seen, the behavioral model does a good job predicting the IP3 performance over a defined region.

Six load impedances are chosen as examples to test the large-signal model. The simulated fundamental tone and the 3rd order intermodulation product are compared with the measurement results. The reflection coefficients of the 6 example loads are listed in Table 4.1 and plotted in Smith Chart, as shown in Figure 4.12. The load examples are chosen to spread over the Smith Chart.

The simulated results are compared with corresponding measurement datasets in Figure 4.13. Good agreements can be observed for all cases. Also given out

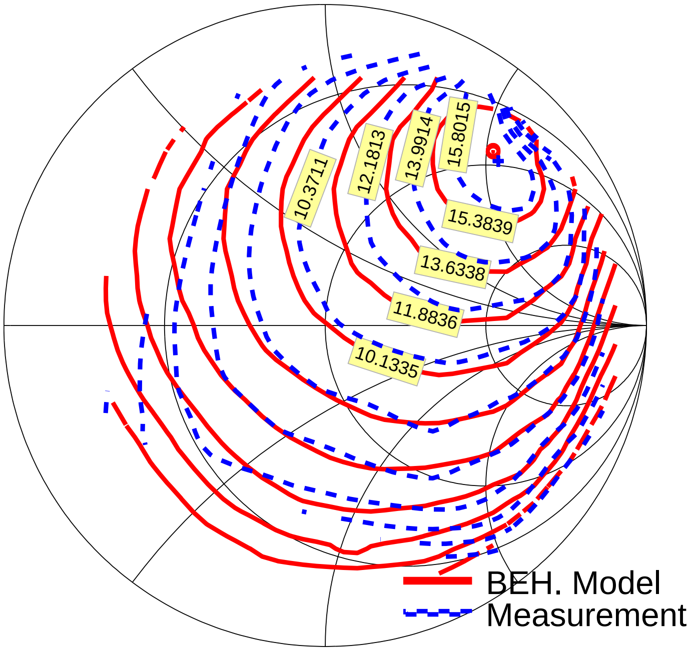

Figure 4.11 Comparison of the measured and simulated IP3 using the large-signal behavioral model.

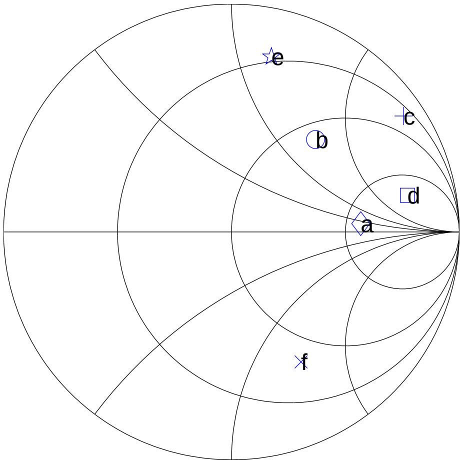

Figure 4.12 Illustration of the six load impedance examples on the Smith Chart. The six loads spread in a large area, showing the robustness of this model to predict the nonlinear effect in a wide load range.

are the simulated results obtained from the large-S21 model. The large-S21 model presents good performance for limited set of load points, such as at (a), (d), (e), and (f). However, at (b) and (c) the simulation results show significant discrepancies. Therefore, the new large-signal behavioral model provides better performance against the large-S21 behavioral model.

Figure 4.14 shows the errors in the simulated fundamental tone at different loads. As can be seen, the new model has much less errors compared with the large-S21 model. Similarly, Figure 4.15 illustrates the errors in the simulated IM3 at different loads. Again, the new model has better performance compared with the large-S21 model.

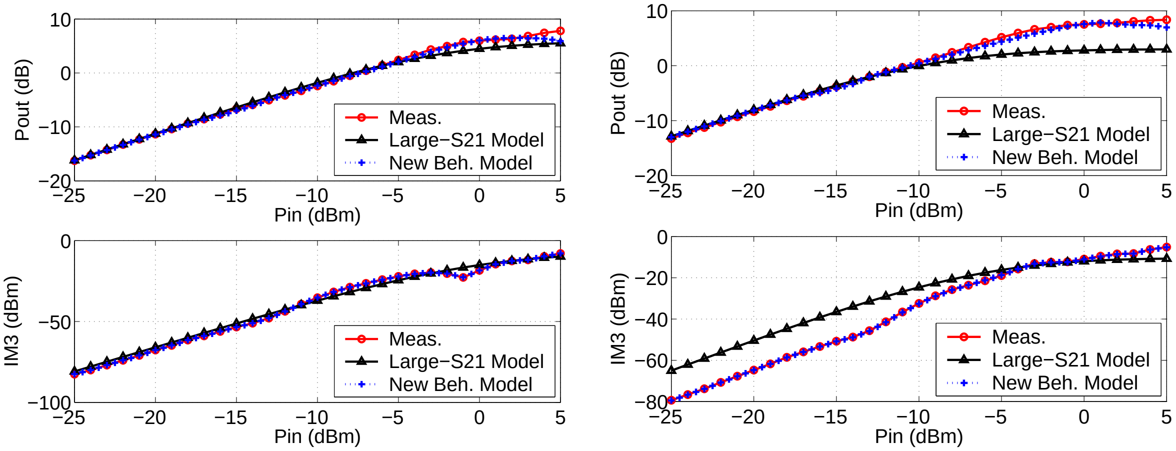

(a) 0.56723+j*0.03630 (b) 0.36904+j*0.40569

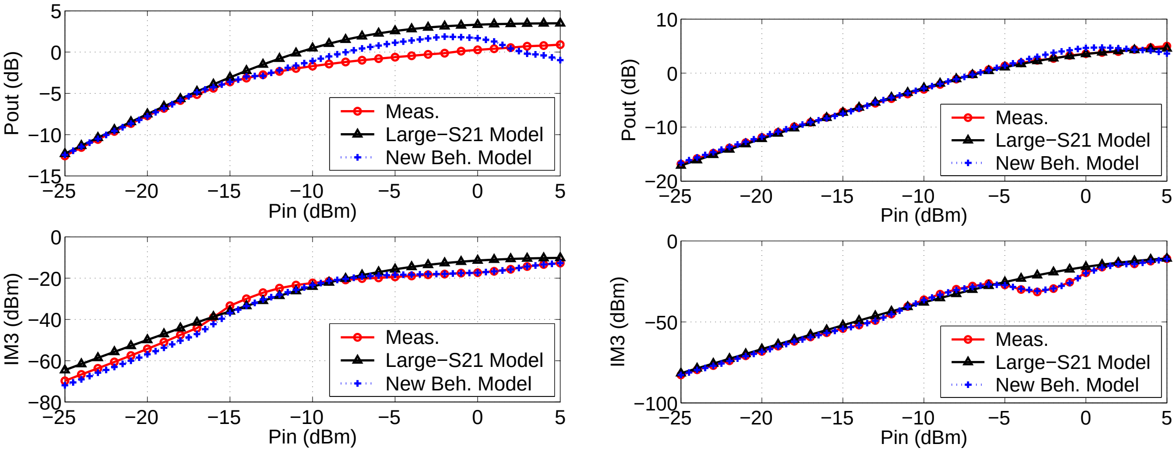

(c) 0.75532+j*0.50893 (d) 0.77211+j*0.16110

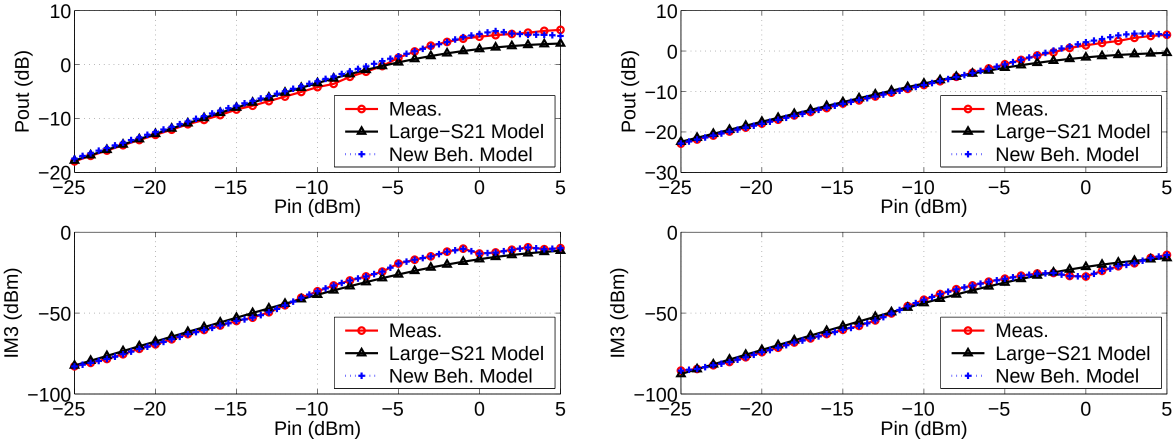

(e) 0.17539+j*0.76875 (f) 0.30559-j*0.57057

Figure 4.13 Comparison of the measured and simulated Pout and IM3 at 6 load impedances.

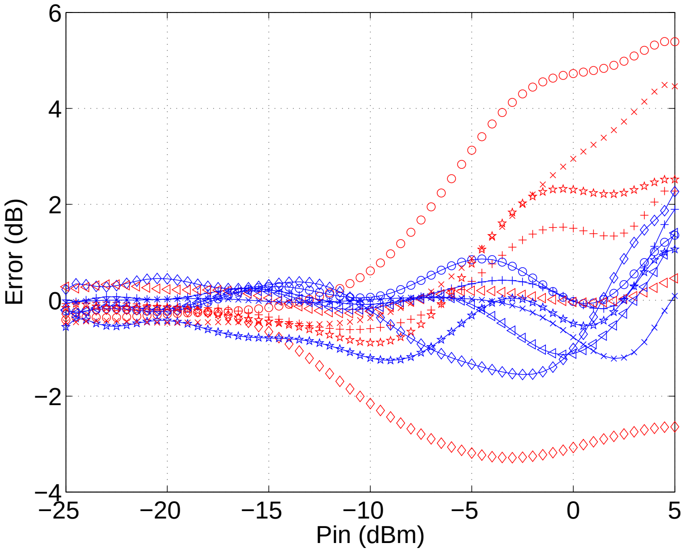

Figure 4.14 The errors of the simulated fundamental tone at 6 loads are plotted. The blue curves represent the errors associated with the newly developed model; the red curves represent the errors associated with the large-S21 model. The new model presents better performance, compared with the large-S21 model.

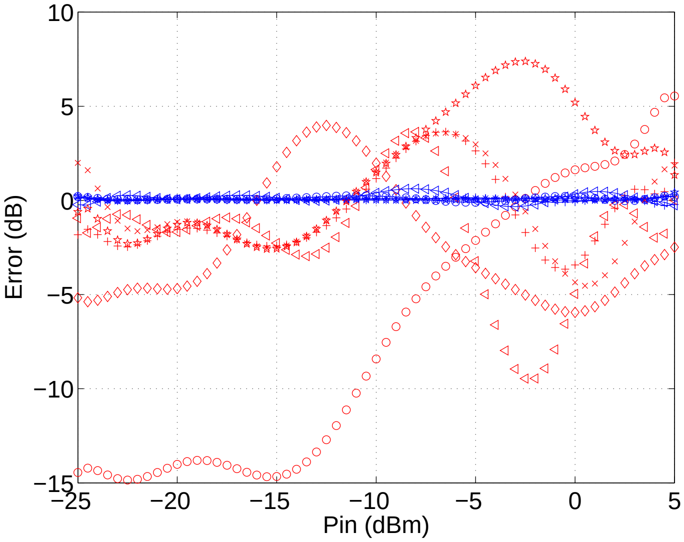

Figure 4.15 The errors of the simulated 3rd order intermodulation product at 6 loads are plotted. The blue curves represent the errors associated with the newly developed model; the red curves represent the errors associated with the large-S21 model. The new model presents better performance, compared with the large-S21 model.

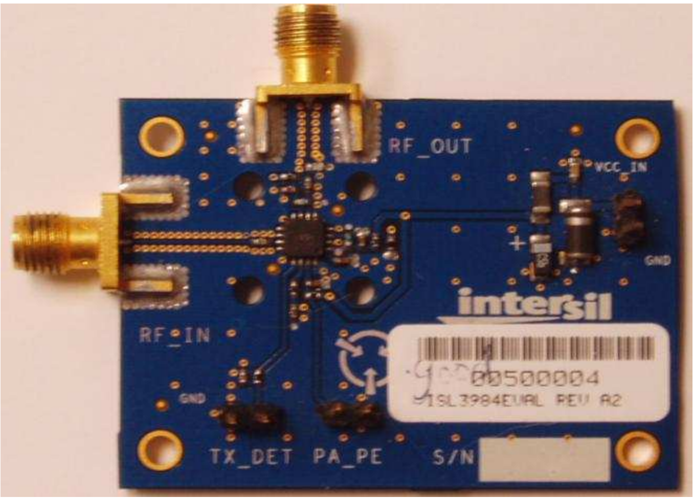

Figure 4.16 Illustration of the ISL3984 power amplifier sample.

4.5.2 Example model of a PA sample

The second example component used is an Intersil power amplifier (ISL3984). Figure 4.16 shows the tested ISL3984 power amplifier sample. Loadpull gain and phase compression measurements were performed on this power amplifier sample at 2450 MHz. The measurement condition is summarized below:

- Frequency: 2450 MHz;
- Input power: -20 dBm to 0 dBm;
- Two tone frequency spacing: 100 KHz;
- Bias: 3.3 V.

To verify the performance of the behavioral model, a swept power harmonic simulation is done in 50 ohm condition, i.e. the source and load impedances are at 50 ohm. The simulated gain and phase compression curves are compared to the measured data in Figure 4.17. Good agreement can be seen in the figure.

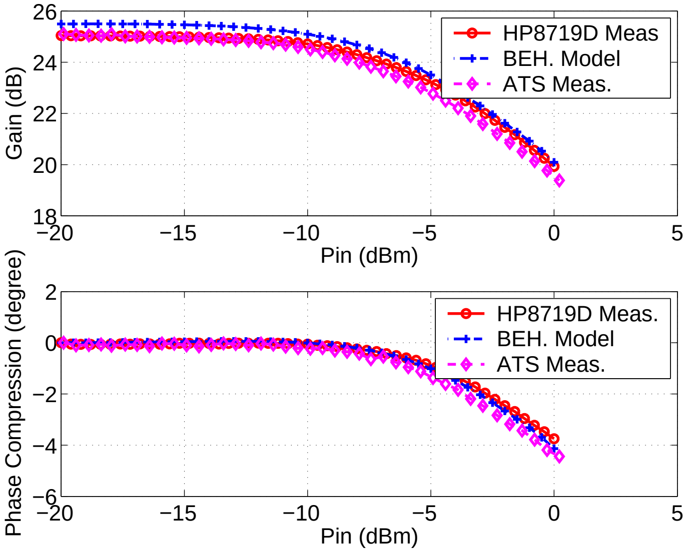

Figure 4.17 Comparison of the simulated and measured gain and phase compression in 50 ohm.

Figure 4.18 compares the simulated and measured output power contours at input power level of -20dBm. The source impedance is set to be conjugately matched. The Γ_S is $0.34051 + \mathrm{j} * 0.58271$. As can be seen, the two datasets agree very well.

Similar to the LNA model, a file-based model is created for the simulation of IM3. Figure 4.19 compares the simulated and measured IM3 contours at input power level of -20dBm. The file-based model predicts the 3rd order intermodulation product accurately under various load conditions.

Six load impedances are chosen as examples to test the large-signal model. The simulated fundamental tone and the 3rd order intermodulation product are compared with the measurement results. The reflection coefficients of the 6 example loads are listed in Table 4.2 and plotted in Smith Chart, as shown in Figure 4.20. The load examples are chosen to spread over the Smith Chart.

The simulated results are compared with corresponding measurement datasets in Figure 4.21. Good agreements can be observed between the simulated results from the proposed model and the measurements. Also given out are the simulated results

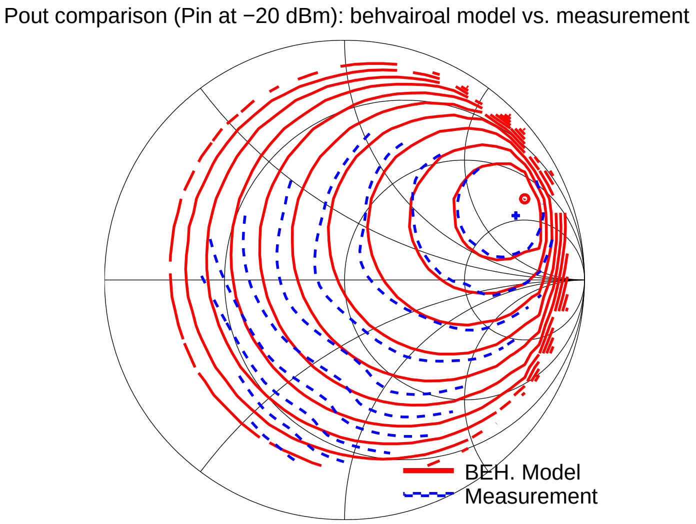

Figure 4.18 Comparison of the simulated output power contour with the measured dataset.

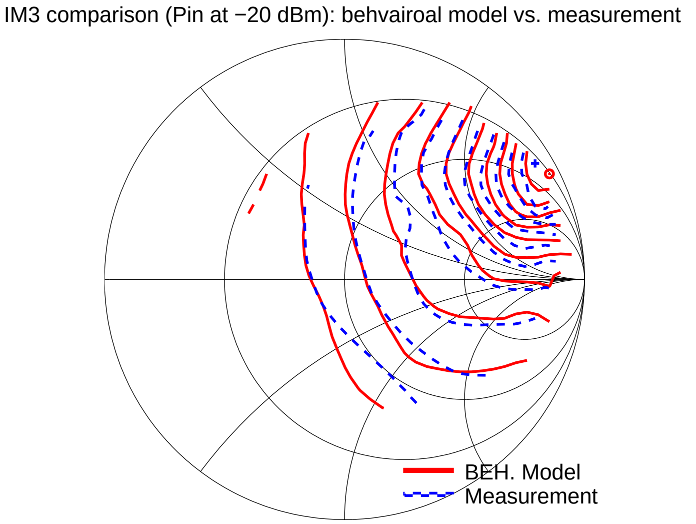

Figure 4.19 Comparison of the simulated IM3 contour using the behavioral model with the measured dataset.

Table 4.2 List of the 6 example load reflection coefficients used to test the PA model.

(a)	0.62561+j*0.39360	(b)	-0.36966+j*0.09652
(c)	0.19215+j*0.33529	(d)	0.87741+j*0.07210
(e)	0.61180+j*0.627895	(f)	0.52078-j*0.53337

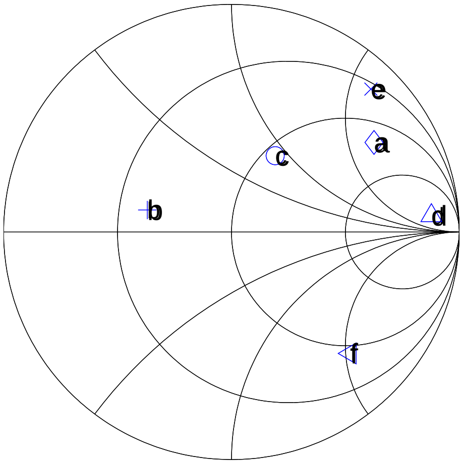

Figure 4.20 Illustration of the six load impedance examples used to test the behavioral model developed for the ISL3984 on the Smith Chart. The six loads spread in a large area, showing the robustness of this model to predict the nonlinear effect in a wide load range.

obtained from the large-S21 model. The large-S21 model presents good performance for limited set of load points, such as at (a), (b), (d), and (e). However, at (c) and (f) the simulation results show significant discrepancies. Therefore, the new large-signal behavioral model provides better performance against the large-S21 behavioral model.

Figure 4.22 shows the errors in the simulated fundamental tone at different loads. As can be seen, the new model has much less errors compared with the large-S21 model. Similarly, Figure 4.23 illustrates the errors in the simulated IM3 at different loads. Again, the new model has better performance compared with the large-S21 model.

Through the comparison results illustrated from the two example models, the validity of the model has been proved. The behavioral model derived from the loadpull gain and phase compression measurements can predict the performance of the DUT under various load conditions and input power levels accurately to some extent.

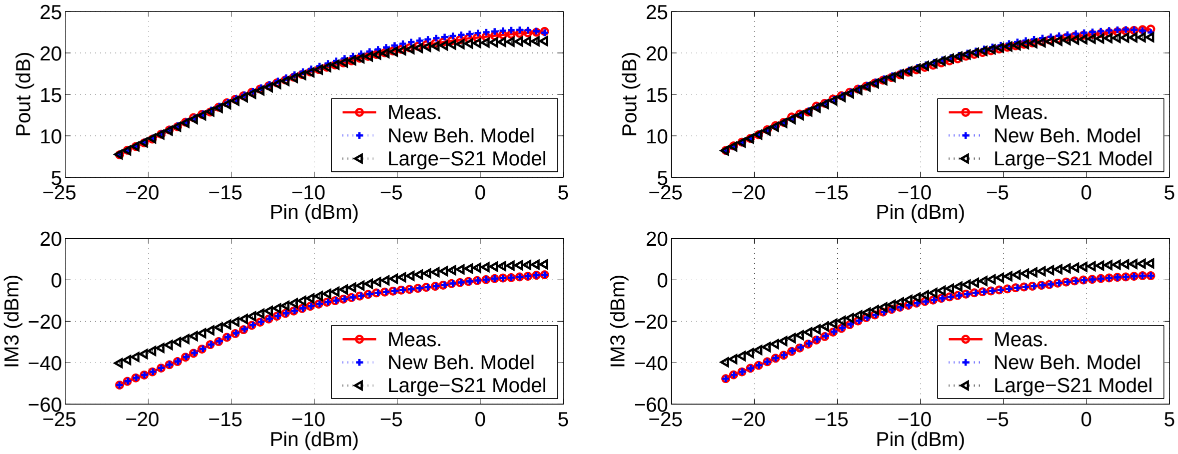

(a) 0.62561+j*0.39360 (b) -0.36966+j*0.09652

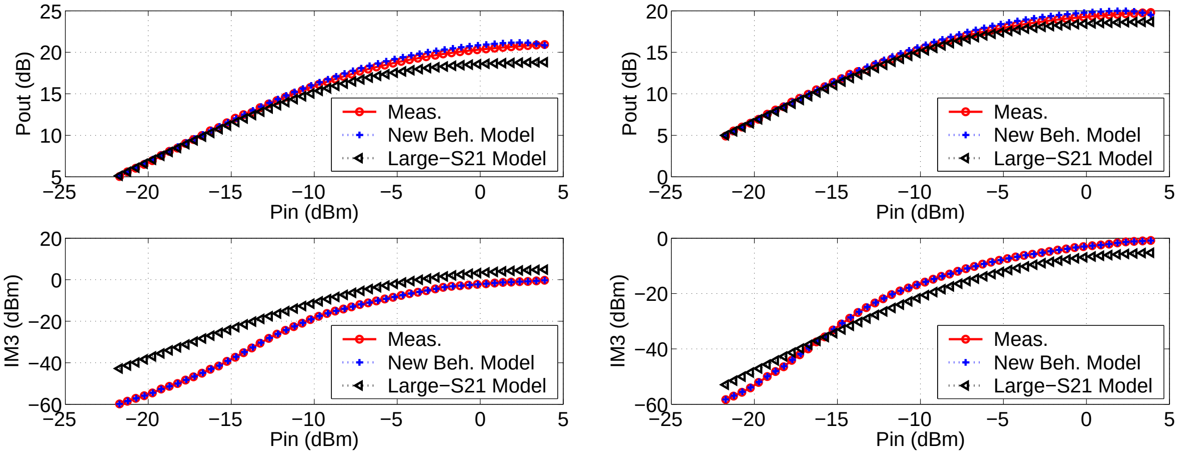

(c) 0.19215+j*0.33529 (d) 0.87741+j*0.07210

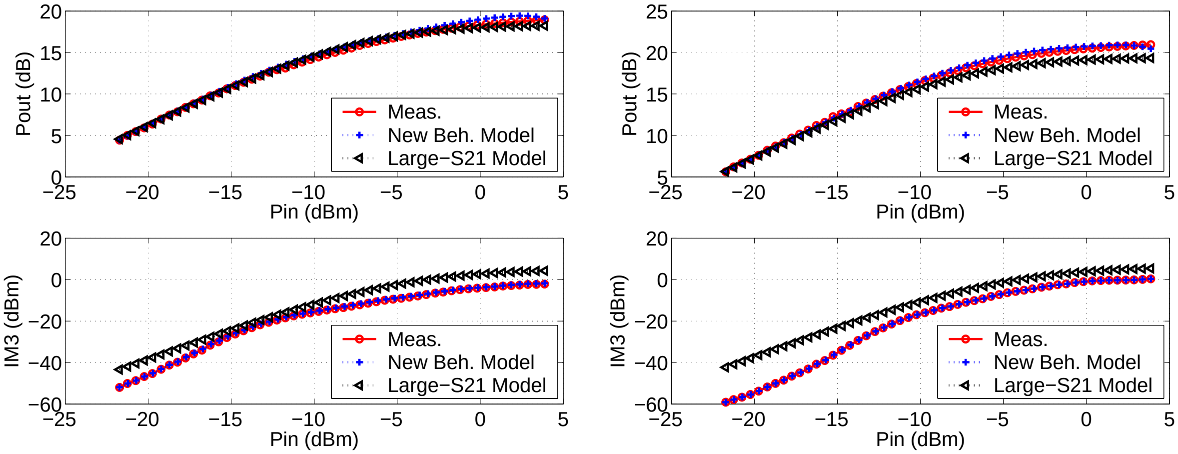

(e) 0.61180+j*0.62789 (f) 0.52078-j*0.53337

Figure 4.21 Comparison of the measured and simulated Pout and IM3 at 6 load impedances.

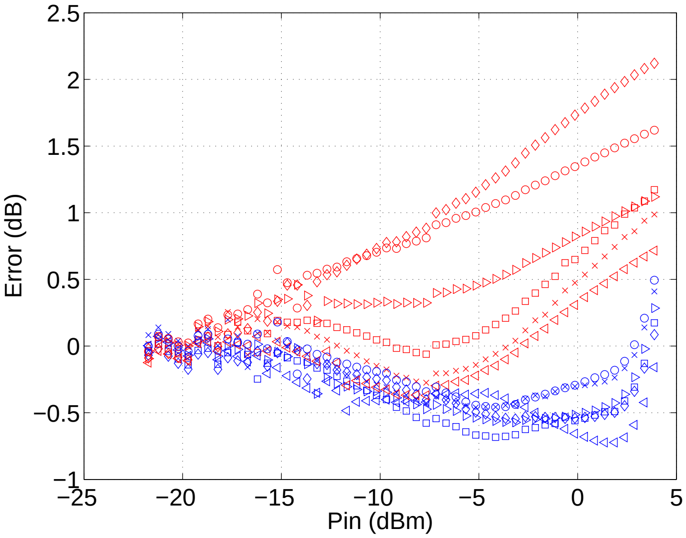

Figure 4.22 The errors of the simulated fundamental tone at 6 loads are plotted. The blue curves represent the errors associated with the newly developed model; the red curves represent the errors associated with the large-S21 model. The new model presents better performance, compared with the large-S21 model.

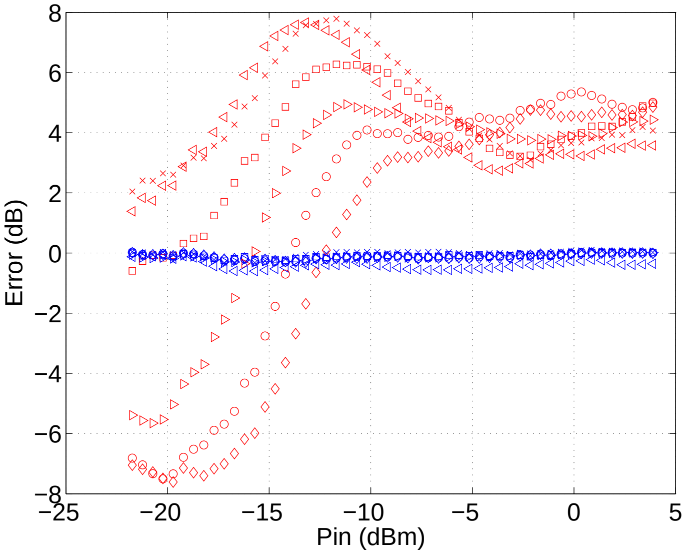

Figure 4.23 The errors of the simulated 3rd order intermodulation product at 6 loads are plotted. The blue curves represent the errors associated with the newly developed model; the red curves represent the errors associated with the large-S21 model. The new model presents better performance, compared with the large-S21 model.

This measurement-based behavioral modeling technique is also demonstrated as simple solution to integrate the loadpull measurement datasets with commercial CAE softwares. The resulted model provides the invaluable insights for designers to study nonlinear components at system levels without losing much accuracy.

4.6 Experimental result 2: simulation-based behavioral model

We have discussed the measurement-based behavioral modeling approach in previous section. The second behavioral modeling example will demonstrate the process to derive a abstract model based on the simulation datasets. An equivalent circuit model for the 30 Watts Cree UGF21030 LDMOS power transistor is used to create the simulation datasets. This circuit model was developed by Modelithics [78].

This model was simulated at 2.17 GHz under swept power and various load conditions. The simulated AM-AM and AM-PM datasets were used to create the large-signal behavioral model. The simulation setup for generating the test datasets is given below:

- Frequency: 2170 MHz;
- Input power: 0 dBm to 35 dBm;
- Two tone frequency spacing: 100 KHz;
- Bias: Vgs is 4 V and Vds is 25 V (biased for deep Class AB amplifier).

Figure 4.24 compares the simulated results from the behavioral model and the circuit model for the gain and phase compression. Good agreements are achieved for the 50 ohm case.

Figure 4.25 and Figure 4.26 show the delivered power simulated under loadpull conditions, at two input power levels (10 dBm and 30 dBm). The source reflect

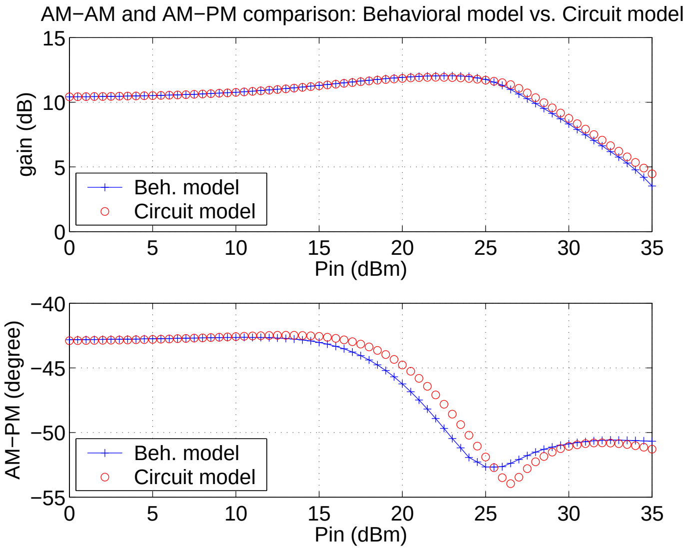

Figure 4.24 Comparison of the simulated gain and phase compression under 50 ohm condition: behavioral model vs. circuit model.

coefficient is set at $-0.55244 - j * 0.23757$. For the small input power level (10 dBm), the behavioral model presents almost identical performance as the circuit model. Even at high power levels (e.g. 30 dBm), the behavioral model still does a good job to predict the drift in the optimal load impedance for the output power.

As one example to demonstrate the importance to have the loadpull AM-PM information in the model creation, two behavioral models were created, one optimized with the AM-PM information and one without.

Figure 4.27 compares the IM3 contours simulated by the behavioral models with and without the AM-PM information. The results are obtained through Envelope simulation of the behavioral model. Obviously, the loadpull AM-PM information does help the large-signal model to do a better job to predict the intermodulation performance. This comparison proves the importance of having the loadpull information for creating a large-signal behavioral model based on loadpull measurements. Notice that not like the previous two example models, the IM3 prediction here doesn't depend on file-based models.

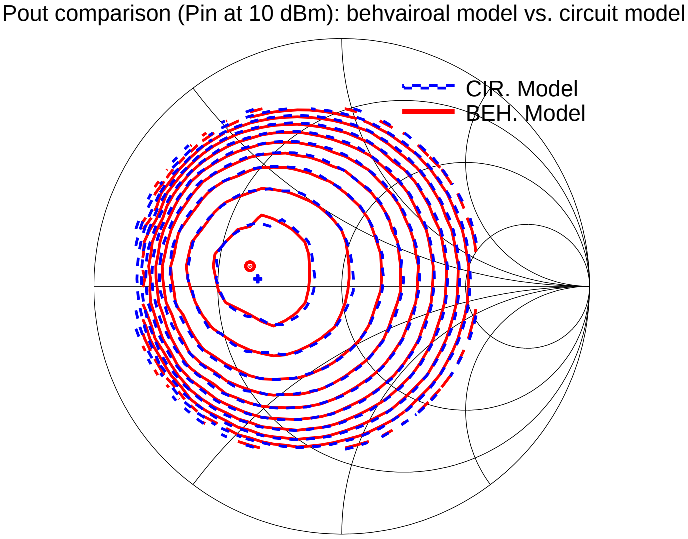

Figure 4.25 Comparison of the simulated Pout contours from the behavioral model and the circuit model at constant Pin of 10 dBm.

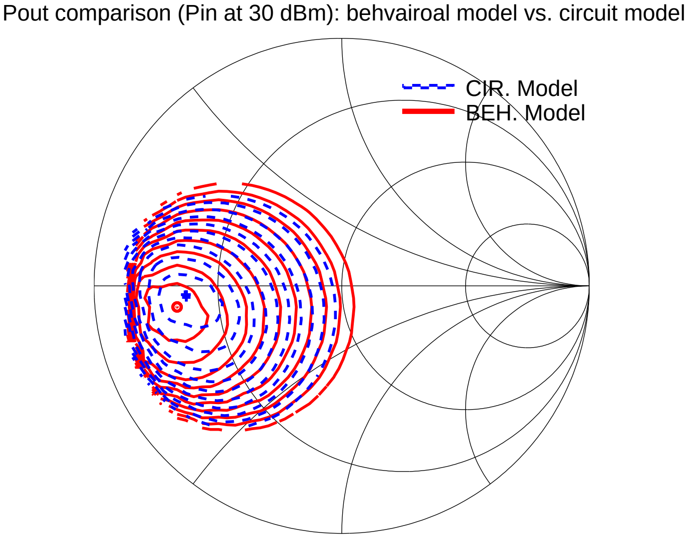

Figure 4.26 Comparison of the simulated Pout contours from the behavioral model and the circuit model at constant Pin of 30 dBm.

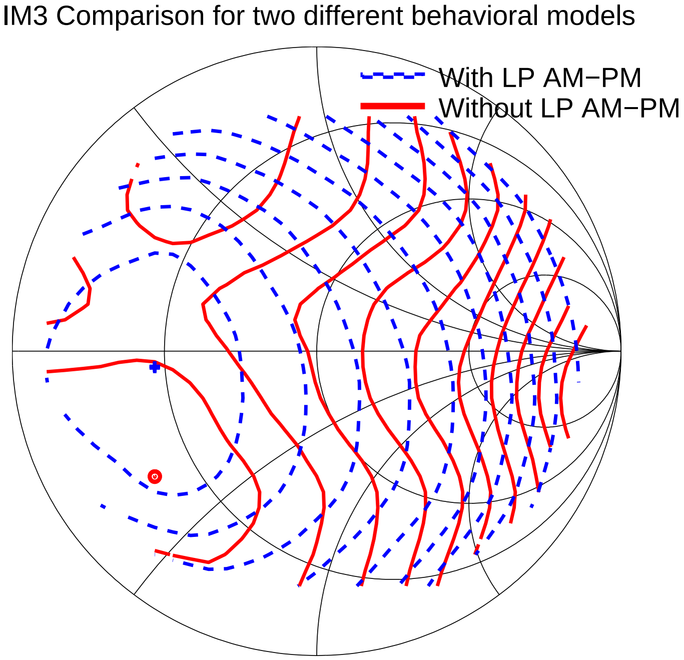

Figure 4.27 Comparison of the simulated IM3 contours from behavioral models: one optimized with loadpull AM-PM information and one without.

Figure 4.28 compares the simulated IM3 contours from the behavioral model (with the AM-PM information) and the circuit model. In general, the model predicts the trend of the IM3 performance. However, since only the fundamental tone is utilized in the model generation, its ability to predict the IM3 is limited. To get better results for the intermodulation products, either file-based model can be used or additional loadpull harmonic measurements will help.

Figure 4.29 evaluates the performance of the behavioral model under two tone stimuli against that of the circuit model. The input power is set to sweep in the simulation. Again, both behavioral models are evaluated. High level agreements can be observed for the simulated datasets from both models.

Notice the difference between the two behavioral models. The model without the AM-PM information predicts a false sweet spot in the IM3 curve. This is avoided through including the AM-PM information in the model generation process.

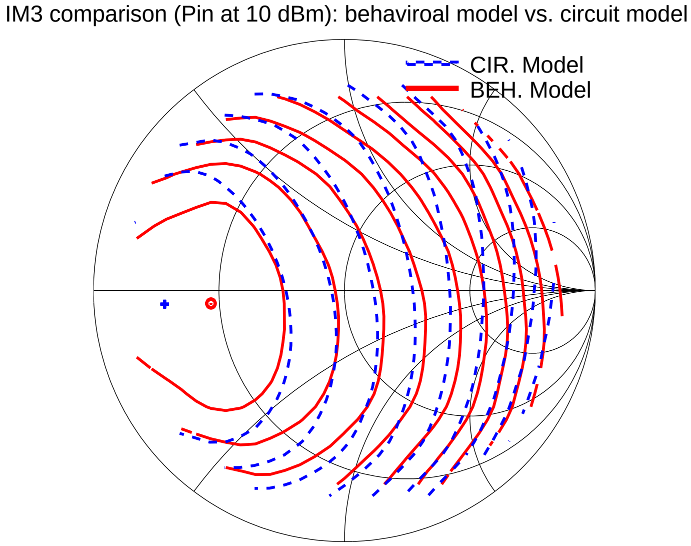

Figure 4.28 Comparison of the simulated IM3 contours from the behavioral and circuit models.

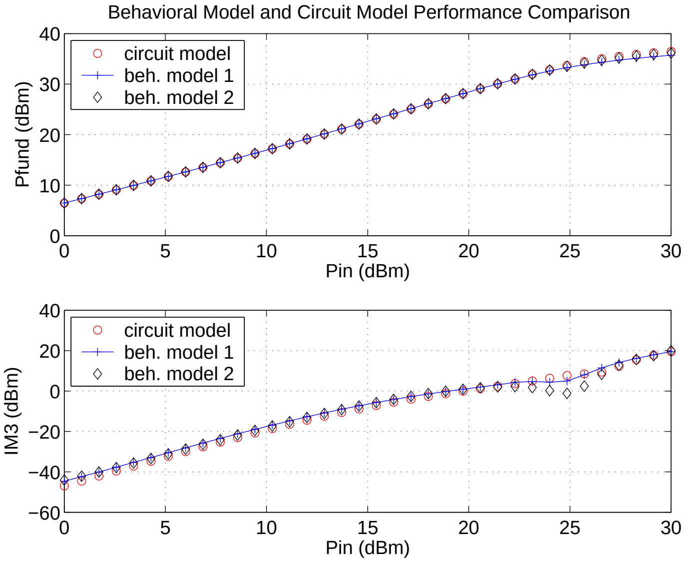

Figure 4.29 Comparison of the simulated IM3 from the circuit model and the behavioral models. Behavioral model 1 is created with the loadpull AM-PM information, while behavioral model 2 isn't. The simulated IM3 Behavioral model 2 shows a fake sweet spot, showing the importance to have the loadpull AM-PM information in the model generation process. The Γ_L is at $-0.80213 - j * 0.08629$.

Table 4.3 Simulation time comparison: behavioral model vs. circuit model. Loadpull harmonic balance simulation at three input power levels is performed for this test.

Type	10 dBm	20 dBm	30 dBm
BEH. Model	2.55 sec	2.66 sec	2.89 sec
CIR. Model	3.08 sec	3.95 sec	4.05 sec

One advantage using behavioral models instead of circuit models is that behavioral models require less simulation time. This will become important when simulating a complete design system, which usually contains dozens of transistors or more.

Table 4.6 compares the simulation time using the behavioral model and the circuit model. The loadpull harmonic balance simulation for 100 load points is performed at three different input power levels: 10 dBm, 20 dBm and 30 dBm. This test was performed on a workstation with a Pentium-4 CPU and 1 GB memory. The behavioral model requires less simulation time, especially at high power levels, as can be observed from the table.

4.7 Conclusion

In this chapter, a behavioral modeling technique is presented that is based directly on the loadpull gain and phase compression measurements. Developed from the large-signal scattering function theory, this technique shows the possibility to generate the large-signal scattering function model using traditional loadpull measurement systems. The large-signal scattering function theory is presented and the analogy between the LSNA and the loadpull measurement systems is drawn. A detail analysis of the model generation process is given out. Three example behavioral models are created to demonstrate the capability of this new technique. Two of them are based on measurements, while one is based on the simulation dataset from a equivalent circuit model. These models are studied from different aspects, including the one tone loadpull and power swept simulation, two tone loadpull and power swept simulation. Good agreements are observed between the model simulated results and measurements, showing the strong capability of this modeling technique.

CHAPTER 5

MEMORY EFFECT MODELING OF POWER AMPLIFIERS IN LOADPULL CONDITIONS

5.1 Introduction

The memory effect in a power amplifier exhibits itself either in the frequency domain as asymmetric spectrum, or time domain as the dynamic AM-AM and AM-PM behavior. This effect is caused by several issues, including input and output tuned network, low frequency dispersion, electrothermal interactions and bias circuitry [3], [4]. The memory effect behavioral modeling of power amplifiers often deals with time domain samples, typically obtained through vector signal analyzers (VSAs) or microwave transition analyzers (MTAs) [39] [79]. The reason to study the test signal in time domain is that the memory effects can be observed easily in time domain through the dynamic AM-AM and AM-PM nonlinear phenomena.

Figure 5.1 shows a typical time domain measurement setup. The baseband I/Q signal is generated through the PC software and downloaded to the arbitrary waveform generator (AWG). The signal generator accepts the modulated signal from the AWG and up-converts it to the desired frequency. The modulated signal is used to drive the DUT; the output signal is down-converted and sampled through the vector signal generator (VSA). The input signal to the DUT can be obtained by directly applying the input signal to the VSA input port. Similar operations, such as down-conversion and sampling, will be performed on the input signal. The input and output samples should be aligned in time so that the correct input-output response can be derived.

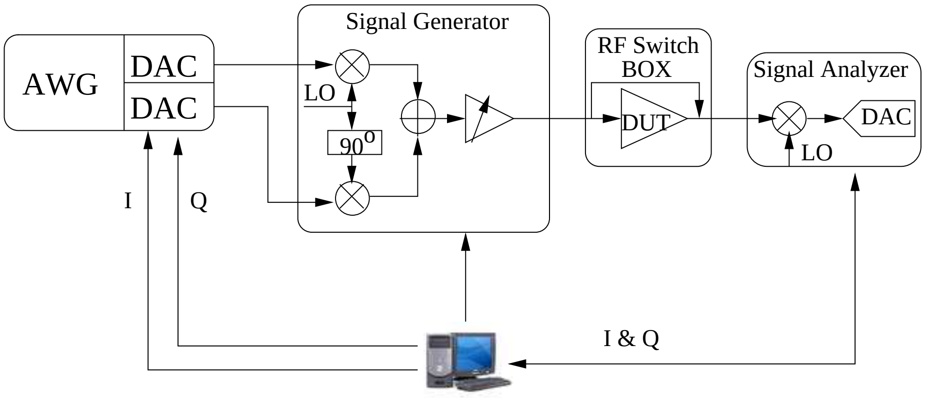

Figure 5.1 Example measurement setup to obtain the time-domain test signal [79].

Once the input and output samples are obtained, the modeling problem is reduced to matching the input samples to the output samples through elaborate mathematical expressions. This has been studied extensively in digital signal processing area [80] [81], although mostly the baseband engineers deal with linear processing. By adding nonlinear blocks in the processing algorithms, a behavioral model can be created that captures both the memory and distortion effects of the amplifier under study.

Lots of modeling techniques have been reported to characterize the memory effect of a power amplifier [34, 79, 82, 83, 84, 85]. Generally speaking, these modeling techniques can be grouped into two categories :

- two-box or three-box modeling techniques [34] [82] and [85] that separate the linear memory effect from the nonlinear behavior and treat them different mathematically; typically, look-up-table or polynomials are used to model the nonlinear gain and phase compression, while linear filtering functions are used to fit the linear memory effect;

- integrated nonlinear modeling techniques [79], [83] and [84], which exploit the capabilities of multi-tap polynomial or dynamic neural network structures to model both the memory effect and the nonlinear gain and compression behavior.

5.1.1 Filtering modeling of memory effects

To simply the modeling problems of the nonlinear amplifiers, the two-box or three-box model structures are proposed that are composed of the linear dynamic time invariant systems and static nonlinear system, e.g [39], [34] and [85]. Successful results have been reported by using these techniques. For example, the method proposed in [82] adopts a two-box modeling structure that has a linear finite impulse filtering (FIR) block and a nonlinear function block. The model diagram is shown in Figure 5.2. The output signal from the FIR block is given in Equation 5.1. This output signal of this memory model can be expressed in Equation 5.2.

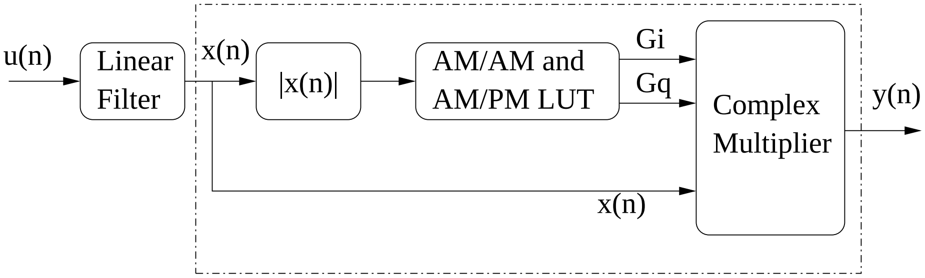

Figure 5.2 Model diagram combining linear filtering and nonlinear LUT sections [82].

$$x(n) = \sum_{i=0}^{M} a_i u(n-i) \tag{5.1}$$

$$y(n) = (G_i + jG_q)x(n) = Gx(n) \tag{5.2}$$

where $x(n)$ and $y(n)$ are the discrete-time input and output samples; the G_i and G_q are the output of the nonlinear block. M represents the memory span determining how many past samples are utilized to predict the current output sample.

Generally, the modeling process utilizing the two-box or three-box structure involves two steps. The first step involves de-embedding the static nonlinearity from the data samples. The second step is to identify the coefficients of the filtering function through optimization.

5.1.2 Neural network modeling of memory effects

Several neural network structures are reported to model the memory effects. One common feature of the reported works is that all of them utilize delayed taps to model the memory effects. The delayed taps are basically a way to combine the current and past values to predict the current output. In general, the output signal can be described by Equation 5.3:

$$y(n) = f_{ANN}[y(n-1), y(n-2), \cdots, y(n-p), x(n), x(n-1), \cdots, x(n-q)] \quad (5.3)$$

where $x(n)$ and $y(n)$ are the discrete-time input and output samples; p and q stand for the memory spans for the input and output samples. f_{ANN} is a nonlinear neural network function.

Isaksson et al [79] proposed using delayed-tap radial basis function neural network (RBFNN) to model the dynamic AM-AM and AM-PM distortion. The RBFNN model can be adjusted through the number of neurons (M) in the hidden layer and the number of delay taps (L) to fit the training series. It is shown in the paper that this type of neural network has better performance than the one-tap parallel Hammerstein model.

Fully recurrent neural network (FRNN) is another type of dynamic neural networks having the capability of learning and then representing the input-output behavior of systems. Luongvinh et al [83] use this network structure to model the memory effects of an amplifier. By using global feedback (feeding the output back to the input), and local interconnections in FRNN (connecting the neurons in the hidden layers), the ability of the network to model nonlinear dynamics of systems can be enhanced. In the reported work [83], a WCDMA signal is used as the training signal. A three-layer FRNN of 10 delay taps and 10 hidden neurons and tanh activation function is constructed.

A time delay neural network (TDNN) is proposed by Ahmed et al [86] to model the memory effect of the PA. The performance of the neural network models utilizing unity and non-unity time delay taps are compared. It is shown that non-unity delay taps will give better results.

Wood et al [87] discusses a modeling method that combines the polynomial based "System Amplifier" model in ADS that models one frequency AM-AM and AM-PM properties and a ANN to model the dynamic properties of the amplifier under test. The ANN is trained upon the difference between the output signals of the System Amplifier and the amplifier under test, over the range of the frequencies and power levels. The dynamical variables that are used are time delays in the port voltages.

5.2 Limitation of current modeling techniques and proposed solution

When we consider using a behavioral model in a simulation, one of the important feature is that the model needs to provide the capability to adjust its performance according to the environment it is embedded in. In this study, the source and load impedances are the main factors that the model should be able to adjust performance to. If we apply this criteria to the techniques discussed above, we will find the limitation of these modeling techniques.

The modeling techniques discussed above deal with power amplifiers operating in one specific load impedance, most likely 50 ohm condition. When the load condition changes, the gain and phase compression properties of the amplifier might change as well. However, the modeling techniques discussed above don't provide the capability to predict this change. This limits the applicability of these models in real world design work, in which the design engineers tend to optimize their products through careful loadpull analysis and matching networks design.

An improved behavioral model is proposed in this chapter to address this limitation. This improved model is basically a two-box model that combines the load-aware large-signal scattering function behavioral model and the linear filtering function model. As shown in Chapter 4, the large-signal scattering function model is capable of predicting the loadpull gain and phase compression. Therefore, it is an excellent candidate. FIR filtering function is utilized to characterize the linear memory effect, similar to [82]. The proposed model is illustrated in Figure. 5.3. The mathematical expression of this model is given in Equation 5.4.

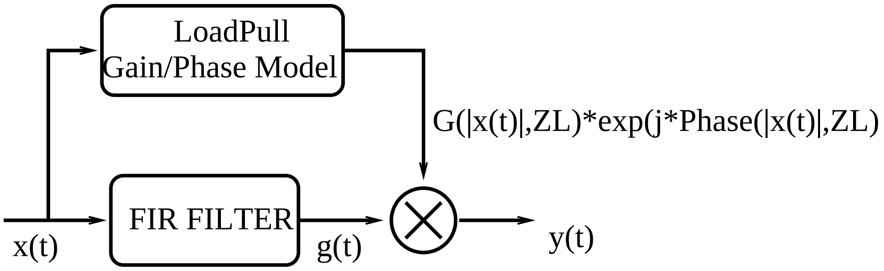

Figure 5.3 Diagram of the proposed memory effect model with the load-related nonlinear gain/compression characterization feature integrated.

$$y(t) = \mathrm{FIR}(x(t)) * G(|x(t)|, Z_L)\mathrm{exp}^{\mathrm{j}\Phi(x(t),Z_L)} \tag{5.4}$$

where $x(t)$ and $y(t)$ are input and output time domain samples; FIR() is the linear filter; $G()$ and $\Phi()$ are the nonlinear gain and phase compression models.

The advantages of this modeling technique includes:

- Compared to the traditional memory effect modeling techniques (as discussed in Section 1), this new technique can adjust the AM-AM and AM-PM nonlinear functions corresponding to the load conditions; this model provides better performance in situations where the load impedance changes;
- Compared to the continuous-wave (CW) loadpull AM-AM and AM-PM model, this new model provides extra capability through the linear block to predict the frequency response of the power amplifier when a wideband modulated signal is applied.

This model diagram is quite similar to the model proposed by Asbeck et al. [88], who used an additional parameter to characterize the dynamic effects associated with time-varying parameters, such as supply voltage or instantaneous temperature. The difference here is that the additional parameter in this new model is the load impedance, that is used to adjust the performance of the nonlinear block.

One important assumption for this modeling structure is that the linear memory effect is independent of the load conditions. The extracted memory effects from different time-domain measured samples at different load impedances should remain the same.

The linear memory effect was conceived to solve the problem with the memoryless narrow-band models such as the AM-AM and AM-PM models. The problem appears when the input signal bandwidth is large enough compared to the system bandwidth, that a CW representation of the system is no longer valid [3].

Therefore, the linear memory effect represents the residual linear frequency response of the system that cannot be characterized by the nonlinear AM-AM and AM-PM models. Conceptually, it is resulted from the frequency response of the input and output tuning network. Since these networks are linear in general, the source and load impedances won't change their behavior. In the proposed model, the linear block will remain constant regardless of the source or load conditions.

5.3 Experimental results

To demonstrate the effectiveness of the proposed model, an example model is developed. Due to the current limitation of the measurement capabilities, the example model is derived from the simulation results of an equivalent circuit transistor model. Specifically, the same Cree 30 Watts LDMOS model discussed previously in Chapter 4 is used in this study.

A 54Mbps WLAN OFDM signal is used as the stimulus to drive the power device. The simulation schematic is shown in Figure 5.4. The simulation setup is listed below:

- RF carrier frequency: 2.17 GHz;
- RF power: 20 dBm;
- Vgs (gate voltage): 4 V;
- Vds (drain voltage): 25 V;
- Time Step: 20 ps;
- Stop Time: 80 us;

The dynamic AM-AM and AM-PM are calculated through Equation 5.5 and 5.6, using the time domain input and output samples. $y(t)$ and $x(t)$ are complex input

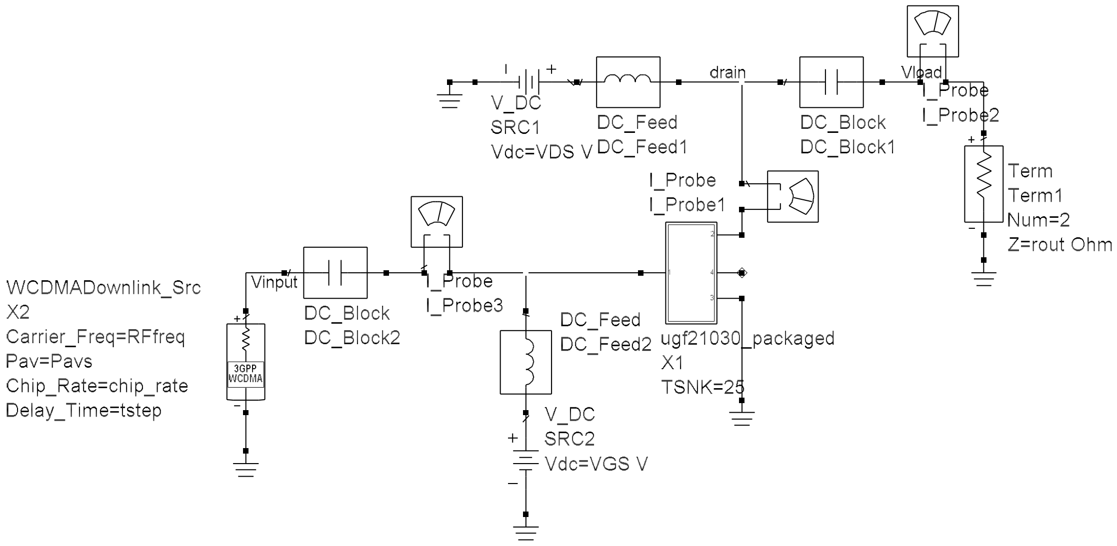

Figure 5.4 Simulation schematic setup: WLAN 54 Mbps OFDM source is used.

and output time samples, respectively. Due to the memory effect, the gain and phase compression will demonstrate dynamic behavior under modulated stimuli, which is shown in Figure 5.5.

$$AM\_AM = \left|\frac{y(t)}{x(t)}\right| \tag{5.5}$$

$$AM\_PM = \Phi\left(\frac{y(t)}{x(t)}\right) \tag{5.6}$$

Figure 5.5 compares the dynamic and static AM-AM and AM-PM performances. By “static”, we mean the AM-AM and AM-PM obtained under CW stimuli. The dynamics shown in the AM-AM and AM-PM obtained under modulated signal stimuli is an evidence of the memory effect.

The linear effect is extracted by subtracting the nonlinear AM-AM and AM-PM from the dynamic curves. Figure 5.6 shows the extracted linear memory effect.

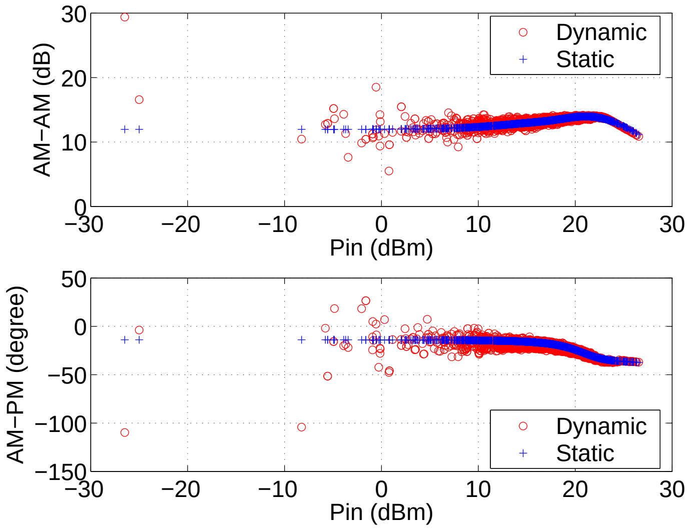

Figure 5.5 Comparison of static and dynamic AM-AM and AM-PM effects. 54 Mbps WLAN signal is used in the modulation simulation setup.

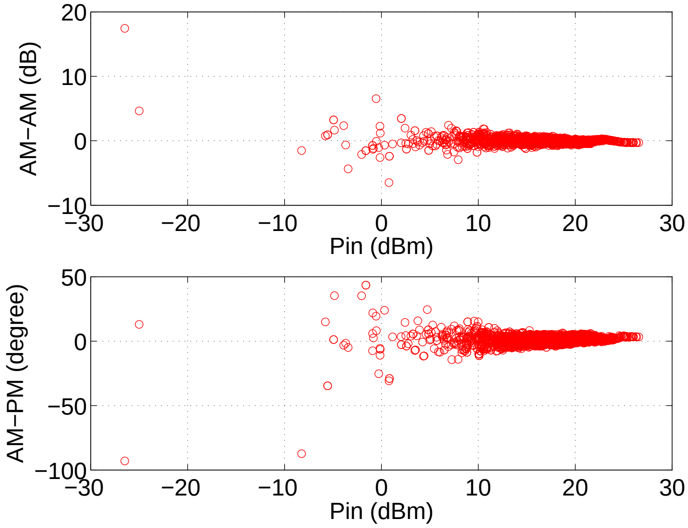

Figure 5.6 Extracted linear memory effect from the dynamic AM-AM and AM-PM effect.

To validate our assumption of the independence of the linear memory on the load impedances, several load impedances are chosen and the simulated results are compared with each other. Figure 5.7 compares the linear memory effects extracted at three different load conditions. The extracted memory effects at these cases demonstrate consistent behavior. The same comparison has been done at several other load conditions; similar results were observed. This consistency proves the validity of the assumption to some extent.

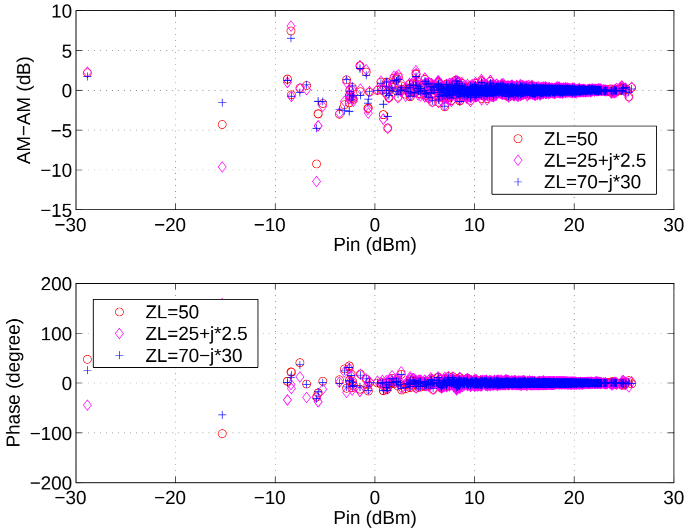

Figure 5.7 The memory effect behaves independently on the load impedances.

The limitation of the traditional memory effect modeling techniques working in a loadpull condition will be demonstrated in Figure 5.8 and Figure 5.9. Suppose we are interested in the performance of an power amplifier at two load impedances. The two loads cause different nonlinear CW AM-AM and AM-PM effects. If the nonlinear block within the model diagram cannot detect the load condition and always uses the same nonlinear function to extract the linear effect, it is very possible that the extracted result won't be linear and will show some residual nonlinearity. Figure 5.8 illustrates this effect.

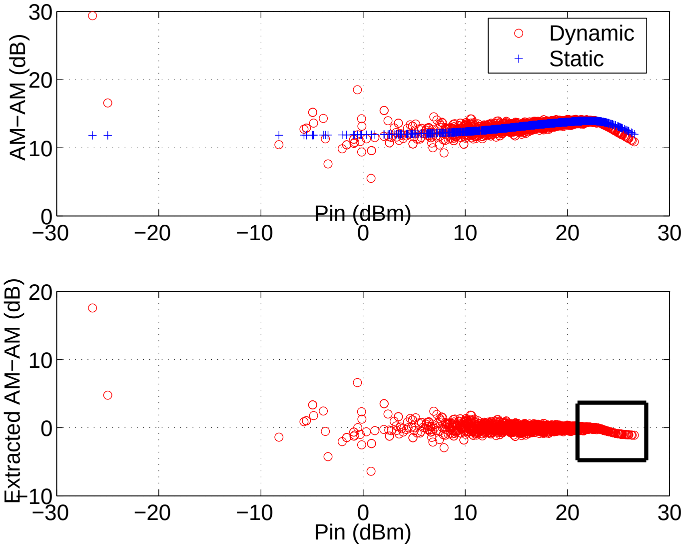

Figure 5.8 Bad extraction of the linear AM-AM and AM-PM distortion.

The nonlinear block in the model is the main contribution to the spectral regrowth. Therefore, if the nonlinear block doesn't reflect the actual AM-AM and AM-PM performance, the predicted spectrum regrowth might be significant different from the desired one, as can be seen in Figure 5.9. Two simulated output spectrums from behavioral models are compared with the simulated result from the circuit model. One of the two behavioral models utilizes the correct AM-AM and AM-PM functions while the other utilizes the AM-AM and AM-PM corresponding to a different load condition. The significant difference between the "bad prediction" and the circuit model simulated result is caused by the nonlinear modeling.

A behavioral model based on the simulation datasets of the LDMOS model is developed. The nonlinear block is the same model as used in chapter 4, which is a large-signal scattering function model derived from the loadpull gain and phase compression simulation. The linear memory effect is characterized by a 5-tap FIR filter. The coefficients are fitted to the extracted linear memory effect. The model is implemented in ADS using the FDD component.

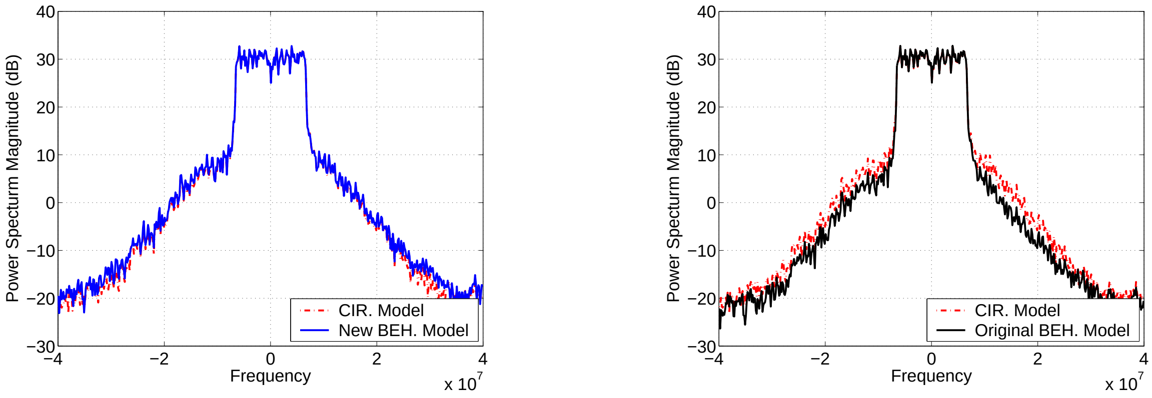

(a)

(b)

Figure 5.9 Illustration of influence of nonlinear AM-AM and AM-PM compression on the output spectrum. In (a), the new model can adjust its nonlinear AM-AM and AM-PM model to adapt to the load condition and predict the spectrum correctly. In (b) the traditional two-box model cannot predict the spectrum correctly because its nonlinear model is developed for 50 ohm. The simulated load impedance is 67.0 + j* 93.8 ohm.

To demonstrate the limitation of the CW loadpull model predicting the dynamics of the AM-AM and AM-PM performance, Figure 5.10 compares the simualted results from the new behavioral model with the linear block and the CW loadpull model. As can be seen, the dynamic effect of the circuit model is captured through the addition of the linear block, which is not predicted by the CW model.

Figure 5.11 compares the predicted memory effect from the linear filtering block with the extracted data. The 5-tap model parameter is listed in Table 5.3.

Table 5.1 The optimized 5-tap FIR coefficients.

B1	B2	B3	B4	B5
0.8787	0.0744	0.1144	-0.1027	0.0343

Figure 5.12 compares the simulated output signal from the behavioral model with that of the circuit model. The modulated signal is a 54 Mbps WLAN signal (which uses 64 QAM modulation). The two datasets present good agreement.

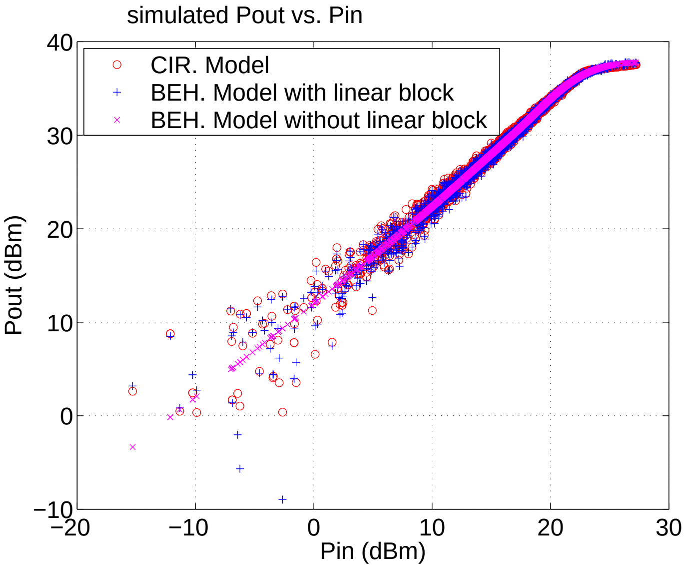

Figure 5.10 Illustration of the effect of the linear block. By adding the linear block to the nonlinear model, the new model can predict the dynamics shown in the AM-AM and AM-PM performance. This is not captured by the CW loadpull model.

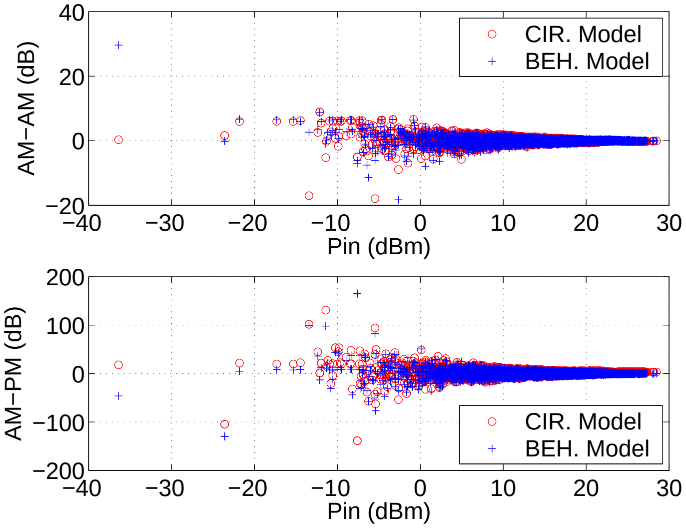

Figure 5.11 Comparison of the simulated linear memory effect: circuit model vs. behavioral model.

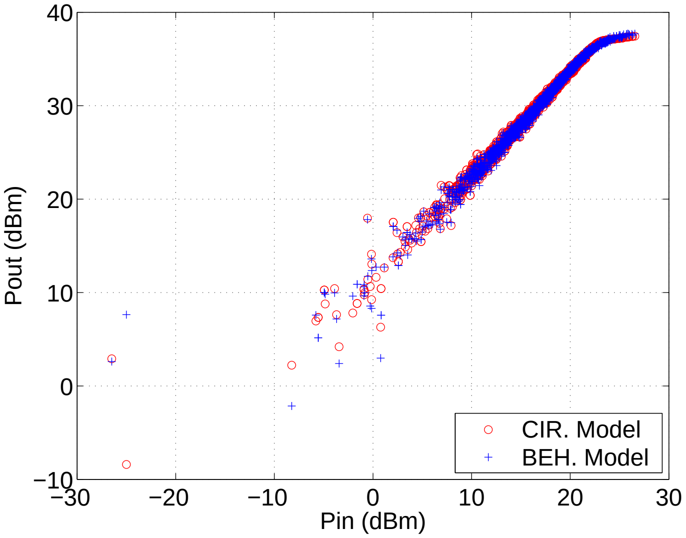

Figure 5.12 Comparison of the simulated output power: behavioral model vs. circuit model. 54 Mbps WLAN signal is used as the input signal.

To explore the capability of this behavioral model to handle different modulated signals, a 6 Mbps WLAN signal (QPSK modulated) is used as the input signal in the simulation. Figure 5.13 compares the results and verifies that the behavioral model can handle different modulated signals.

Figure 5.14 shows the comparison of the output spectrums obtained from the behavioral model and the circuit model. The output spectrums from two models are very similar. This is expected because the simulated time samples from the two models agree to each other very well and that the spectrum is obtained through Fourier analysis of the time domain signal.

The ACPR associated with the upper and lower sideband is simulated for three load impedances, i.e. 67.0 + j* 93.8 ohm, 50 ohm and 5 ohm. Table 5.2 and Table 5.3 compare the simulated lower and upper ACPR of the circuit model with that of the behavioral model. The average input power is set at 20 dBm. The load is 67.0 + j* 93.8 ohm. The newly proposed model presents better performance against the traditional two-box model, since the traditional two-box model cannot adapt its

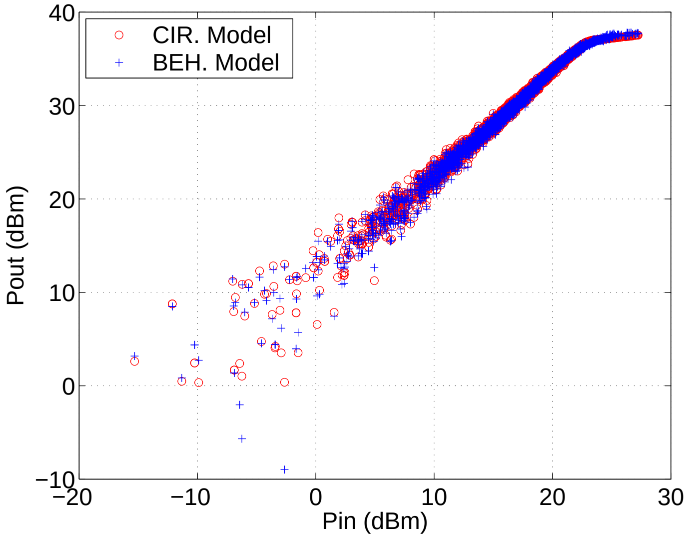

Figure 5.13 Verification of the behavioral model with a 6 MBps WLAN signal. The simulated output signals from both behavioral model and circuit model match very well.

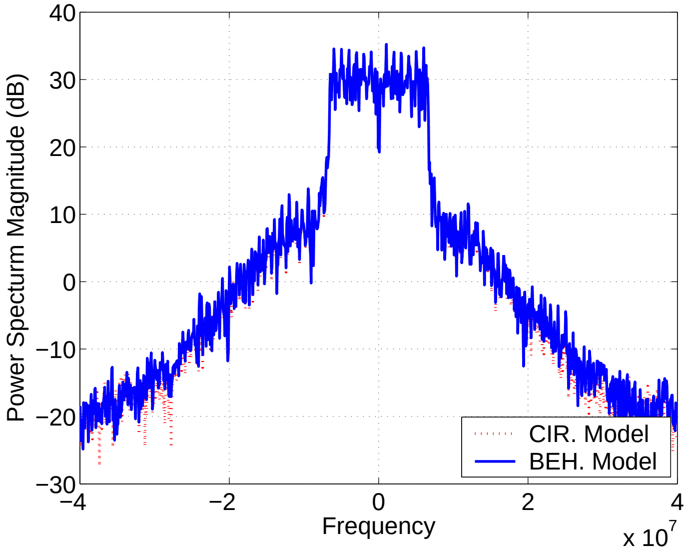

Figure 5.14 Comparison of the simulated and measured output spectrum of the example power amplifier.

performance with respect to the load conditions. Compared to the CW loadpull model, the new model has better prediction, due to the addition of the linear block.

Table 5.2 Comparison of the simulated ACPR for lower sideband (67.0+j*93.8 ohm). Average input power is set at 20 dBm.

	Lower Sideband	Difference
Circuit model	-34.477	
Loadpull two-box beh. model	-33.516	0.961
Traditional two-box beh. model	-37.003	2.526
CW loadpull beh. model	-33.241	1.236

Table 5.3 Comparison of the simulated ACPR for upper sideband (67.0+j*93.8 ohm). Average input power is set at 20 dBm.

	Upper Sideband	Difference
Circuit model	-33.639	
Loadpull two-box beh. model	-33.215	0.324
Traditional two-box beh. model	-35.682	2.043
CW loadpull beh. model	-32.72	0.919

Table 5.4 and Table 5.5 compare the simulated lower and upper ACPR of the circuit model with that of the behavioral model. The load is 50 ohm. For this case, the traditional and the new two-box loadpull model have the same performance, because the nonlinear blocks in both models characterize the AM-AM and AM-PM at 50 ohm very well.

Table 5.4 Comparison of the simulated ACPR for lower sideband (50 ohm). Average input power is set at 20 dBm.

	Lower Sideband	Difference
Circuit model	-37.513	
Loadpull two-box beh. model	-37.003	0.51
Traditional two-box beh. model	-37.003	0.51
CW loadpull beh. model	-36.610	0. 903

Table 5.5 Comparison of the simulated ACPR for upper sideband (50 ohm). Average input power is set at 20 dBm.

	Upper Sideband	Difference
Circuit model	-35.188	
Loadpull two-box beh. model	-35.682	0.494
Traditional two-box beh. model	-35.682	0.494
CW loadpull beh. model	-36.17	0.982

The upper and lower ACPR simulated from different models at 5 ohm load are compared in Table 5.6 and Table 5.7. As can be seen, the new model predicts the ACPR better than the other two behavioral models.

Table 5.6 Comparison of the simulated ACPR for lower sideband (5 ohm). Average input power is set at 20 dBm.

	Lower Sideband	Difference
Circuit model	-33.573	
Loadpull two-box beh. model	-32.805	0.767
Traditional two-box beh. model	-37.003	3.43
CW loadpull beh. model	-32.423	1.15

Table 5.7 Comparison of the simulated ACPR for upper sideband (5 ohm). Average input power is set at 20 dBm.

	Upper Sideband	Difference
Circuit model	-32.489	
Loadpull two-box beh. model	-32.073	0.416
Traditional two-box beh. model	-35.682	3.193
CW loadpull beh. model	-31.767	0.722

5.4 Conclusion

In this chapter, we proposed a new behavioral model to characterize the memory effect in loadpull conditions. This new model combines the load-aware large-signal scattering function model developed in Chapter 4 with a linear filtering block. This model has the same two-box structure as some of the traditional modeling techniques do. The reason to include the load dependency as the additional feature to the existing two-box modeling technique is to capture the load-related gain and phase compression variation. Without this capability, the linear memory effect may not be extracted correctly, as demonstrated in Figure 5.8. Also without this load-aware capability, the model is not suitable for some applications where engineers might experience different load conditions to optimize their designs.

An example behavioral model is created based on the simulation results of an LDMOS circuit model. Results have been given to demonstrate the improvement of the new model over the traditional memory models and the CW loadpull model. The performance of the new model to predict the output signals from the power device under wideband modulated signals (WLAN) is compared to the circuit model performance. Good prediction of the output spectrums and ACPRs is observed. From these comparison results, the model shows promise for real world applications. A program has been developed in Matlab to automate the model generation process.

CHAPTER 6

CONCLUSIONS AND FUTURE STUDY

6.1 Conclusions

Behavioral modeling has received significant interest recently. This is primarily because of the changes in the current design practices. More and more engineers tend to use off-shelf IC blocks, such as LNAs and PAs, in their designs to simplify the product structure, minimize the discrete components, reduce design complexity, and cut the time to market. This new design methodology generates significant demand for accurate behavioral models for these blocks, since it is often the case that the details of the circuit are proprietary and models are not provided along with the devices. Power amplifiers are the main component of interest in this dissertation.

Through the literature review given in Chapter 2, it is found that most of the reported behavioral models are not suitable for many practical applications. One of the specific feature that is missing is the capability to work adaptively in a loadpull condition. The previously proposed models deal with constant load condition (usually 50 ohm) and don't provide the capabilities to adjust the model behavior with respect to varying source and load impedances. On the other hand, engineers tend to study these off-shelf components under different load conditions to optimize their designs. Therefore, there is a gap between the academic research results and many practical applications.

Large-signal scattering function theory provides an elegant solution to this problem by studying the nonlinear effects of the amplifier under realistic driving signals. Specific instrumentations have been developed to generate this kind of model. Since the limit access to the instrument, this theory hasn't been widely accepted yet.

The primary focus of this dissertation is to come up with a practical and low-cost behavioral modeling technique based on the widely available measurement systems (in this research, the loadpull measurement systems are of interest). The main feature that is pursued is the capability to predict the loadpull performances of IC blocks.

The proposed modeling technique is based on loadpull gain and phase compression measurements. AM-AM measurement under various load conditions is a common routine in current loadpull measurement systems. However, AM-PM loadpull measurement hasn't received as much attention. It is found in this dissertation that this information is important for deriving accurate behavioral models to predict the nonlinear effects of power amplifiers. By incorporating these two measurement datasets in the modeling process, it is possible to create a behavioral model that can capture the load-related nonlinearities of a power amplifier.

Three example behavioral models are developed using this technique. The first two models are derived from loadpull AM-AM and AM-PM measurements. The performance of the derived models are compared with simple large-S21 models. According to the results, the new models provide better prediction of gain compression at different load conditions than the large-S21 models do. By applying a file-based model, the models can reproduce the intermodulation products. The capability of the large-S21 models predicting the IM3 performance is, however, limited.

The third example model is given as a demonstration on how to create an abstract behavioral model from a circuit-level model. The example model is derived from the simulated loadpull AM-AM and AM-PM datasets. It is verified under different conditions, including 50 ohm gain and phase compression, one-tone loadpull and two-tone loadpull simulations. The results show good agreements between the simulated datasets from the circuit-level model and the abstracted behavioral model.

The second problem this dissertation tackles is to improve the loadpull model developed in Chapter 4 to include the memory effect modeling capability. As presented in the literature review, the current memory effect modeling techniques haven't taken into account the load-related gain and phase compression performance of a power amplifier. Most of the models can only work properly in one load condition, typically 50ohm. When the load is changed, it is very likely that the models will fail.

To fix the problem, one can simply add a load-aware nonlinear model, like the one proposed in Chapter 4, and combine it with the linear block. The new model assumes the same two-box structure. The resulted model can be flexible enough to be applied in varying load situations. One important assumption for this modeling technique is that the linear memory effect is independent on the load conditions, which is confirmed through the simulation result of an LDMOS circuit model.

An example behavioral model is derived based on a LDMOS circuit model simulation results. The upper and lower ACPRs are simulated and compared with different behavioral models. According to the example results, the loadpull model with the memory effect captured shows its advantage in predicting the spectral regrowth and ACPR, compared with the traditional two-box model as well as the CW loadpull model.

6.2 Recommendation for future studies

Although the proposed modeling technique has solved some problems, there are still lots of areas that can be improved.

First of all, the proposed modeling technique is based on the loadpull AM-AM and AM-PM measurements. According to the analysis of the modeling technique given in Chapter 4, only the fundamental tones at the input and output ports of the power amplifier under study are correlated through the incident and scattering wave variables. No harmonics are taken into account during the model creation process.

Therefore, the resulted model, even though being capable of predicting the compression properties correctly, cannot predict the time domain input and output signal correctly. The time domain signal predicted by the model will be a perfect sinusoidal signal. However, the actual time domain signals at the input and output ports are no longer sinusoidal signals when the input signal is high. They are composed of multiple harmonics, depending on how hard the device is driven.

One approach to re-create the distorted time-domain signal is to take the higher harmonics into account at both the input and output ports, just like the large-signal scattering function modeling technique proposed in [47, 71]. Harmonic loadpull measurement may be useful towards this improvement. The improvement comes at the cost of increasing complexity in the model and the required measurements, which also makes the model difficult to be derived and applied in practical applications.

This harmonic loadpull measurements can be done through traditional loadpull measurement systems or through the LSNA system. The LSNA system, in essence, is an active loadpull measurement system. It offers integrated calibration and measurement capabilities that are powerful and flexible to meet different requirements. It also provides post-analysis capability to process the measured data and display in appropriate formats. By using a LSNA, it would be easier to get a complete large-signal scattering function model. The down-side of this approach is its high cost and therefore limited accessability.

The proposed loadpull memory model has been proven to be able to give better prediction of the power amplifier performance under digital modulated signals than traditional . The results given in Chapter 5 are based on simulation datasets. Theoretically the memory effect is independent on the load conditions. However, this hasn't been verified experimentally, due to the instrument limitation. A two port vector signal analyzer is required to verify this statement experimentally. The main purpose to have this instrument is to sample and measure the input and output signal synchronously. Otherwise, some digital processing steps are required to align the input and output streams.

Two steps are involved in the measurement to study the load effect on linear memory effect. The input and output signals of the power amplifier under study should be sampled and measured simultaneously at various load conditions. The linear memory effect can be extracted by removing the nonlinear AM-AM and AM-PM effects from the output signal samples. For each load condition, the corresponding AM-AM and AM-PM compression curves measured using the CW signal is used in the extraction process. The remaining signal after the extraction is the linear memory effect for different load conditions. By comparing these signals, we can find out whether the load conditions will have significant effects on the linear memory performance. The experimental verification of the loadpull memory model will be another area for the future study.

Currently the proposed memory effect model has a two-box structure. However, according to [3], the two-box structure has limitations in predicting the nonlinear memory effect, or long-term memory effect. A dynamic feedback path is required to represent this effect attributed to electrothermal and/or bias circuitry dynamics. The limitation of the two-box structure is one of the reason for the differences observed between the ACPRs simulated from the new model and the circuit model. Therefore, it would be interesting to see how the addition of the feedback path into the model helps improving the model performance.

REFERENCES

[1] D. Root, J. Wood, and N. Tufillaro, "New techniques for non-linear behavioral modeling of microwave/rf ics from simulation and nonlinear microwave measurements," in *Proc. Design Automation Conference, 2003*, June 2003, pp. 85–90.

[2] P. Wambacq and W. Sansen, *Distortion Analysis of Analog Integrated Circuits.* Boston, MA: Kluwer Academic Publishers, 1998.

[3] J. C. Pedro and S. A. Maas, "A comparative overview of microwave and wireless power-amplifier behaviroal modeling approaches," *IEEE Trans. Microwave Theory Tech.*, vol. 53, pp. 1150–1163, Apr. 2005.

[4] J. C. Pedro and N. B. Carvalho, *Intermodulation Distortion in Microwave and Wireless Circuits.* Norwood, MA: Artech House, 2003.

[5] J. S. Kenney, W. Woo, L. Ding, R. Raich, H. Ku, and G. T. Zhou, "The impact of memory effects on predistortion linearization of RF power amplifiers," in *Proc. of the 8th Int. Symp. on Microwave and Optical Techn.*, Montreal, Canada, June 2001, pp. 189–193.

[6] F. Launay, Y. Wang, and S. Toutain, "M-ary PSK signal power spectrum at the output of a nonlinear power amplifier," in *Proc. IEEE MTT-S*, vol. 3, Seattle, WA USA, June 2002, pp. 2197–2200.

[7] H. Lai and Y. Bar-Ness, "Minimum distortion power polynomial model (MDP-PM) of nonlinear power amplifiers and its application on analog predistorters," in *Proc. IEEE VTC '99*, vol. 3, Amsterdam Netherlands, Sept. 99, pp. 1501–1505.

[8] H. Songbai, L. Mingyu, D. Hongmin, and Y. Juebang, "Analysis of CDMA RF channel nonlinear distortion," in *Proc. IEEE Comm. Circuits and Systems and West Sino Expositions '02*, vol. 1, July 2002, pp. 474–477.

[9] A. Springer, T. Frauscher, B. Adler, D. Pimingsdorfer, and R. Weigel, "Impact of nonlinear amplifiers on the UMTS system," vol. 2, Sept. 2000, pp. 455–460.

[10] Y. Guo and J. Cavallaro, "Post-compensation of RF non-linearity in mobile OFDM systems by estimation of memory-less polynomial," in *Proc. IEEE ISCAS '02*, vol. 1, May 2002, pp. 26–29.

[11] F.-L. Lin, S.-F. Chen, L.-F. Chen, and H.-R. Chuang, "Computer simulation and measurement of error vector magnitude (EVM) and adjacent-channel power ratio (ACPR) for digital wireless communication RF power amplifiers," in *Proc. IEEE VTC '99*, vol. 4, Sept. 1999, pp. 2024–2028.

[12] G. Zhou, "Analysis of spectral regrowth of weakly nonlinear power amplifiers," vol. 4, 2000, pp. 357–359.

[13] A. Saleh, "Frequency-independent and frequency-dependent nonlinear models of TWT amplifiers," *IEEE Trans. Commun.*, vol. 29, pp. 1715–1720, Nov. 1981.

[14] I.-S. Park, E. Powers, and G. Xu, "Parallel adaptive predistortion for RF power amplifier linearization," in *Proc. IEEE Globecom '97*, vol. 1, Nov. 1997, pp. 3–8.

[15] J. Li and M. Kavehrad, "OFDM-CDMA systems with nonlinear power amplifier," in *Proc. IEEE WCNC '99*, vol. 13, New Orleans, LA USA, Sept. 1999, pp. 1167–1171.

[16] M. Tummla, M. Donovan, B. Watkins, and R. North, "Volterra series based modeling and compensation of nonlinearities in high power amplifiers," in *Proc. IEEE ICASSP '97*, vol. 3, Munich, Germany, Apr. 1997, pp. 2417–2420.

[17] K.-S. Jin, Y. Shin, and S. Im, "A predistorter for nonlinear distortion in multicode CDMA systems," in *Proc. 9th IEEE International Symposium on personal, indoor and mobile radio communications, 1998*, vol. 3, Boston, MA USA, Sept. 1998, pp. 1481–1485.

[18] G. White, A. Burr, and T. Javornik, "Modeling of nonlinear distortion in broadband fixed wireless access systems," *Electronics Letters*, vol. 39, pp. 686–687, Apr. 2003.

[19] A. Ghobani and M. Sheikhan, "The effects of solid state power amplifier (SSPA) nonlinearities on M-PSK and M-QAM signal transmission," in *6th Int. Conf. on Digital Processing of Signals in Communications*, Loughborough, UK, 1991, pp. 193–197.

[20] C. Rapp, "Effects of HPA-nonlinearity on a 4-DPSK/OFDM-signal for a digital sound broadcasting system," in *Proc. of 2nd European Conf. on Satellite Communications*, Liege, Belgium, Oct. 1991, pp. 179–184.

[21] *Internal technical report on behavioral modeling project for low noise amplifiers, Modelithics, inc, Tampa, FL, 2003.*

[22] S. Hischke and J. Habermann, "New results on the effects of nonlinear amplifiers on DOQPSK and pi/4-DQPSK signals," in *Proc. 9th IEEE International Symposium on personal, indoor and mobile radio communications, 1998*, vol. 3, Boston, MA USA, Sept. 1998, pp. 1481–1485.

[23] J. O'Toole and T. Brazil, "Novel neural network-bessel transform for behavioural modelling of a power amplifier," in *High Frequency Postgraduate Student Colloquium 2000*, Dublin Ireland, Sept. 2000, pp. 45–50.

[24] A. Pages-Zamora, M. Lagunas, and T. Jimenez, "Memoryless predistortion of nonlinear amplifiers based on fourier series based models," in *Proc. 8th IEEE Signal Processing Workshop on Statistical Signal and Array Processing, 1996*, Corfu Greece, June 1996, pp. 375–378.

[25] Honkanen, M., and S. G. Haggman, "New aspects on nonlinear power amplifier modeling in radio communication system simulations," in *8th IEEE International Symposium on Personal, Indoor and Mobile Radio Communications, 1997.*, vol. 3, Helsinki Finland, Sept. 1997, pp. 844–848.

[26] M. Honkanen, O. Pollanen, J. Tanskanen, E. Jarvinen, and S. G. Haggman, "Comparison of measured and simulated pi/4-DQPSK adjacent channel power using a functional high power amplifier model," in *Proc. 48th IEEE VTC '98*, vol. 3, Ottawa, Ont. Canada, May 1998, pp. 2459–2463.

[27] H. Ku and J. S. Kenney, "Behavioral modeling of power amplifiers considering IMD and spectral regrowth asymmetries," in *IEEE MTT-S digest*, vol. 2, June 2003, pp. 799–802.

[28] T. S. L. Goh, R. D. Pollard, and S. Boussakta, "ACPR prediction of multi-carrier systems through behaviroural modelling of power amplifiers using measured two-tone transfer characteristics and statistical techniques."

[29] H. Ku, M. Mckinglet, and J. S. Kenney, "Extraction of accurate behavioral modeling for power amplifiers with memory effects using two-tone measurements," in *IEEE MTT-S digest*, vol. 2, June 2002, pp. 983–986.

[30] J. Liu, H. Arslan, and L. P. Dunleavy, "Adaptive power amplifier model and its usage in ofdm system," in *Topical Conference on Wireless Communication Technology '03*, Oct. 2003.

[31] J. Liu, H. Arslan, L. P. Dunleavy, A. Webster, and J. Paviol, "Impact of carrier frequency depedent power amplifier behavior on 802.11a wlan system," in *Proceedings of European Microwave conference*, Oct. 2004.

[32] H. B. Poza, Z. A. Sarkozy, and H. L. Berger, "A wideband data link computer simulation model," in *Proc. NAECON Conf, 1975.*

[33] C. J. Clark, C. P. Silva, A. A. Moulthrop, and M. S. Muha, "Power-amplifier characterization using a two-tone measurement technique," *IEEE Trans. Microwave Theory Tech.*, vol. 50, pp. 1590–1602, June 2002.

[34] F. Launay, Y. Wang, S. Toutain, S. Barataud, J. Nebus, and R. Quere, "Nonlinear amplifier modeling taking into account HF memory frequency," in *Proc. IEEE MTT-S '02*, vol. 2, Seattle, WA USA, June 2002, pp. 865–868.

[35] C. Silva, C. Clark, A. Moulthrop, and M. Muha, "Optimal-filter approach for nonlinear power amplifier modeling and equalization," in *Microwave Symposium Digest., 2000 IEEE MTT-S International*, vol. 1, Boston, MA USA, June 2000, pp. 437–440.

[36] J. Ibanez-Diaz, C. Pantaleon, I. Santamaria, T. Fernandez, and D. Martinez, "Nonlinearity estimation in power amplifiers based on undersampled temporal data," in *Proc. 17th IEEE Instrumentatioin and Measurement Technology Conference, 2000*, vol. 3, Baltimore, MD USA, May 2000, pp. 1266–1271.

[37] E. Aschbacher and M. Rupp, "Modeling and identification of nonlinear power-amplifier with memory for nonlinear digital adaptive pre-distortion," in *Proc. of IEEE SPAWC workshop, 2003*, Rome, Italy, June 2003.

[38] E. G. Jeckeln, H.-Y. Shih, E. Martony, and M. Eron, "Method for modeling amplitude and bandwidth dependent distortion in nonlinear RF devices," in *2003 IEEE MTT-S Digest*, vol. 3, June 2003, pp. 1733–1736.

[39] C. J. Clark, G. Chrisikos, M. S. Muha, A. A. Moulthrop, and C. P. Silva, "Time-domain envelope measurement technique with application to wideband power amplifier modeling," *IEEE Trans. Microwave Theory Tech.*, vol. 46, pp. 2531–2540, Dec. 1998.

[40] M.S.Muha, C. Clark, A.A.Moulthrop, and C.P.Silva, "Validation of power amplifier nonlinear block models," in *1999 IEEE MTT-S Digest*, vol. 2, June 1999, pp. 759–762.

[41] N. Borges de Carvalho and J. Pedro, "A comprehensive explanation of distortion sideband asymmetries," *IEEE Trans. Microwave Theory Tech.*, vol. 50, pp. 2090–2101, Sept. 2002.

[42] H. Ku, M. D. McKinley, and J. S. Kenney, "Quantifying memory effects in RF power amplifiers," *IEEE Trans. Microwave Theory Tech.*, vol. 50, pp. 2843–2849, Dec. 2002.

[43] C. Maziere, T. Reveyrand, S. Mons, D. barataud, J. Nebus, R. Quere, A. Mallet, L.Lapierre, and J. Sombrin, "A novel behavorial model of power amplifier based on a dynamic envelope gain approach for the system level simulation and design," in *2003 IEEE MTT-S Digest*, vol. 2, June 2003, pp. 769–772.

[44] A. Cidronali, C. Accillaro, M. Myslinski, D. Schreurs, and G. Manes, "A state-space modeling approach for dynamic nonlinear microwave system based on large signal time domain measurements," in *IEEE MTT-S Digest*, June 2005.

[45] D. Root, J. Wood, N. Tufillaro, D. Schreurs, and A. Pekker, "Systematic behavioral modeling of nonlinear microwave/rf circuits in the time domain using techniques from nonlinear dynamic systems," in *Proceedings of the 2002 IEEE International Workshop on BAMS*, Oct. 2002, pp. 71–74.

[46] S. A. Maas, *Nonlinear Microwave Circuits.* Boston, MA: Artech House, 1988.

[47] J. Verspecht, M. V. Bossche, and F. Verbeyst, "Characterizing components under large signal excitation: defining sensible 'large signal s-parameters'?!" in *49th ARFTG Conference Digest*, June 1997, pp. 109–117.

[48] J. Verspecht and P. V. Esch, "Accurately characterizing hard nonlinear behavior of microwave components with the nonlinear network measurement system: Introducing 'nonlinear scattering functions'," in *Proceedings of the 5th International Workshop on Integrated Nonlinear Microwave and Millimeterwave Circuits*, Oct. 1998, pp. 17–26.

[49] J. Verspecht, "Everything you've always wanted to know about hot-s22 (but we're afraid to ask)," in *Workshop at the International Microwave Symposium*, June 2002.

[50] Maury Microwave Corporation, Ontario, CA, USA, www.maurymicrowave.com.

[51] Focus Microwaves inc., Dollard-des-Ormeaux, Quebec, Canada, www.focus-microwaves.com.

[52] J. F. Sevic, G. Albright, W. Schuerch, and G. M. Simpson, "Simultaneous load-pull and real-time infrared thermal imaging of RF/Microwave power transistors," *Proceedings of 63th ARFTG Conference*, pp. 13–20, 2004.

[53] C. Clark, G. Chrisikos, M. Muha, A. Moulthrop, and C. Silva, "Time-domain envelope measurement technique with application to wideband power amplifier modeling," *IEEE Transactions on Microwave Theory and Techniques*, vol. 46, pp. 2351–2540, Dec. 1998.

[54] J. Liu, L. P. Dunleavy, and H. Arslan, "Exploration of power amplifier performance using a digital demodulation loadpull measurement procedure," in *Proceedings of ARFTG conference*, June 2005.

[55] J. S. Park, S. R. Park, H. J. Roh, and K. H. Koo, "Power amplifier back-off analysis with am-to-pm for millimeter-wave ofdm wireless lan," in *Proc. IEEE RAWCON '01*, Waltham, MA USA, Aug. 2001, pp. 189–192.

[56] S. Cripps, "A theory for the prediction of gaas fet load-pull power contours," in *Microwave Symposium Digest, MTT-S International*, vol. 83, May 1983, pp. 221–223.

[57] F. Raab, P. Asbeck, S. Cripps, P. Kenington, Z. Popovic, N. Pothecary, J. Sevic, and N. Sokal, “Power amplifiers and transmitters for rf and microwave,” *IEEE Trans. Microwave Theory Tech.*, vol. 50, pp. 814–826, Mar. 2002.

[58] *8719D, 8720D and 8722D Network Analyzer User's Guide*, Agilent Technologies, inc., Feb 1999.

[59] “Using Vector Modulation Analysis in the Integration, Troubleshooting and Design of Digital RF Communication Systems,” Product note HP 89400-8.

[60] M. McKinley, K. Remley, M. Myslinski, J. Kenney, D. Schreurs, and B. Nauwelaers, “EVM calculation for broadband modulated signals,” *Proceedings of 64th ARFTG Conference*, pp. 45–52, Dec. 2004.

[61] S. Yamanouchi, K. Kunihiro, and H. Hida, “An Efficient Algorithm for simulating Error Vector Magnitude in Nonlinear OFDM Amplifiers,” *IEEE Custom Integrated Circuits Conference*, pp. 129–132, 2004.

[62] C. Lee, V. Postoyalko, and T. O'Farrell, “Analysis and Simulation of AM-AM/PM Nonlinear Distortion due to Direct Laser Modulation in Radio over Fiber Systems,” *International Topical Meeting on Microwave Photonics*, pp. 137–140, Nov. 2002.

[63] A. Webster, J. Liu, H. Arslan, L. Dunleavy, and J. Paviol, “Measurement-based Modeling of a 5 GHz WLAN Transmitter,” *Proceedings of IEEE RAWCON conference*, pp. 403–406, Oct. 2004.

[64] H. Ku and J. Kenney, “Estimation of Error Vector Magnitude using Two-tone Intermodulation Distortion Measurements,” *IEEE MTT-S International digest*, vol. 1, pp. 17–20, June 2001.

[65] C. Potter, “Uncertainty and Budgets Applied to Error Vector Magnitude (EVM) for Digital Modulation Systems,” *Proceedings of 61st ARFTG Conference*, pp. 103–109, June 2003.

[66] “IEEE 802.11a WLAN standard,” Sept. 1999.

[67] *FLL120MK GaAs FET specification sheet*, Fujitsu Compound Semiconductor, inc., CA, USA.

[68] Advanced Design System from Agilent Technologies, inc., CA, USA, www.agilent.com.

[69] Microwave Office from Applied Wave Research, inc.,CA, USA, www.microwaveoffice.com.

[70] J. Verspecht, "Large-signal network analysis - going beyond sparameters," in *52nd ARFTG Short Course Notes*, Dec. 2003.

[71] J. Verspecht, D. Root, J. Wood, and A. Cognata, "Broad-band, multi-harmonic frequency domain behavioral models from automated large-signal vectorial network measurements," in *IEEE MTT-S Digest*, June 2005.

[72] J. Verspecht, D. F. Williams, D. Schreurs, K. A. Remley, and M. D. McKinley, "Linearization of large-signal scattering functions," *IEEE Transactions on microwave theory and techniques*, vol. 53, pp. 1369–1376, Apr. 2005.

[73] J. Olah and S. Gupta, "Power amplifier design using measured loadpull data," *Microwave Engineering Europe*, Aug. 2003.

[74] R. L. Carlson, "Meld load-pull test with eda tools," *Microwave and RF*, Apr. 2003.

[75] W. Clausen, J. Capwell, L. Dunleavy, T. Weller, J. Verspecht, J. Liu, and H. Arslan, "Black-box modeling of rfic amplifiers for linear and non-linear simulations," *Microwave Product Digest*, Oct. 2004.

[76] The MathWorks, Inc., MA, USA, www.mathworks.com.

[77] G. Gonzalez, *Microwave Transistor Amplifiers: Analysis and Design (2nd Edition).* Prentice Hall, 1996.

[78] Modelithics, inc., Tampa, FL, USA, www.modelithics.com.

[79] M. Isaksson, D. Wisell, and D. Ronnow, "Nonlinear behavioral modeling of power amplifiers using radial-basis function neural networks," in *IEEE MTT-S Digest*, June 2005.

[80] A. Antoniou, *Digital Filters : Analysis, Design and Applications.* USA: McGraw-Hill, 1993.

[81] S. W. Smith, *The Scientist and Engineer's Guide to Digital Signal Processing.* USA: California Technical Publishing, 1997.

[82] T. Liu, S. Boumaiza, M. Helaoui, H. B. Nasr, and F. M. Ghannouchi, "Behavior modeling procedure of wideband rf transmitters exhibiting memory effects," in *IEEE MTT-S Digest*, June 2005.

[83] D. Luongvinh and Y. Kwon, "Behavioral modeling of power amplifiers using fully recurrent neural networks," in *IEEE MTT-S Digest*, June 2005.

[84] T. Liu, S. Boumaiza, and F. M. Ghannouchi, "Dynamic behavioral modleing of 3g power amplifiers using real-valued time-delay neural networks," *IEEE Trans. Microwave Theory Tech.*, vol. 52, pp. 1025–1033, Mar. 2004.

[85] P. Crama and Y. Rolain, “Broadband measurement and identification of a wiener-hammerstein model for an rf amplifier,” in *ARFTG Conference Digest*, Dec. 2002, pp. 49–57.

[86] A. Ahmed, E. R. Srinidhi, and G. Kompa, “Efficient pa modeling using neural network and measurement setup for memory effect characterization in the power device,” in *IEEE MTT-S Digest*, June 2005.

[87] J. Wood, J. Horn, and D. Root, “Spice model for am-pm conversion introduced by weakly nonlinear circuits,” in *IEEE MTT-S Digest*, June 2005.

[88] P. M. Asbeck, H. Kobayashi, M. Iwamoto, G. Hanington, S. Nam, and L.E.Larson, “Augmented behavioral characterization for modeling the nonlinear response of power amplifiers,” in *2002 IEEE MTT-S Digest*, vol. 1, June 2002, pp. 135–138.

ABOUT THE AUTHOR

Jiang Liu obtained his BSEE at Nanjing University of Posts and Telecommunications in 1996 and MSEE at University of South Florida in 2002. His research focuses on development of advanced RF and microwave measurement systems and nonlinear behavioral modeling of RF and microwave circuits and systems.